letnik/volume **52** - št./no. **2/06** - str./pp. **73-140**
Ljubljana, feb./Feb. 2006, zvezek/issue **490**

STROJNIŠKI VESTNIK

JOURNAL OF MECHANICAL ENGINEERING

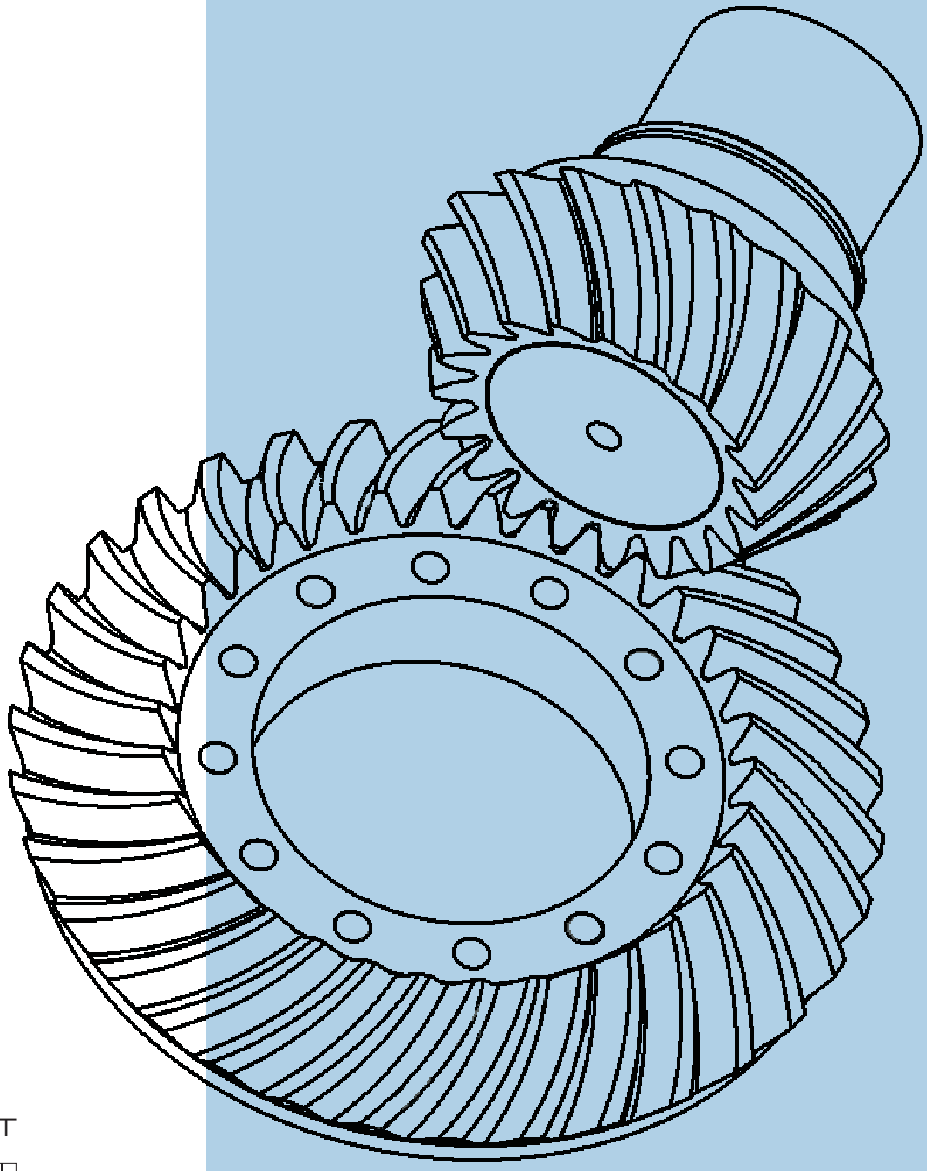

cena 800 SIT

9 770039 248001

ISSN 0039-2480

Vsebina - Contents

Strojniški vestnik - Journal of Mechanical Engineering
letnik - volume 52, (2006), številka - number 2
Ljubljana, februar - February 2006
ISSN 0039-2480

Izhaja mesečno - Published monthly

Strojniški vestnik - Journal of Mechanical Engineering 52(2006)2, 74-84
UDK - UDC 620.179.12/.13:539.388.1
Izvirni znanstveni članek - Original scientific paper (1.01)

Modeliranje naključnih termomehanskih napetostno-deformacijskih stanj

Thermo-Mechanical Modelling of Stochastic Stress-Strain States

Marko Nagode - Matija Fajdiga
(Fakulteta za strojništvo, Ljubljana)

Deformacijski postopek je najbolj razširjena metoda napovedovanja dobe trajanja dinamično obremenjenih delov na področju malociklične trdnosti. Uporablja se tako pri nizkih, srednjih kakor tudi visokih temperaturah, če je temperatura med obratovanjem nespremenljiva. Deformacijski postopek je računsko izjemno hiter in narekuje le uporabo analiz elastičnosti s končnimi elementi. Zaradi številnih prednosti, razširjenosti in potencialnih možnosti je bil prilagojen tako, da je uporaben tudi za spremenljive temperature. Napetostno-deformacijsko stanje je popisano s Prandtlovimi operatorji. Postopek temelji na stabilnih histereznih zankah, pri čemer lezenje ni upoštevano. Analiziran je tudi vpliv filtriranja konic sunkov. Narejena je primerjava izsledkov raziskav z rezultati meritev in Skeltonovim modelom.

(Ključne besede: utrujanje termomehansko, enačbe konstitutivne, stanja napetostno-deformacijska, modeliranje)

The isothermal strain-life approach is the most commonly used approach for determining fatigue damage, particularly in low-cycle fatigue. It is used for low, medium and high temperatures if the temperature remains constant during the test. Computationally, it is extremely fast and generally requires elastic finite-element analyses only. For this reason it has been adapted for variable temperatures. The local temperature-stress-strain behaviour is modelled with an operator of the Prandtl type. The hysteresis loops are supposed to be stabilized and no creep is considered. The consequences of reversal point filtering are analysed. Finally, the approach is compared to several thermo-mechanical fatigue tests and the Skelton model.

(Keywords: thermomechanical fatigue, constitutive equations, stress strain states, modelling)

0 UVOD

Številni izdelki, npr. motorji z notranjim zgorevanjem, izpušni in hladilni sistemi, turbine, jedrski reaktorji, so v času uporabe obremenjeni z naključnimi termomehanskimi obremenitvami (TMU), ki lahko privedejo do utrujenostnih razpok [1]. Z razvojnega vidika je zato pomembna napoved dobe trajanja izdelka v razvojnih fazah pred preskušanjem prototipov oziroma izdelkov. Doba trajanja je odvisna predvsem od obremenitev, uporabljenih materialov, oblike izdelka in okoliščin. Za njeno dokazovanje se uporabljajo naslednji preizkusi ([2] in [3]):

- deformacijsko nadzorovani malociklični preizkus (MCUP - LCF) pri nespremenljivi temperaturi,
- termomehanski preizkus delov in izdelkov in
- toplotni sunek.

0 INTRODUCTION

Many products, like internal combustion engines, exhaust and cooling systems, turbines, nuclear reactors, are subjected to stochastic thermo-mechanical fatigue (TMF) loading that can cause fatigue failures during their usage [1]. From the development perspective, fatigue-life prediction in the development phases before prototype or product testing is important. Fatigue life depends primarily on loads, applied materials, product geometry and environmental effects. Its approval is generally based on the following tests ([2] and [3]):

- isothermal strain-controlled low-cycle fatigue (LCF) tests,
- TMF tests on specimens and components,
- thermal shock tests.

MCUP se izvajajo prednostno, ker so v primerjavi z drugimi preprostejši [4]. Poleg tega se opravljajo že več desetletij, postopek testiranja in zapisovanja rezultatov testiranj pa je standardiziran [2]. Obstajajo tudi baze podatkov o materialnih lastnostih, potrebnih za napoved dobe trajanja malociklično obremenjenih delov. Končni cilj je razviti metodologijo napovedovanja dobe trajanja, ki bo omogočala zanesljive napovedi brez termomehanskih testiranj in testiranj s toplotnim sunkom. Področje je poglobljeno predstavljeno v [3] do [9].

V prispevku je obravnavan problem napovedovanja napetostno-deformacijskih stanj ob upoštevanju spremenljive temperature obratovanja. Predpostavimo, da je vpliv lezenja in prehodnih pojavov, npr. utrjevanja ali mehčanja, neznaten. Napovedovanje napetostno-deformacijskih stanj torej temelji na stabilnih histereznih zankah in konstitutivnih enačbah elastoplastičnosti. Izmed razpoložljivih reoloških modelov ([9] do [11]) je bil izbran model vzporedno vezanih vzmeti in drsnikov [11], izražen s Prandtlovim modelom s temperaturno odvisnimi gostotami in temperaturno neodvisnimi drsnimi površinami. Model omogoča razširitev deformacijskega postopka na področje spremenljivih temperatur, pri čemer se velika hitrost računanja ne zmanjša.

Napetostno nadzorovan in temperaturno preoblikovan reološki model je obravnavan v [12] in [13]. V primeru deformacijskega nadzora potrebujemo enakovreden, a drugačen model.

V drugem poglavju so obravnavane temperaturno odvisne napetostno-deformacijske krivulje in ocenjevanja parametrov. V tretjem poglavju je prikazan razvoj temperaturno preoblikovanega in deformacijsko nadzorovanega modela vzmet – drsnik. V četrtem poglavju so analizirane posledice izločanja konic sunkov. V petem poglavju je opisano ujemanje novega modela z rezultati preizkusov in s Skeltonovim modelom, v zadnjem poglavju pa so podani pomembnejši sklepi.

1 TEMPERATURNO ODVISNE NAPETOSTNO-DEFORMACIJSKE KRIVULJE

Ker večina materialov preide po nekem manjšem številu obremenitvenih ciklov v stabilno področje, se za napoved dobe trajanja navadno uporabijo materialne lastnosti, ki ustrezajo polovični dobi trajanja preskušanca. Temperaturni časovni poteki obremenitev so v splošnem naključni. V literaturi je mogoče najti napetostno-deformacijske krivulje za le nekaj različnih

In terms of complexity, LCF tests are favoured because of their simplicity [4]. In addition, because they have been carried out for decades, the testing procedures and data recording is standardized [2]. There also exist databases with material properties required for the fatigue-life prediction of low-cycle loaded parts. The final goal is, therefore, to develop a methodology of fatigue-life prediction that will enable reliable estimations by avoiding expensive TMF and thermal shock tests. The methodology is discussed comprehensively in [3] to [9].

The present work is concerned with a cyclic stress-strain response prediction suitable for variable temperatures. Assuming that creep and transient effects, such as cyclic hardening and cyclic softening and their effect on damage accumulation are negligible, the hysteresis loops are supposed to be stabilized and the constitutive equations for elastoplasticity are applicable for stress-strain behaviour modelling. From among the available models ([9] to [11]), the strain-controlled spring-slider model [11] with temperature-dependent Prandtl densities and temperature-independent yield surfaces has been chosen. It enables the extension of the isothermal strain-life approach to non-isothermal problems by preserving a high computational speed.

The stress-controlled and temperature-modified spring-slider model is explained in [12] and [13]. However, if the strain is controlled, an equivalent but distinct spring-slider is required.

In Section 2 the temperature-dependent cyclic stress-strain curves and parameter assessment is discussed. In Section 3 the temperature-modified strain-controlled spring-slider model is developed. In the 4th section the consequences of reversal point filtering are analysed. In Section 5 the spring-slider model is compared to several TMF tests, and the final section lists the conclusions.

1 TEMPERATURE-DEPENDENT CYCLIC STRESS-STRAIN CURVES

Most metals approach a cyclically stable state after a certain number of cycles. Cyclically stable or half-life material properties are usually used in fatigue analyses. Generally speaking, the temperature–time history is stochastic, but cyclic stress–strain curves for only a few distinct temperatures can be found in the literature. To

temperatur. Napoved napetostno-deformacijskih stanj pri temperaturah, pri katerih napetostno-deformacijske krivulje ne obstajajo, je mogoča z uporabo interpolacije, aproksimacije ali neparametričnih metod. Predvsem slednje so se v zadnjem času izkazale za najboljše. Za popis elastoplastičnih lastnosti gradiv se najpogosteje uporablja Ramberg-Osgoodova enačba [14]:

obtain the material parameters that have not been measured, linear parameter interpolation, approximation or non-parametric methods can be used. The latter turned out to be the most appropriate recently. Elasto-plastic hardening solids are most frequently modelled by the Ramberg–Osgood relation [14]:

$$\varepsilon = g(\sigma, T) = \frac{\sigma}{E(T)} + \left(\frac{\sigma}{K'(T)} \right)^{1/n'(T)} \quad (1),$$

kjer je $E(T)$ modul elastičnosti, $K'(T)$ in $n'(T)$ pa sta utrjevalni koeficient in utrjevalni eksponent. Interpolacija je bila obravnavana v [12].

where $E(T)$ is Young's modulus and $K'(T)$ and $n'(T)$ are the cyclic hardening coefficient and the cyclic hardening exponent respectively. Parameter interpolation has been dealt with in [12].

2 MODELIRANJE NAPETOSTNO-DEFORMACIJSKIH STANJ

V [12] je bilo dokazano, da Masingov model in spominski modeli niso veljavni, če se temperatura med obremenitvenim potekom spreminja. Masing je izsledke svojih raziskav utemeljil z reološkim modelom vzmet – drsnik in predpostavil, da so parametri modela neodvisni od časa [11]. Da bi odpravili omejitve omenjenih modelov, je bil model vzmet – drsnik temperaturno spremenjen ([12] in [13]). Model v sedanji obliki je primeren za modeliranje elastoplastičnih lastnosti gradiv in nelinearnega kinematičnega utrjevanja pri sočasnem nadzoru napetosti. Če je deformacija nadzorna spremenljivka, je na sliki 1 prikazan primernejši model za modeliranje napetostno-deformacijskih stanj.

Iz ravnotežja na segmentu vzmet – drsnik je mogoče izraziti celotno deformacijo ε: $\varepsilon = \varepsilon_{qj} + \varepsilon_{\alpha j}$. Deformacija drsnika $|\varepsilon_{qj}|$ ne more nikoli preseči navidezne drsne deformacije q_j. Deformacija vzmeti

2 STRESS-STRAIN-TEMPERATURE BEHAVIOUR

It has been shown in [12] that the Masing and Memory models are not valid if the temperature varies during the cycle. Masing based his finding on the rheological spring-slider model and assumed that the model parameters are time independent [11]. Therefore, the spring-slider model has been adapted for variable temperatures ([12] and [13]). The model developed so far is capable of modelling elasto-plastic hardening solids and non-linear kinematic hardening under stress control. If the strain is controlled, the rheological spring-slider model depicted in Fig. 1 proves to be more convenient.

From the equilibrium in a single spring-slider segment, the total strain ε is obtained $\varepsilon = \varepsilon_{qj} + \varepsilon_{\alpha j}$, where the slider strain $|\varepsilon_{qj}|$ can never exceed the fictive yield strain q_j. The spring strain can now be expressed as:

$$\varepsilon_{\alpha j} = \varepsilon - \mathrm{sign}(\varepsilon - \varepsilon_{\alpha j}) \min\{q_j, |\varepsilon - \varepsilon_{\alpha j}|\} \quad (2)$$

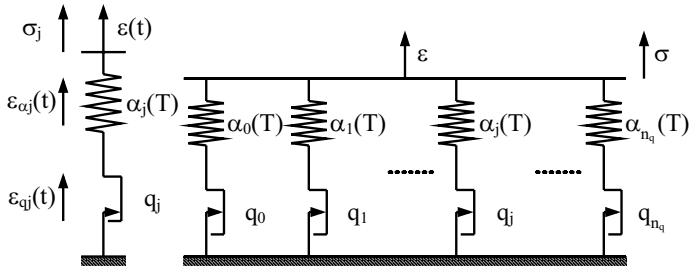

Sl. 1. *Reološki model vzmet – drsnik*
Fig. 1. *Rheological spring-slider model*

ustreza operatorju ohlapa s splošno začetno vrednostjo ([15] do [17]):

and corresponds exactly to the play operator with the general initial value ([15] to [17]):

$$\varepsilon_{\alpha j}(t_i) = \max\{\varepsilon(t_i) - q_j, \min\{\varepsilon(t_i) + q_j, \varepsilon_{\alpha j}(t_{i-1})\}\} \tag{3}$$

za $0 < t_1 < t_2 < \cdots < t_n$. Trenutna deformacija $\varepsilon_{\alpha j}(t_i)$ je odvisna od deformacije v predhodnem trenutku $\varepsilon_{\alpha j}(t_{i-1})$, imenovanem spominska točka. Predpostavimo, da zaostalih deformacij ni. Odtod izhaja $\varepsilon_{\alpha j}(0) = 0$ in $\sigma_j(0) = 0$. Napetost v odseku vzmet – drsnik je tedaj:

for $0 < t_1 < t_2 < \cdots < t_n$. Thus, the current strain state $\varepsilon_{\alpha j}(t_i)$ depends on the previous state $\varepsilon_{\alpha j}(t_{i-1})$ called the memory point. Presumably, there is no residual strain initially, so $\varepsilon_{\alpha j}(0) = 0$ and $\sigma_j(0) = 0$. The stress in the spring-slider segment is then:

$$\sigma_j(t_i) = E_j(T_i)\varepsilon_{\alpha j}(t_i) = \alpha_j(T_i)\varepsilon_{\alpha j}(t_i) \tag{4}$$

$T_i = T(t_i)$ in $\alpha_j(T_i)$ je Prandtlova gostota. S seštevanjem napetosti po posameznih odsekih je mogoče izraziti celotno napetost s Prandtlovimi operatorji ([15] do [17]):

where $T_i = T(t_i)$ and $\alpha_j(T_i)$ is the Prandtl density. Adding the spring-slider stresses results in the total stress in the form known as the operator of the Prandtl type ([15] to [17]):

$$\sigma(t_i) = \sum_{j=0}^{n_q} \alpha_j(T_i)\varepsilon_{\alpha j}(t_i) \tag{5}$$

s temperaturno odvisnimi gostotami. Ker je operator rege, definiran v en. (3), neodvisen od časa in temperature, ga je treba spremeniti tako, da bo zagotavljal ravnotežje v odseku vzmet – drsnik tudi pri spremenljivih temperaturah.

Če je v trenutku t_{i-1} j-ti odsek v ravnotežju, pomnožimo en. (3) z $\alpha_j(T_{i-1})$ (sl. 2). Odtod izhaja:

with temperature-dependent Prandtl densities. The play operator given in Eq. (3) is independent of time and temperature. Therefore, it is modified to assure equilibrium in the spring-slider.

Let us presume that at t_{i-1} the spring-slider segment *j* is in equilibrium and multiply Eq. (3) by $\alpha_j(T_{i-1})$ (Fig. 2). This yields:

$$\sigma_j(t_{i-1}) = \max\{(\varepsilon(t_{i-1}) - q_j)\alpha_j(T_{i-1}), \min\{(\varepsilon(t_{i-1}) + q_j)\alpha_j(T_{i-1}), \sigma_j(t_{i-2})\}\} \tag{6},$$

kjer velja $\sigma_j(t_{i-2}) = \sigma_j(t_{i-1})$. Če se v koraku $[t_{i-1}, t_i]$ spremenita temperatura ali deformacija, se meje operatorja ohlapa premaknejo in:

where the memory point $\sigma_j(t_{i-2}) = \sigma_j(t_{i-1})$. If the temperature or strain change in the interval $[t_{i-1}, t_i]$, then the boundaries of the play operator move and:

$$\sigma_j(t_i) = \max\{(\varepsilon(t_i) - q_j)\alpha_j(T_i), \min\{(\varepsilon(t_i) + q_j)\alpha_j(T_i), \sigma_j(t_{i-1})\}\}$$

Če nato enačbo delimo z $\alpha_j(T_i)$, dobimo:

If the equation is divided by $\alpha_j(T_i)$, then:

$$\varepsilon_{\alpha j}(t_i) = \max\left\{\varepsilon(t_i) - q_j, \min\left\{\varepsilon(t_i) + q_j, \frac{\sigma_j(t_{i-1})}{\alpha_j(T_i)}\right\}\right\} \tag{7}$$

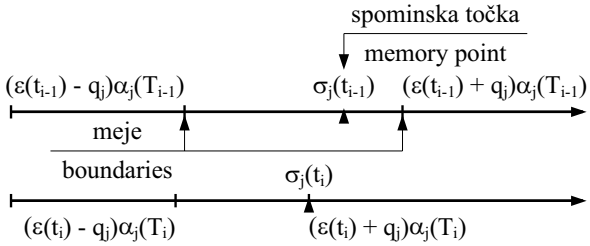

Sl. 2. *Ravnotežje v modelu vzmet – drsnik*
Fig.2. *Equilibrium in the spring-slider model*

in nazadnje:

$$\varepsilon_{\alpha j}(t_i) = \max\left\{\varepsilon(t_i) - q_j, \min\left\{\varepsilon(t_i) + q_j, \frac{\alpha_j(T_{i-1})}{\alpha_j(T_i)}\varepsilon_{\alpha j}(t_{i-1})\right\}\right\} \quad (8),$$

kjer je $\sigma_j(t_{i-1}) = \alpha_j(T_{i-1})\varepsilon(t_{i-1})$. Z enačbama (8) in (5) je mogoče modelirati napetostno-deformacijska stanja tudi v primeru naključno spreminjajočih se temperatur, saj temperaturno spremenjen operator ohlapa vedno zagotavlja ravnotežje v vseh odsekih vzmet – drsnik.

Ker so ponovitvene napetostno-deformacijske krivulje znane, je Prandtlove gostote mogoče izračunati vnaprej. Naj bo $n_q + 1$ navideznih drsnih deformacij enakomerno razporejenih med ničelno in največjo pričakovano amplitudo deformacije (sl. 3). Za vsako navidezno drsno deformacijo q_j v območju $j = 0,\ldots,n_q$ in vsako temperaturo T_k v območju $k = 0,\ldots,n_T$ je z en. (1) mogoče izračunati deformacije $\varepsilon_j(T_k)$ in napetosti $\sigma_j(T_k)$. Prandtlove gostote izračunamo tako, da v en. (5) vstavimo napetosti:

and finally:

as $\sigma_j(t_{i-1}) = \alpha_j(T_{i-1})\varepsilon(t_{i-1})$. When Eq. (8) is inserted into Eq. (5), the temperature-dependent stress-strain behaviour can be modelled, since the temperature-modified play operator guarantees the equilibrium in the spring-slider segments at any time and temperature.

As the temperature-dependent cyclic stress-strain curves are known, the Prandtl densities can be precalculated. Let us disperse $n_q + 1$ fictive yield strains equidistantly between the zero strain and the maximum expected strain amplitude (Fig. 3). Thus, for each fictive yield strain q_j in the range $j = 0,\ldots,n_q$ and each temperature T_k in the range $k = 0,\ldots,n_T$, the strain $\varepsilon_j(T_k)$ and the stress $\sigma_j(T_k)$ can be determined from Eq. (1). By inserting q_j and $\sigma_j(T_k)$ into Eq. (5) the Prandtl densities are obtained:

$$\alpha_j(T_k) = \frac{1}{\Delta q}(\sigma_{j+1}(T_k) - 2\sigma_j(T_k) + \sigma_{j-1}(T_k)) \quad j = 0,\ldots,n_q \quad k = 0,\ldots,n_T \quad (9),$$

kjer je $\sigma_{-1}(T_k) = \sigma_0(T_k) = 0$, širina razreda navidezne drsne deformacije pa je Δq.

Prandtlove gostote je pametno izračunati vnaprej, jih shraniti v preglednico rešitev ter šele nato modelirati napetostno-deformacijska stanja z enačbama (8) in (5). Tako ohranimo veliko hitrost računanja.

where $\sigma_{-1}(T_k) = \sigma_0(T_k) = 0$ and the fictive yield strain class width is Δq.

The Prandtl densities can be precalculated and stored in a table before the stress-strain-temperature trajectory modelling using Eqs. (8) and (5) starts. In this way a high computational speed is preserved.

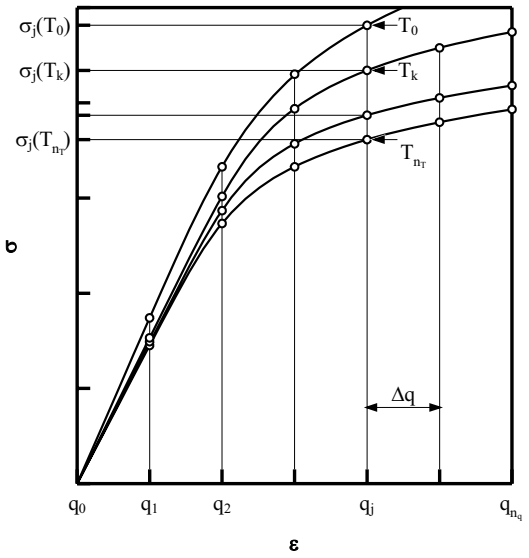

Sl. 3. *Temperaturno odvisne napetostno-deformacijske krivulje*
Fig. 3. *Temperature dependent cyclic stress-strain curves*

3 POSLEDICE IZLOČANJA KONIC SUNKOV

Če so materialne lastnosti časovno neodvisne, temperature pa nespremenljive, lahko poteke obremenitev pred začetkom modeliranja napetostno-deformacijskih stanj zgostimo in tako izločimo le zaporedje konic sunkov brez časovne komponente. Poteke obremenitev pregledujemo sproti in izločamo vse točke, ki niso lokalni ekstremi ter obremenitvene cikle, ki ne prispevajo k zbiranju poškodb [17]. Ker se z zgoščevanjem poteki močno skrajšajo, je deformacijski postopek numerično bistveno hitrejši od zahtevnejših postopkov in se zato tudi pogosto uporablja.

Če se temperatura med posameznimi konicami sunkov spreminja, lega naslednje konice ni več odvisna le od lege predhodne konice, ampak tudi od prehoda med njima. Slika 4 prikazuje vpliv spreminjanja temperature na krivuljo σ-ε za zlitino 9Cr2Mo, ki se začne v točki 0 ($T_0 = 270$ °C), gre skozi točki 1 ($T_1 = 570$ °C) in 2 ($T_2 = 270$ °C) ter se konča v točki 3 ($T_3 = 570$ °C). Predpostavimo, da sta poteka deformacij in temperatur nezgoščeni in izračunajmo krivuljo napetost-deformacija (glej debelo polno črto) po enačbah iz prejšnjega poglavja. En. (8) zagotavlja ravnotežje v odsekih vzmet – drsnik v vseh točkah, označenih s trikotniki. Izkaže se, da se izračunane napetosti ne

3 CONSEQUENCES OF REVERSAL POINT FILTERING

For rate-independent material behaviour and constant temperature, only the reversal points in the load histories are needed for stress-strain trajectory modelling and cycle counting. Load histories can thus be compressed and the time component can be eliminated. The load histories are scanned online and any point that is not the reversal point is discharged from the history. Similarly, all reversal points corresponding to a change in amplitude smaller than a certain threshold are filtered [17]. As history compression results in a considerable reduction of history lengths the strain-life approach is much faster than competing ones. For this reason it has been used frequently.

However, if the temperature changes between reversal points, the position of the next point does not depend only on the current point, but also on the transition between the points. Fig. 4 shows the influence of temperature variations on the σ-ε trajectory for a 9Cr2Mo alloy. It starts at point 0 ($T_0 = 270$ °C), goes through points 1 ($T_1 = 570$ °C) and 2 ($T_2 = 270$ °C) and ends at point 3 ($T_3 = 570$ °C). Let us suppose that the strain and temperature histories are not filtered and calculate the stress-strain-temperature trajectory as explained in the preceding section (the thick solid line). Eq. (8) ensures equilibrium in the spring-slider model at any point indicated by triangle markers. It has been observed that the stresses do not necessarily coincide

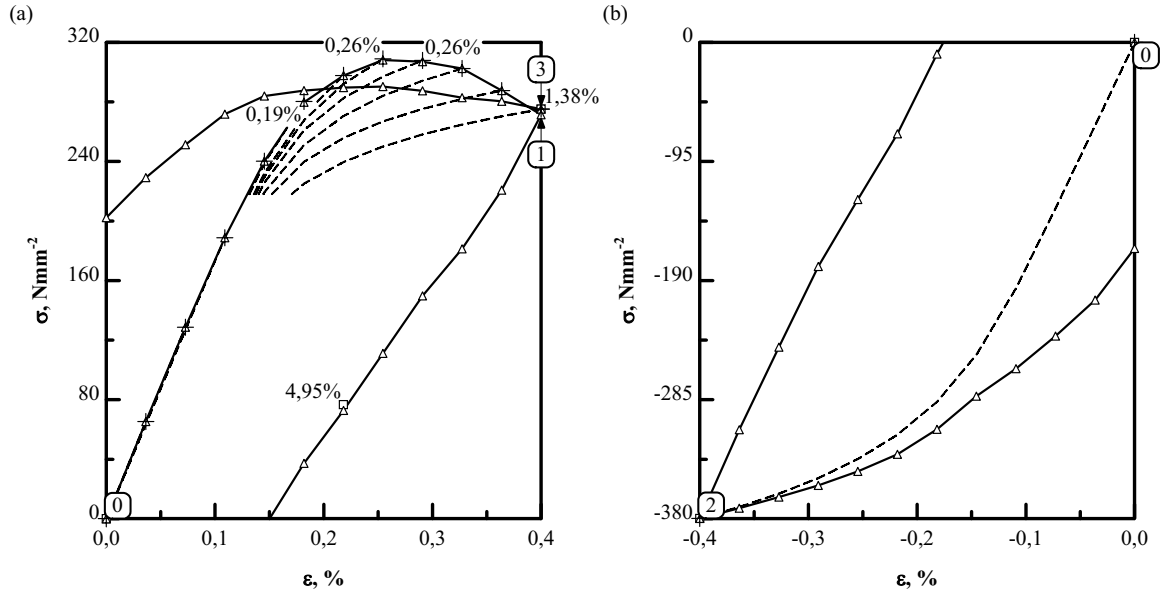

Sl. 4. *Vpliv temperature na spremembe σ-ε krivulj*
Fig. 4. *Influence of temperature variations on σ-ε trajectory*

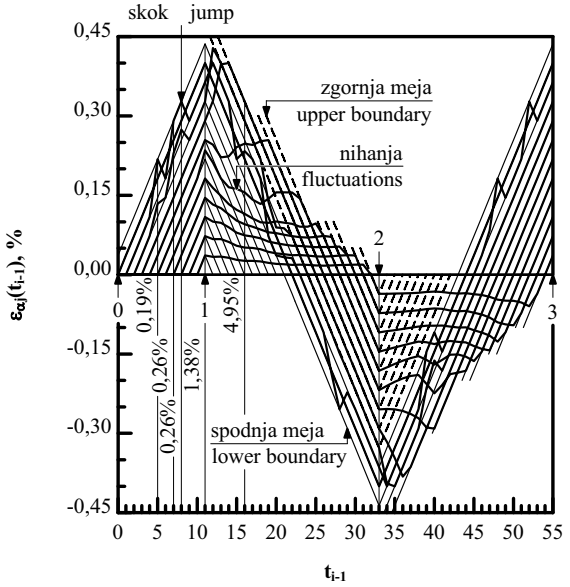

Sl. 5. *Spominske točke pri spremenljivi temperaturi*
Fig. 5. *Memory point history at variable temperature*

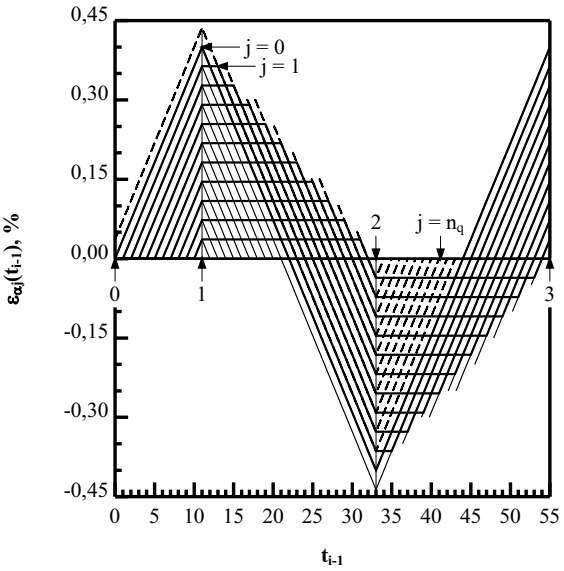

Sl. 6. *Spominske točke pri nespremenljivi temperaturi*
Fig. 6. *Memory point history at constant temperature*

ujemajo vedno z napetostmi na izotermnih napetostno-deformacijskih krivuljah (črtkane črte s simboli v obliki križcev). S tem je dokazan vpliv prehodov med konicami sunkov na krivuljo σ-ε. Podobna odstopanja se pojavijo v primeru zgoščenih potekov obremenitev, kjer se lega točk v ravnini σ-ε računa le za konice sunkov (kvadratni simboli). Odstopanja so odvisna od spominskih točk in temperaturnih sprememb med konicami sunkov.

Na slikah 5 in 6 so prikazani poteki spominskih točk za $j = 0,\ldots,n_q$ operatorjev ohlapa (debele polne črte), omejenih z zgornjimi (tanke črtkane črte) in spodnjimi (tanke polne črte) mejami. Točke 0 do 3 ustrezajo konicam sunkov. Če je temperatura $T_0 = \cdots = T_3 = 570\,°\mathrm{C}$, se spominske točke vedno ujemajo z eno od meja oziroma ostajajo nespremenjene (sl. 6). Če pa se temperatura spreminja (sl. 5), lahko spominske točke preskočijo z ene meje na drugo ali pa med njimi nihajo. To je torej razlog za odstopanja napetosti.

S slike 5 je razvidno, da so odstopanja neodvisna od dolžine krivulje σ-ε. Ko ε spremeni smer in se začno spominske točke približevati spodnji ali zgornji meji, se začno odstopanja zmanjševati. Ker ostajajo odstopanja po vrednosti vedno omejena, je izločanje konic sunkov sprejemljivo tudi v primeru spremenljivih temperatur.

with those on the isothermal cyclic stress-strain curves (the dashed lines with cross markers). This way the influence of transitions between reversal points on the σ-ε curve is proved. Similar deviations are observed in the case of the compressed load histories, where the point positions in the σ-ε plane are calculated at load reversals only (square markers). The deviations depend on the memory points and the temperature variations between the reversal points.

In Figs. 5 and 6 the memory-point histories for the $j = 0,\ldots,n_q$ play operators (thick solid lines) bounded by their upper (thin dashed line) and lower (thin solid line) boundaries are shown. Points 0 to 3 correspond to the reversal points. If the temperature $T_0 = \cdots = T_3 = 570\,°\mathrm{C}$, the memory points coincide with one of the boundaries or stay constant, as depicted in Fig. 6. However, if the temperature changes (see Fig. 5), the memory points can jump from one boundary to another or fluctuate between the boundaries. This is actually why stress deviations occur.

From Fig. 5 it can be observed that the deviations do not depend on the length of the σ-ε trajectory. Whenever ε changes its direction and memory points start to approach either the lower or upper boundaries, the deviations start to decrease. As deviation are always limited, only reversal points should be processed under variable temperatures, too.

4 PREVERJANJE

Deformacijsko nadzorovan in temperaturno spremenjen model, sestavljen iz vzporedno vezanih odsekov vzmet – drsnik, smo primerjali z več preizkusi TMU, ki jih je opravil Skelton [4] pri 0,6 % celotne deformacije zlitine 9Cr2Mo. Temperaturno odvisni parametri, ki se pojavljajo v Ramberg-Osgoodovi enačbi, podatki o materialu in eksperimentalnih tehnikah so pojasnjeni v [2], [4] in [18].

Pri prikazu poteka deformacij in temperatur običajno nanašamo deformacije na ordinatno, temperature pa na abscisno os [4]. V prispevku sta obravnavani pot PKRM in zahtevna ponovitev (črtkana črta), prikazani na sliki 7. Medtem ko predstavlja pot PXRM 45° deltoidni cikel, izveden proti smeri urnega kazalca, je pot PMRK enaka ciklu, izvedenem v smeri urnega kazalca. Podobno velja tudi za 135° deltoidni cikel, omejen s točkami PKRZ. Cikla pravokotne oblike PXRZ in PKRM sta poimenovana 45° in 135° pravokotni cikel. Poti GEHF in GFHE tvorita dvojni termični cikel ter cikel zahtevne oblike je prikazan s črtkano črto.

Izmerjene histerezne zanke so omejene s križci na slikah 8 in 9. Trikotniki označujejo napetostno-deformacijske krivulje, izračunane s Skeltonovim [4] algoritmom, debele polne črte pa krivulje, ocenjene po našem algoritmu.

S slike 8 je razvidno, da je napoved obremenitvenih ciklov, izvedenih v smeri proti urnemu kazalcu, boljša od napovedi ciklov, izvedenih

4 VERIFICATION

The strain-controlled and temperature-modified spring-slider model is compared to several TMF tests conducted by Skelton [4] at a total strain range of 0.6% on the 9Cr2Mo alloy. The temperature-dependent parameters associated with the Ramberg-Osgood relation as well as the material data and experimental methods are given in [2], [4] and [18].

In deciding the temperature-strain path, the convention is to plot strain on the vertical axis and temperature on the horizontal axis [4]. The paper concerns the path PKRM and the complex cycle (dashed line) given in Fig. 7. The path PXRM represents a 45° kite cycle performed in an anticlockwise way while the corresponding clockwise cycle is taken in the PMRX order. A similar scheme applies in the 135° kite cycle PKRZ. The parallelogram-shaped PXRZ and PKRM are labelled as the 45° zero strain and the 135° zero strain respectively. Finally, the anticlockwise GEHF and the clockwise GFHE bi-thermal cycles as well as the complex cycle given in the dashed line are considered.

The observed hysteresis loops from the tests are plotted as crosses in Figs. 8 and 9. The triangle markers and the thick solid lines denote the stress-strain trajectories modelled by the Skelton [4] and our algorithm respectively.

It is clear that in Fig. 8 the shapes of the anticlockwise loops are predicted well, whereas for

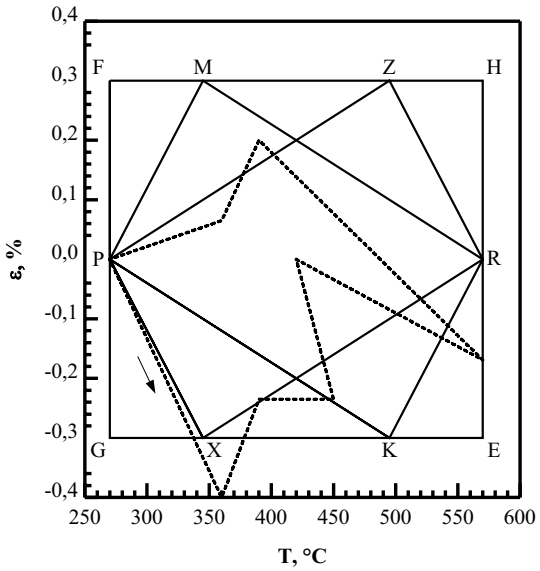

Sl. 7. *Vrste TMU ciklov*
Fig. 7. *TMF cycle types*

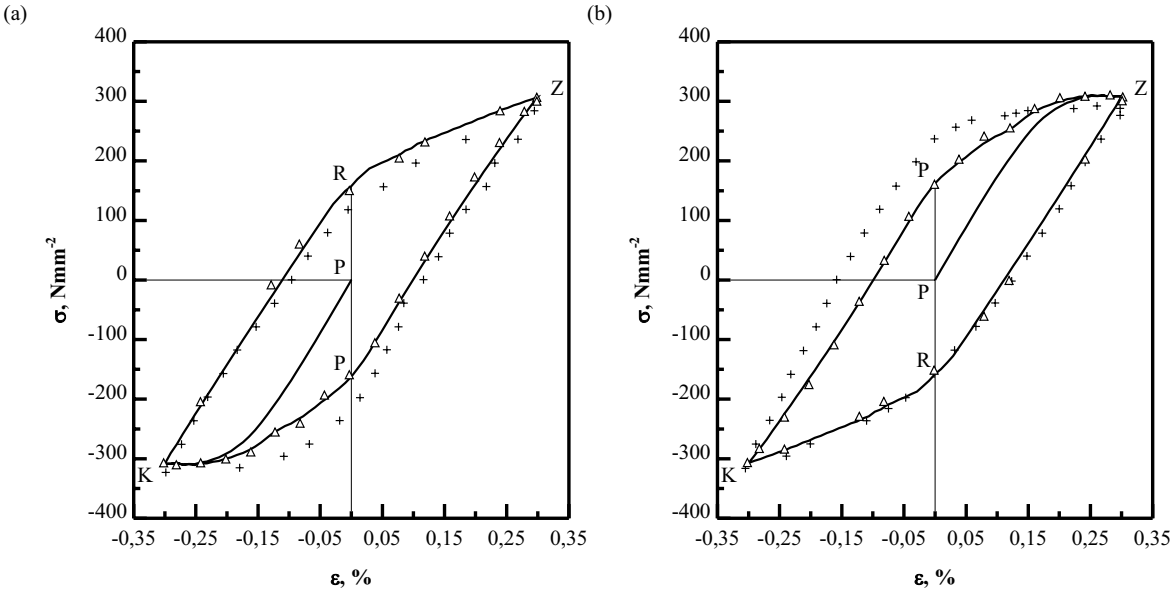

Sl. 8. *TMU 135° zanka (a) proti smeri urnega kazalca (b) v smeri urnega kazalca*
Fig. 8. *TMF loop 135° kite (a) anticlockwise, (b) clockwise*

v smeri urnega kazalca. Pri slednjih so testne histerezne zanke širše od napovedanih. Širše histerezne zanke niso le posledica nelinearnega ohlajanja, pač pa predvsem nekaterih parametrov, ki doslej še niso bili prepoznani. Ujemanje med Skeltonovimi in našimi rezultati je skoraj popolno. Postopek je bil nazadnje uspešno preverjen na ciklu zahtevne oblike, prikazani na sliki 9.

the clockwise style tests the observed loops are wider. The wider loops do not appear just because of non-linear cooling. Consequently, some parameters undefined so far seem to be more influential. The agreement between the Skelton [4] and our algorithm is almost perfect. The method was finally applied to the complex cycle of Fig. 9 successfully.

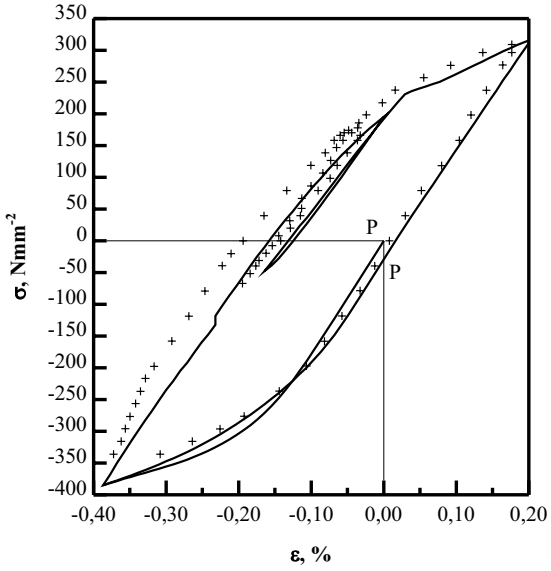

Sl. 9. *Zahtevna TMU zanka*
Fig. 9. *Complex TMF loop*

5 SKLEP

Deformacijski postopek je alternativa napetostnemu postopku napovedovanja utrujenostne poškodbe, ki se uporablja predvsem, če se pojavi tečenje. V prispevku je predstavljen in z več TMU preizkusi preverjen temperaturno spremenjen deformacijski postopek napovedovanja napetostno-deformacijskih stanj. Razvit in preverjen je bil deformacijsko nadzorovani model, sestavljen iz vzporedno vezanih odsekov vzmet – drsnik, ki omogoča modeliranje lokalnih temperaturno-napetostno-deformacijskih stanj. Za primer napetostnega nadzora je bil v [12] razvit enakovreden model. Izločanje konic sunkov je za elastoplastična gradiva sprejemljivo. Velika hitrost računanja običajnega deformacijskega postopka se ohrani. Razviti model je formalno dobro definiran z modelom Prandtlovega tipa in pomeni posplošenje Skeltonovih [4] izsledkov. Čeprav predlagani model ne omogoča napovedovanja lezenja in nekaterih drugih pojavov, lahko dosežemo izboljšano napoved temperaturno-napetostno-deformacijskih stanj na podlagi standardnih MCV preizkusov.

5 CONCLUSIONS

The strain-life approach is an alternative to the stress-life approach for determining fatigue damage, particularly when yielding occurs. An online temperature-modified strain-life approach has been developed and verified through several TMF tests. The spring-slider model has been developed and verified to enable local temperature-stress-strain trajectory modelling. The model is applicable if the strain is controlled or else the model given in [12] can be used. Reversal point filtering turned out to be acceptable for elasto-plastic hardening solids. The high computational speed of the classical strain-life approach can thus be preserved. The developed model is a generalization of the Skelton [4] findings and is formally well defined through an operator of the Prandtl type. Although neither creep damage nor some other effects can be assessed by the proposed approach, an improved temperature-stress-strain state prediction based on standardized LCF tests is possible.

6 LITERATURA
6 REFERENCES

[1] Constantinescu A, Charkaluk E, Lederer G, Verger L (2004) A computational approach to thermomechanical fatigue. *Int J Fatigue*, 26, 805-818.

[2] Skelton RP, Webster GA (1996) History effects on the cyclic stress-strain response of a polycrystalline and single crystal nickel-base superalloy. *Materials Science and Engineering*, A216, 139-154.

[3] Charkaluk E, Bignonnet A, Constantinescu A, Dang Van K (2002) Fatigue design of structures under thermomechanical loadings. *Fatigue Fract Engng Mater Struct*, 25, 1199-1206.

[4] Skelton RP (2004) Hysteresis, yield, and energy dissipation during thermo-mechanical fatigue of a ferritic steel. *Int J Fatigue*, 26, 253-264.

[5] Ellison EG, Smith EM (1973) Predicting service life in a fatigue-creep environment. In: Carden AE, McEvily AJ, Wells CH, editors. Fatigue at elevated temperatures. *ASTM STP 520*, pp 575-612.

[6] Sehitoglu H (1992) Thermo-mechanical fatigue life prediction methods. In: Mitchell MR, Landgraf RW, editors. Advances in fatigue lifetime predictive techniques. *ASTM STP 1122*, pp 47-76.

[7] Cai C, Liaw PK, Ye M, Yu J (1999) Recent developments in the thermomechanical fatigue life prediction of superalloys. *J Mater*, 51(4).

[8] Chaboche JL, Gallerneau F (2001) An overview of the damage approach of durability modelling at elevated temperature. *Fatigue Fract Engng Mater Struct*, 24, 405-418.

[9] Chaboche JL (1989) Constitutive equations for cyclic plasticity and cyclic viscoplasticity. *Int J Plast*, 5, 247-302.

[10] Krempl E, Khan F (2003) Rate (time)-dependent deformation behaviour: an overview of some properties of metals and solid polymers. *Int J Plast*, 19, 1069-1095.

[11] Conle A, Oxland TR, Topper TH (1988) Computer-based prediction of cyclic deformation and fatigue behaviour. In: Solomon HD, Halford GR, Kaisand LR, Leis BN, editors. Low cycle fatigue. *ASTM STP 942*, pp 1218-1236.

[12] Nagode M, Zingsheim F (2004) An online algorithm for temperature influenced fatigue-life estimation: strain-life approach. *Int J Fatigue*, 26, 155-161.
[13] Nagode M, Hack M (2004) An online algorithm for temperature influenced fatigue-life estimation: stress-life approach. *Int J Fatigu*e, 26, 163-171.
[14] Ramberg W, Osgood WR (1943) Description of stress-strain curves by three parameters. Technical note no. 902, *NACA*.

Avtorjev naslov: prof.dr. Marko Nagode
prof.dr. Matija Fajdiga
Univerza v Ljubljani
Fakulteta za strojništvo
Aškerčeva 6
1000 Ljubljana
marko.nagode@fs.uni-lj.si
matija.fajdiga@fs.uni-lj.si

Author's Address: Prof.Dr. Marko Nagode
Prof.Dr. Matija Fajdiga
University of Ljubljana
Faculty of Mechanical Eng.
Aškerčeva 6
SI-1000 Ljubljana, Slovenia
marko.nagode@fs.uni-lj.si
matija.fajdiga@fs.uni-lj.si

Prejeto: 2.11.2005
Received:
Sprejeto: 16.11.2005
Accepted:
Odprto za diskusijo: 1 leto
Open for discussion: 1 year

Strojniški vestnik - Journal of Mechanical Engineering 52(2006)2, 85-100
UDK - UDC 621.431.37:629.063.6
004.94
Izvirni znanstveni članek - Original scientific paper (1.01)

Računalniško modeliranje gibanja goriva in njegov vpliv na konstrukcijo rezervoarja

Computational Modelling of Fuel Motion and Its Interaction with the Reservoir Structure

Matej Vesenjak[1] - Zoran Ren[1] - Heiner Müllerschön[2] - Stephan Matthaei[3]
([1]Fakulteta za strojništvo, Maribor; [2]DYNAmore GmbH, Stuttgart-Vaihingen; [3]DaimlerCrysler AG, Stuttgart)

Računalniški modeli vozil za simuliranje trkov vedno natančneje opisujejo obnašanje resničnih vozil. Rezervoar za gorivo je eden izmed elementov vozil, katerega računalniški modeli so bili do sedaj zelo poenostavljeni. Takšni modeli upoštevajo le vztrajnost mase goriva, ki je z masnimi točkami pritrjena na steno rezervoarja, vendar pa je vpliv gibanja goriva v rezervoarju popolnoma zanemarjen.

Prispevek opisuje nove računalniške modele, s katerimi je mogoče simulirati deformacijo rezervoarja za gorivo ob upoštevanju gibanja goriva pri trku vozila. V ta namen so bile vrednotene štiri metode simuliranje gibanja tekočine (Lagrange, Euler, poljubnostna Lagrange-Eulerjeva metoda - PLE in hidrodinamika zglajenih delcev - HZD) v rezervoarju preproste oblike, analizirane z eksplicitnim programom LS-DYNA. Računalniški rezultati so bili primerjani s poprej objavljenimi preizkusnimi opazovanji, pri čemer je bila ugotovljena zelo dobra primerljivost med rezultati.

Najprimernejši metodi (HZD in PLE) sta bili kasneje uporabljeni v dinamičnih simulacijah dejanskega rezervoarja za gorivo. Simulacije so pokazale, da predstavljeni modeli rezervoarja ob upoštevanju gibanja goriva zagotavljajo mnogo natančnejše rezultate v primerjavi z znanimi poenostavljenimi modeli.

(Ključne besede: gibanje goriva, Lagrangev opis, Eulerjev opis, ALE, SPH, vplivi tekočina - trdnina)

Computational models of vehicles for crash simulations are ever more precisely describing the behaviour of real vehicles. A fuel-tank is a typical vehicle element that has been very simplified in the computational models used so far. Such models have considered only the influence of the fuel mass inertia, which was point-wise connected to the tank walls, with total neglect of the fuel motion in the tank.

This paper describes new computational models that allow for a simulation of the fuel-tank deformation considering the fuel motion during a vehicle crash. For this purpose four different methods for describing fluid motion (Lagrangian, Eulerian, Arbitrary Lagrange-Eulerian description - ALE, SPH) were evaluated on a simple reservoir problem, analysed with the explicit dynamic code LS-DYNA. The computational results were compared with previously published experimental observations and a good correlation of the results was observed.

The most appropriate methods, SPH and ALE, were afterwards used in dynamic simulations of a real fuel-tank. The simulations showed that by also taking into consideration the fuel motion, the proposed computational models provide more accurate results in comparison with the previously used, simplified models.

(Keywords: fuel motion, Lagrangian description, Eulerian description, ALE, SPH, fluid structure interaction)

0 UVOD

V zadnjem času postajajo numerične simulacije v avtomobilizmu vse pomembnejše. Njihov cilj ni več zgolj določitev globalnega obnašanja vozil, temveč tudi natančnejše obnašanje posameznih

0 INTRODUCTION

In recent years numerical simulations in automotive engineering have gained in importance. Their aim is not only the determination of the global vehicle behaviour but also the behaviour of single

sestavnih delov. Pri razvoju konstrukcije novega vozila ali izboljšavi konstrukcije že znanega vozila so za računalniško simuliranje komponent najpogosteje uporabljene analize po metodi končnih elementov. V mnogih primerih simuliranje posameznih komponent ni zadostno, zato morajo biti v analizo vključene komponente oziroma celotni sklopi, ki vplivajo drug na drugega. Reševanje problemov postane zahtevnejše, kadar so sestavni elementi sklopa iz dveh ali več fizikalnih sistemov, ki medsebojno vplivajo. Kadar medsebojno vplivata dva ali več fizikalnih sistemov in je rešitev posameznega brez upoštevanja ostalih nemogoča, govorimo o vezanih problemih [20].

Eden izmed delov vozila, pri katerem vplivata dva fizikalna sistema, je rezervoar za gorivo. V preteklih simulacijah je bilo simuliranje rezervoarjev zelo poenostavljeno, saj vpliv gibanja tekočine na obnašanje rezervoarja ni bil obravnavan. Upoštevana je bila le masa goriva, ki je bila porazdeljena po posameznih vozliščih sten rezervoarja zaradi upoštevanja vztrajnostnih sil. Gibanje goriva pri trku vozila, ki ima velik vpliv tako na deformacijo rezervoarja kakor tudi njegovih nosilnih elementov, pa je bilo popolnoma zanemarjeno. Omenjene poenostavitve so bile neizogibne zaradi omejene uporabe simulacijskih programskih paketov, vendar pa novejši programski paketi omogočajo tudi učinkovito reševanje več fizikalnih sistemov hkrati. V prispevku so opisani in vrednoteni različni numerični modeli, s katerimi je mogoče opisati gibanje in vpliv tekočine na trdnino s programskim sistemom LS-DYNA [10]. LS-DYNA temelji na metodi končnih elementov in je bila prvotno namenjena reševanju dinamičnih problemov v mehaniki trdnin. Modeliranje odzivov v dinamiki trdnin je zato zelo dobro razvito. Modeliranje vezanih problemov med tekočino in trdnino pa še vedno ostaja izziv. Primerjava metod in njihova uporabnost je ponazorjena na praktičnem primeru gibanja tekočine v rezervoarju s preprosto geometrijo. Z eksperimentalnimi meritvami pa so primerjani tudi rezultati analiz [11].

1 MEDSEBOJNI VPLIV TEKOČINE IN TRDNINE

Eden izmed najpogosteje obravnavanih vezanih problemov v inženirski praksi je medsebojni vpliv tekočine in trdnine, zaradi česar so se razvili različni postopki reševanja teh problemov. K razvoju algoritmov za računanje vezanih problemov je pripomogel tudi silovit razvoj

components. In the case of computational component simulation, during the designing phase of a new vehicle structure or during the design improvements of existing vehicle designs, finite-element method analyses are most often used. In many cases, however, simulating separate components is not sufficient. Therefore, other components or assemblies that interact with each other have to be included in the analysis. The solution process becomes more sophisticated when the assembly components consist of two or more different physical systems that interact. When two or more physical systems interact with each other and an independent solution of one system is impossible without a simultaneous solution of the others, such systems are known as coupled [20].

One of the vehicle components where two physical systems interact is the fuel-tank. In previous simulations the model of the tank was very simplified, since the fluid motion's influence on the tank's behaviour was not considered. Only the fuel mass was taken into account, which was distributed at discrete nodes along the tank walls to account for the fuel inertia forces. The fuel motion during a vehicle crash, which has a large influence on tank deformation and its supporting elements, was thus completely neglected. Such simplifications were necessary due to the limitations of the simulation software used. However, some recent releases of simulation software already allow for an effective solution of several physical systems simultaneously. In this paper different computational models that allow for consideration of the fluid motion and its influence on the structure are described and evaluated with the software LS-DYNA [10]. LS-DYNA is based on the finite-element method and it was originally designed for solving structural dynamic problems. Therefore, its ability to model structural responses in general is well defined. However, the modelling of a coupled fluid-structure interaction is still quite challenging. A comparison of the methods and their applicability is illustrated on a practical example, describing the fuel motion in a reservoir with simple geometry. The computational results are further compared with the experimental measurements [11].

1 FLUID-STRUCTURE INTERACTION

One of the most popular coupled problems in engineering is the interaction between the fluid and the structure, which consequently results in different approaches to solving such a problem. The development of coupled problems solution algorithms was also influenced by the rapid develop-

računalniške opreme, saj so tovrstne analize računsko zelo zahtevne. Vezane probleme je z uporabo različnih programskih paketov mogoče reševati na dva načina:

- z uporabo dveh programskih paketov: eden za določitev območja tekočin in eden za ločeno določitev rešitve območja trdnine. Takšni programski paketi (npr. CFX in Nastran) so po navadi povezani z vmesnikom, ki nadzoruje izmenjavo potrebnih podatkov o robnih pogojih ([4] in [19]);
- z uporabo programskega paketa, ki omogoča hkratno reševanje dveh ali več vezanih fizikalnih sistemov (npr. ADINA, ANSYS, LS-DYNA).

Programski paket LS-DYNA omogoča dinamično ugotavljanje medsebojnega vpliva med tekočino in trdnino z eksplicitno integracijsko shemo. V LS-DYNI je vpliv tekočine mogoče opisati in simulirati na dva načina: (i) s stičnimi silami (uporabno pri Lagrangevem in SPH modelu) in (ii) s kriterijem poroznosti snovi, ki v vsakem opazovanem elementu določi silo, ki je potrebna za vzpostavitev ravnotežja med tekočino in trdnino (uporabno pri Eulerjevem in modelu PLE) ([1], [6], [10] in [12]).

2 RAZLIČNI OPISI DOMEN

2.1 Lagrangev opis

Lagrangev opis se običajno uporablja za opis problemov v mehaniki trdnin. Problem se opiše z velikim številom masnih delcev, pri čemer se opazuje gibanje vsakega posameznega delca v prostoru in času (sl. 1). Problem je natančno določen, kadar poznamo gibanje vseh delcev [17].

ment of computer hardware, because such simulations are computationally very intensive. Coupled problems can be solved in two ways, by using commercial software:

- with the use of two commercial codes: one for solving the fluid domain and one to separately determine the solid-domain solution. Such codes (e.g., CFX and Nastran) are usually connected via an interface that controls the necessary boundary conditions' data exchange ([4] and [19]);
- with use of a commercial software that simultaneously solves a multi-physics problem (e.g., ADINA, LS-DYNA, ANSYS).

The LS-DYNA code is capable of establishing a dynamic interaction between the fluid and the structure with an explicit integration scheme. In LS-DYNA it is possible to describe and simulate the influence of the fluid on the structure, and vice versa, in two ways: (i) with contact forces (applicable for Lagrangian and SPH model) and (ii) with a leakage criteria, which in each observed element determinates the force that is necessary to establish equilibrium conditions between the fluid and the structure (applicable for Eulerian and ALE model) ([1], [6], [10] and [12]).

2 DIFFERENT DOMAIN DESCRIPTIONS

2.1 Lagrangian description

The Lagrangian formulation is usually used for describing solid mechanics problems. The problem is described with a large number of mass particles, where the motion of every single particle is observed in space and time (Fig. 1). The problem is exactly defined when the motion of all the particles is known [17].

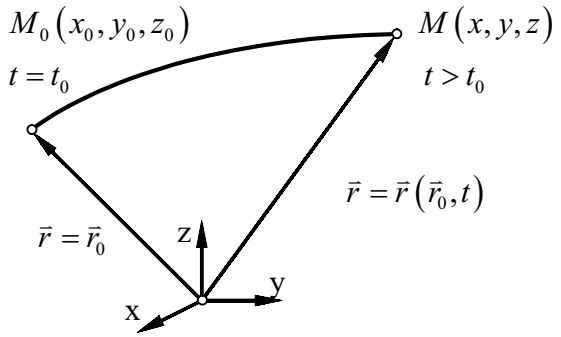

Sl. 1. *Lagrangev opis [17]*
Fig. 1. *Lagrangian formulation [17]*

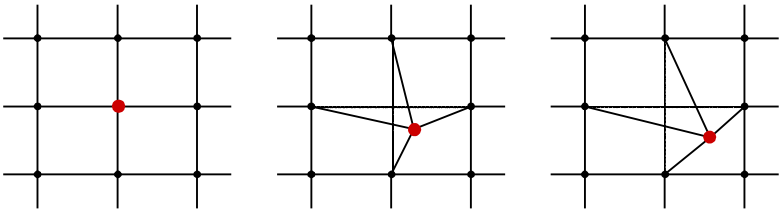

Sl. 2. *Deformacija mreže pri Lagrangevem opisu*
Fig. 2. *Mesh deformation in the Lagrangian formulation*

Lagrangev način opisa gibanja je preprost in nezahteven za uporabo, dokler gre za posamezni masni delec. V primeru proučevanja problema z velikim številom masnih delcev pa postane izredno zahteven in zapleten [17].

Pri Lagrangevem opisu predstavlja en končni element isti delež materiala celoten potek analize. Mreža končnih elementov je pritrjena na material med celotnim računskim postopkom, zaradi česar se pomika z materialom. Slika 2 prikazuje način reševanja preprostega primera tekočine z Lagrangevim opisom. Predpostavljeno je, da obremenitev deluje le na sredinsko vozlišče. Rezultat te obremenitve je pomik vozlišča v računskem časovnem koraku. Če vpliv obremenitve ne preneha, oz. se spremeni, vozlišče v naslednjem časovnem koraku ponovno zavzame novo lego in mreža se vedno bolj deformira, saj sledi toku materiala.

Ker mreža končnih elementov sledi materialu, ima relativen pomik medsebojno povezanih vozlišč izrazit vpliv na deformacijo končnih elementov. S premikom elementov se prenašajo tudi masa, gibalna količina in energija [2]. Enačba o ohranitvi mase se lahko v Lagrangevem opisu v parcialni diferencialni obliki zapiše kot:

$$\frac{\partial \rho}{\partial t} + \rho \cdot \frac{\partial v_i}{\partial x_i} = 0 \qquad (1),$$

kjer sta ρ gostota in v hitrost materiala (mreže). Za nestisljiv material je znano, da je div(v) = 0. Lagrangev opis ohranitve mase se lahko zapiše tudi v obliki algebrajske enačbe kot:

$$\rho \cdot J = \rho_0 \qquad (2),$$

kjer je J Jacobijeva matrika med trenutno in referenčno obliko. Ohranitev gibalne količine je v Lagrangevem opisu podana kot:

$$\rho \cdot \frac{\partial v_i}{\partial t} = \frac{\partial \sigma_{i,j}}{\partial x_i} + \rho \cdot b_i \qquad (3),$$

The Lagrangian formulation is very simple and easy to use for one or only a few mass particles. However, the method becomes very complicated and complex for a description of large number of mass particles [17].

In the Lagrangian formulation, one finite element represents the same part of the material throughout the course of the analysis. The finite-element mesh is fixed to the material during the entire computational process and therefore moves with the material. Figure 2 illustrates the solution process of a simple fluid problem using the Lagrangian formulation. It is presumed that the loading influences only the central node. The result of the loading is the shift of that node in a computational time step. If the influence of the loading does not stop or change, the node takes a new position in the next time step and the mesh deforms even more, since the mesh follows the material flow.

Since the mesh follows the material, the relative movement of connecting nodes can result in a significant deformation of the finite elements. Mass, momentum and the energy are transported with the movement of the elements [2]. The mass conservation equation can be, in partial differential equation form, written for the Lagrangian description as:

where ρ is the density and v is the velocity of the material (mesh). For an incompressible material it is known that div(v) = 0. The Lagrangian description for the mass conservation can also be written in an algebraic equation as:

where J is the Jacobian between the current and reference configuration. Conservation of momentum in terms of the Lagrangian description gives:

kjer sta σ Cauchy-jeva napetost in b masna sila (sila na enoto mase). Tretja enačba predstavlja ohranitev energije in se lahko v primeru izključno mehanskega postopka zapiše kot:

where σ is the Cauchy stress and b is the body force (a force per unit mass). The third equation represents the energy conservation and can be, in a purely mechanical process, written as:

$$\rho \cdot \frac{\partial u}{\partial t} = \sigma_{i,j} \cdot \frac{\partial v_i}{\partial x_i} \tag{4},$$

kjer je u notranja energija na enoto mase.

Pomanjkljivost Lagrangevega opisa postane razvidna v primerih s skrajno popačeno mrežo, saj njihov opis vedno temelji na mreži. Popačenost mreže vpliva na natančnost metode in zato na rezultat analize. Sprejemljiva možnost za izboljšanje Lagrangevega modela je ponovno mreženje domene problema.

where u is the internal energy per unit mass.

The disadvantage of the Lagrangian description becomes evident in cases of an extremely distorted mesh, because their formulation is always based on mesh. When the mesh is heavily distorted, the accuracy of the formulation and hence the solution will be severely affected. A possible option to enhance the Lagrangian model is to re-mesh the problem domain.

2.2 Eulerjev opis

Pri Eulerjevem opisu, ki se navadno uporablja za reševanja problemov računalniške dinamike tekočin, se problem opazuje v določeni prostorski točki in ne sledi gibanju posameznega delca (sl. 3). V enem časovnem koraku Δt gredo skozi točko številni masni delci, katerih gibanje je v trenutku prehoda natančno določeno. V opazovani točki se veličine polja spreminjajo s časom.

Ohranitev mase je v Eulerjevem opisu zapisana kot:

2.2 Eulerian description

In the Eulerian formulation, which is commonly used for solving computational fluid dynamic problems, the problem is being observed at separate points in space that do not follow the particles motion (Fig. 3). In one time step, Δt, several mass particles can pass through the observed point. Their motion is exactly determined at the moment of passing through that point. The field variables at the observed point are time dependent.

In the Eulerian formulation the mass conservation is written as:

$$\frac{D\rho}{Dt} + \rho \cdot \frac{\partial v_i}{\partial x_i} = 0 \tag{5},$$

kjer je $\frac{D}{Dt} = \frac{\partial}{\partial t} + v_i \cdot \frac{\partial}{\partial x_i}$ snovski oziroma hitrostni odvod, ki podaja časovno spremembo veličine in prostorsko spremembo veličine zaradi nehomogenosti hitrostnega polja (vsota lokalnega in konvektivnega odvoda).

Ohranitev gibalne količine je izražena:

where $\frac{D}{Dt} = \frac{\partial}{\partial t} + v_i \cdot \frac{\partial}{\partial x_i}$ is the total time derivative that is physically the time rate of the change following a moving material element (sum of the local and the convective derivative).

The conservation of momentum can be expressed as:

$$\rho \cdot \frac{Dv_i}{Dt} = \frac{\partial \sigma_{i,j}}{\partial x_i} + \rho \cdot b_i \tag{6}.$$

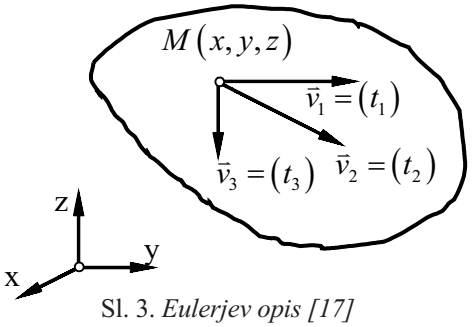

Sl. 3. *Eulerjev opis [17]*
Fig. 3. *Eulerian formulation [17]*

In ohranitev energije se lahko zapiše:

$$\rho \cdot \frac{Du}{Dt} = \sigma_{i,j} \cdot \frac{\partial v_i}{\partial x_i} \quad (7).$$

Temeljna razlika med Lagrangevim in Eulerjevim postopkom je v tem, da so pri Lagrangevem opisu veličine *x*, *y* in *z* spremenljive koordinate gibljivega delca. Pri Eulerjevem opisu pa te koordinate pomenijo mirujoče koordinate določene točke polja [17].

Kljub temu da se Eulerjeva mreža med analizo v LS-DYNI navidezno ne premika ali deformira, se dejansko spreminjata njena lega in oblika, vendar le v posameznem časovnem koraku ([13], [14] in [16]). Razlog za to je uporaba Lagrangevega opisa v posameznih časovnih korakih, ki je naprednejša v LS-DYNI. Eulerjeva mreža je v LS-DYNI obravnavana na poseben način (sl. 4). Uporaba Eulerjeve mreže je ponazorjena na enakem primeru, ki je bil uporabljen pri Lagrangevem opisu. Zaradi obremenitev na sredinsko vozlišče opazovano vozlišče spremeni lego v enem računalniškem časovnem koraku (mreža se deformira). Po časovnem koraku se analiza ustavi in izvedeta se naslednji dva približka [5]:

- premik vozlišč: vsem vozliščem Eulerjeve mreže, ki so zaradi obremenitev spremenila svojo lego, se ponovno določi izhodiščna lega;
- interpolacija vmesnih rezultatov: vse notranje veličine (napetost, tokovna polja, hitrostno polje), ki se nanašajo na vozlišča s spremenjeno lego, so interpolirane tako, da imajo ustrezno prostorsko porazdelitev kakor pred premikom vozlišč. Tako premik vozlišč ne vpliva na porazdelitev notranjih veličin.

Opisani postopek se ponavlja v vseh časovnih korakih celotne analize in ponuja uporabniku nepremično in nedeformirano Eulerjevo mrežo.

And the conservation of the energy can be written as:

The basic difference between the Lagrangian and the Eulerian formulations is that in the Lagrangian formulation the magnitudes *x*, *y* and *z* are variable coordinates of a moving particle; in the Eulerian formulation those coordinates represent the steady coordinates of the defined field point [17].

Although the Eulerian mesh in LS-DYNA appears not to move or deform during the analysis, it does actually change its position and form, but only within a single time step ([13], [14] and [16]). The reason for this is the use of the Lagrangian formulation in single time steps, which is much more advanced in the LS-DYNA. The Eulerian mesh in LS-DYNA is treated in a special way (Fig. 4). To illustrate the use of an Eulerian mesh the same example is used as at the Lagrangian formulation. Because of the central node loading, the observed node changes its position during one computational time step (mesh deforms). After the time step the analysis stops and the following two approximations are performed [5]:

- mesh smoothing: all the nodes of the Eulerian mesh that have been displaced due to loading are moved to their original position;
- advection: the internal variables (stresses, flow fields, velocity field) for all the nodes that have been moved are recomputed (interpolated) so that they have the same spatial distribution as before the mesh smoothing. In this way the mesh smoothing does not affect the internal variable distribution.

The described procedure is repeated for each time step of the analysis and provides the analyst with a non-movable and undeformable Eulerian mesh.

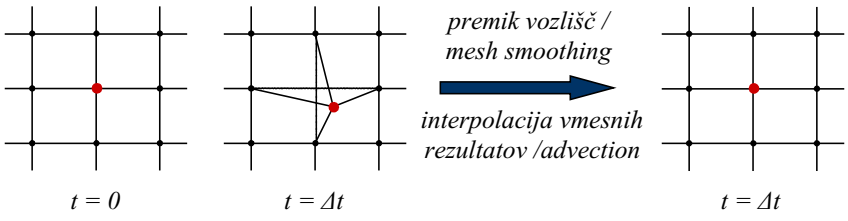

Sl. 4. *Deformacija mreže pri Eulerjevem opisu*
Fig. 4. *Mesh deformation in the Eulerian formulation*

2.3 Poljubnostni Lagrange-Eulerjev opis (PLE)

Značilnosti Lagrangevega in Eulerjevega opisa napovedujejo, da bi bilo računalniško ustrezno združiti omenjena opisa in poudariti njune prednosti ter se izogniti njunim pomanjkljivostim. Ta zamisel je vodila do razvoja poljubnostnega Lagrange-Eulerjevega opisa (PLE). V tem opisu se mreža lahko deloma premika in deformira, ker sledi materialu (Lagrangev opis), hkrati pa dopušča, da material teče skozi mrežo (Eulerjev opis).

Povezava med konvektivno hitrostjo c_i, hitrostjo materiala v_i in hitrostjo mreže $\hat{v}_i$ je definirana kot:

$$c_i = v_i - \hat{v}_i \tag{8}.$$

Glede na gibanje materiala in mreže se ohranitvene enačbe mase, gibalne količine in energije zapišejo kot:

$$\frac{\partial \rho}{\partial t} + c_i \cdot \frac{\partial \rho}{\partial x_i} + \rho \cdot \frac{\partial v_i}{\partial x_i} = 0 \tag{9}$$

$$\rho \cdot \frac{\partial v_i}{\partial t} + \rho \cdot c_i \cdot \frac{\partial v_i}{\partial x_i} = \frac{\partial \sigma_{i,j}}{\partial x_i} + \rho \cdot b_i \tag{10}$$

$$\rho \cdot \frac{\partial u}{\partial t} + \rho \cdot c_i \cdot \frac{\partial u}{\partial x_i} = \sigma_{i,j} \cdot \frac{\partial v_i}{\partial x_i} \tag{11}.$$

Iz zgornjih enačb je razvidno, da v primeru, ko sta hitrost mreže in hitrost materiala enaka, izpeljemo Lagrangev opis. Kadar se material premika in mreža miruje (hitrost mreže je enaka konvektivni hitrosti), pa izpeljemo Eulerjev opis (preglednica 1) [2].

Računalniški algoritem reševanja opisa ALE v LS-DYNI je podoben opisanemu postopku Eulerjevega opisa ([13], [14] in [16]). Razlikuje se le v premiku vozlišč. V Eulerjevem opisu so vozlišča premaknjena nazaj na izhodiščne lege, pri čemer se

2.3 Arbitrary Lagrange-Eulerian description (ALE)

The features of the Lagrangian and Eulerian descriptions suggest that it would be computationally beneficial to combine these two descriptions so as to strengthen their advantages and to avoid their disadvantages. This idea led to the development of the Arbitrary Lagrange-Eulerian formulation. In this formulation the mesh partly moves and deforms because it follows the material (Lagrangian formulation), while at the same time the material can also flow through the mesh (Eulerian formulation).

The relationship between the convected velocity, c_i, the material velocity, v_i, and the mesh velocity, $\hat{v}_i$, is defined as:

Regarding the material and the mesh movement, the mass, the momentum and the energy conservation equations can be written as:

From the above equations it is obvious that if the mesh and material velocity are equal this would give the Lagrangian description, and if the material moves and the mesh remains steady (the mesh velocity is equal to convected velocity) this would give the Eulerian description (Table 1) [2].

The ALE algorithm in LS-DYNA is similar to the described Eulerian computational procedure ([13], [14] and [16]). The only difference is the mesh smoothing. In the Eulerian formulation the nodes are moved back to their original positions, while in

Preglednica 1. *Primerjava kinematike PLE, Lagrangevega in Eulerjevega opisa*
Table 1. *Comparison of the kinematics for the ALE, Lagrangian and Eulerian formulations*

		PLE ALE	Lagrange	Euler
pomik / displacement	material mreža / mesh	u_i $\hat{u}_i$	u_i $\hat{u}_i = u_i$	u_i $\hat{u}_i = 0$
hitrost / velocity	material mreža / mesh	v_i $\hat{v}_i$	v_i $\hat{v}_i = v_i$	v_i $\hat{v}_i = 0$
pospešek / acceleration	material mreža / mesh	a_i $\hat{a}_i$	a_i $\hat{a}_i = a_i$	a_i $\hat{a}_i = 0$

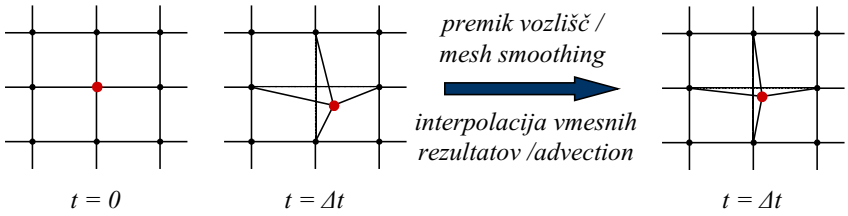

Sl. 5. *Deformacija mreže pri PLE opisu*
Fig. 5. *Mesh deformation in the ALE formulation*

pri opisu PLE nova lega premaknjenih vozlišč izračuna glede na povprečno oddaljenost do sosednjih vozlišč (sl. 5).

Podobna numerična shema je uporabljena v drugih primerljivih programskih sistemih (npr. MSC/Dytran).

Prednost Lagrange-Eulerjevega opisa se pokaže, kadar želimo slediti določeni napetosti in se mora mreža samodejno zgoščevati. Drug primer je analiza rezervoarjev s tekočino, pri kateri je upoštevano gibanje tekočine v rezervoarju, mejna ploskev pa se zaradi vpliva med trdnino in tekočino ves čas spreminja (sl. 6).

Kljub temu pa lahko uporaba PLE opisa povzroči popačenost elementov, kar lahko vpelje nevarne napake v numeričnih simulacijah. V določenih primerih PLE opis povzroči nepričakovano ustavitev računskega postopka. To se običajno zgodi zaradi zelo majhnih časovnih korakov, kot posledica zelo majhnih deformiranih Lagrangevih elementov ali celo negativne prostornine končnih elementov.

2.4 Metoda hidrodinamike zglajenih delcev (MHZD)

Stanje sistema je pri metodi hidrodinamike zglajenih delcev (MHZD) opisano z določenim

the ALE formulation the positions of the moved nodes are calculated according to the average distance to the neighbouring nodes (Fig. 5).

A similar calculation scheme is also used in other comparable codes (e.g., MSC/Dytran).

The advantage of the ALE formulation is evident when a stress front needs to be followed and the mesh is automatically refined. Another example is the analysis of fluid tanks, where the fluid's movement inside the tank is of interest and the boundary surface is continuously changing due to the interaction between the fluid and tank surfaces (Fig. 6).

However, using the ALE formulation can also result in a highly distorted mesh, which can introduce large errors in numerical simulations. In some cases the ALE formulation can encounter unexpected terminations in the computational process, usually due to very small time steps following from very small, deformed Lagrangian elements or even negative element volumes.

2.4 Smoothed Particle Hydrodynamics (SPH)

In the SPH method, the state of the system is represented by a set of particles (Fig. 7) that pos-

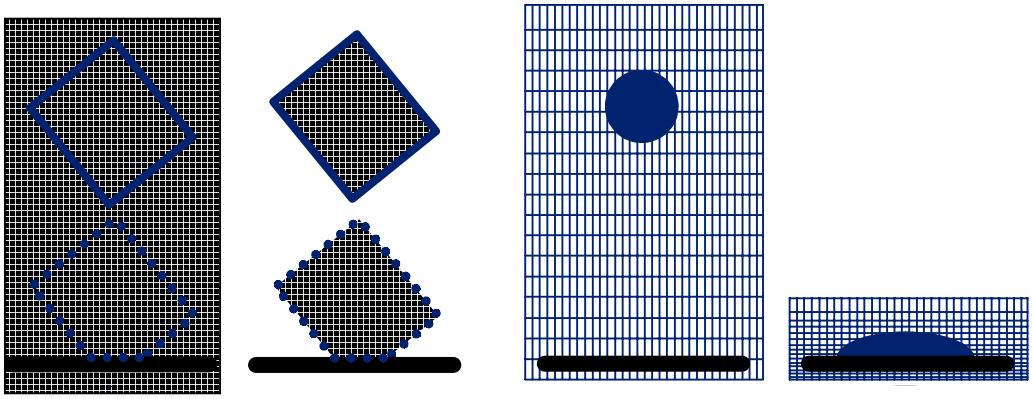

Sl. 6. *Uporaba PLE opisa*
Fig. 6. *Applications of the ALE formulation*

številom delcev. Le-ti posamezno vsebujejo materialne lastnosti in se gibljejo na osnovi temeljnih ohranitvenih enačb. MHZD je brezmrežna Lagrangeva metoda delcev, ki so jo razvili Lucy, Gingold in Monaghan z začetnim namenom simulirati astro-fizikalne probleme ([5], [7] do [9] in [15]). Kasneje je bila MHZD obsežno preučena in razširjena za reševanje dinamičnih odzivov trdnih materialov pa tudi za simuliranje toka tekočine z velikimi deformacijami. MHZD ima pred običajnimi brezmrežnimi metodami določene prednosti. Najpomembnejša prednost je prilagodljivost, ki je dosežena v začetnem koraku približka spremenljivih veličin (npr. gostote, hitrosti, energij). Le-ta je izvedena v vsakem časovnem koraku in temelji na trenutni krajevni porazdelitvi delcev s poljubno lego. Zaradi prilagodljivosti približka metoda HZD ni odvisna od poljubne porazdelitve delcev. Zaradi tega lahko obravnava zelo dobro probleme z izrednimi deformacijami. Naslednja prednost metode HZD je kombinacija Lagrangevega opisa in približka delcev.

V nasprotju z drugimi brezmrežnimi metodami, pri katerih so brezmrežna vozlišča uporabljena le kot interpolacijske točke, vsebujejo zglajeni delci tudi materialne lastnosti in so tako namenjeni kot aproksimacijske točke ter materialni elementi. Ti delci so se zmožni gibati v prostoru, prenašati vse računalniške podatke in dodatno oblikovati računalniški sistem za reševanje parcialnih diferencialnih enačb, ki opisujejo ohranitvene zakone. Metoda HZD je razdeljena na dva ključna dela. Prvi del je predstavitev integrala funkcij polja, drugi del pa predstavlja aproksimacijo delcev. Omenjeni postopek je uporabljen za izpeljavo parcialnih diferencialnih enačb v navadne diferencialne enačbe v diskretizirani obliki v odvisnosti le od časa [9].

Ohranitvene enačbe mase, gibalne količine in energije MHZD lahko zapišemo kot:

sess individual material properties and move according to the governing conservation equations. SPH as a meshfree, Lagrangian, particle method was developed by Lucy, Gingold and Monaghan, initially to simulate astrophysical problems ([5], [7] to [9] and [15]). Later the SPH method was extensively studied and extended to the dynamic response with material strength as well as dynamic fluid flows with large deformations. It has some special advantages over the traditional mesh-based numerical methods. The most significant is the adaptive nature of the SPH method, which is achieved at the very early stage of the field variable (i.e., density, velocity, energy) approximation that is performed at each time step based on a current local set of arbitrarily distributed particles. Because of the adaptive nature of the SPH approximation, the formulation of the SPH is not affected by the arbitrariness of the particle distribution. Therefore, it can handle problems with extremely large deformations very well. Another advantage of the SPH method is the combination of the Lagrangian formulation and the particle approximation.

Unlike the mesh-free nodes in other mesh-free methods, which are only used as interpolation points, the SPH particles also carry material properties, functioning as both approximation points and material components. These particles are capable of moving in space, carry all the computational information, and thus form the computational frame for solving the partial differential equations describing the conservation laws. The SPH formulation is divided into two key steps. The first step is the integral representation (kernel approximation) of the field function, and the second is the particle approximation (discretization). This procedure is applied to the particle differential equations to produce a set of ordinary differential equations in a discretized form with respect only to time [9].

The SPH equations for the conservation of mass, momentum and energy can be written as:

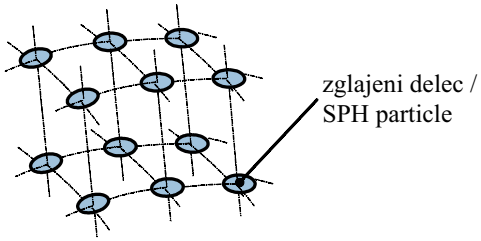

Sl. 7. *Model po MHZD*
Fig. 7. *SPH model*

$$\frac{\partial \rho_i}{\partial t} = \sum_{j=1}^{N} m_j \cdot v_{ij} \cdot \frac{\partial W_{ij}}{\partial x_i} \tag{12}$$

$$\frac{\partial v_i}{\partial t} = \sum_{j=1}^{N} m_j \cdot \left(\frac{\sigma_i}{\rho_i^2} + \frac{\sigma_j}{\rho_j^2} \right) \cdot \frac{\partial W_{ij}}{\partial x_i} \tag{13}$$

$$\frac{\partial u_i}{\partial t} = \sum_{j=1}^{N} m_j \cdot \frac{\sigma_i \cdot \sigma_j}{\rho_i \cdot \rho_j} \cdot v_{ij} \cdot \frac{\partial W_{ij}}{\partial x_i} \tag{14},$$

kjer je N število delcev v območju vpliva delca i; W_{ij} predstavlja gladilno funkcijo delca i, izvrednoteno v delcu j, in je tesno povezana z gladilno razdaljo; v_{ij} pa je relativna hitrost med delcem i in delcem j [9].

Glavna možna prednost MHZD je v tem, da ne potrebuje medsebojno povezane prostorske mreže in se s tem izogne problemu popačenosti elementov pri velikih deformacijah. V primerjavi z Eulerjevim opisom je učinkovitejša, saj je treba modelirati le materialna območja in ne vseh območij, kjer bi material lahko obstajal. Kljub vsem obetom pa je metoda HZD razmeroma nova, v primerjavi z običajnim Lagrangevim in Eulerjevim opisom z mrežo elementov, z znanimi problemi na področju stabilnosti, zveznosti in izpolnjevanju ohranitvenih enačb [15].

3 PRIMERJALNA ŠTUDIJA RAZLIČNIH POSTOPKOV REŠEVANJA PRAKTIČNEGA PRIMERA

3.1 Opis problema in računalniški model

Analizirani problem sestoji iz zaprtega rezervoarja iz poliakrilnega stekla (PMMA), v začetnem mirujočem stanju, napolnjen s 60% vode in 40% zraka (sl. 8). Rezervoar je pritrjen na sani (pritrjen v navpični smeri) in pospešen z vzdolžnim časovno odvisnim pospeškom z največjo vrednostjo približno 30 g v času t = 40 ms. Časovno odvisna sprememba proste površine vode in tlak v točki 1, v rezervoarju iz polikarilnega stekla z debelino sten 30 mm, sta bila predhodno določena s preizkusom [11].

Rezervoar je modeliran z lupinskimi Belytschko-Tsayevimi lupinskimi elementi s štirimi vozlišči in tremi integracijskimi točkami po debelini elementa [3]. Za rezervoar je bil uporabljen elastičen materialni model s podatki, ki ustrezajo poliakrilnemu steklu (ρ = 1180 kg/m^3, E = 3000 MPa in ν = 0,35). Spodnja ploskev rezervoarja je bila modelirana kot toga. Za modeliranje vode in zraka so bili, odvisno od uporabljene metode, uporabljeni prostorninski

where N is the number of particles in the support domain of the particle i; W_{ij} is the smoothing function of the particle i evaluated at the particle j, and is closely related to the smoothing length; and v_{ij} is the relative velocity between the particles i and j [9].

The main potential advantage of the SPH technique is that it does not require an interconnected spatial mesh and thus avoids the problem of mesh distortion during large deformations. Compared with the Eulerian description, it is more effective, since only the material's regions of interest need to be modelled, and not all the regions where the material might exist. With all this promise, however, the SPH technology is relatively new, compared to standard mesh-based Lagrangian and Eulerian descriptions, with remaining known problems in the areas of the stability, consistency and conservation [15].

3 COMPARATIVE STUDY OF DIFFERENT APPROACHES TO SOLVING A PRACTICAL EXAMPLE

3.1 Problem description and computational model

The analysed problem consists of a closed container reservoir at rest, 60% filled with water and 40% with air (Fig. 8). The reservoir was attached to a sled (fixed in the vertical direction) and subjected to a longitudinal time-dependent acceleration with a peak acceleration of approximately 30 g at time t = 40 ms. The time-dependent variation of the water surface shape and water pressure at point 1 was previously measured in experimental testing of a reservoir made of PMMA plates with 30-mm thickness [11].

The reservoir was modelled with four-noded Belytschko-Tsay shell elements with three integration points through the thickness [3]. The elastic material model is used for the reservoir container, with the material data corresponding to the PMMA material (ρ = 1180 kg/m^3, E = 3000 MPa and ν = 0.35). Only the bottom surface of the reservoir was modelled as rigid. For the water and air solid elements and SPH particles were used, depending on the ap-

elementi in zglajeni delci. Za modeliranje vode (ρ = 1000 kg/m^3 pri 293 K) in zraka (ρ = 1 kg/m^3 pri 293 K) je bil uporabljen konstitutivni model Null (Type 9) [6]. Domena tekočine je opisana z materialnim modelom, ki zanemari strižne napetosti. Z uporabo nizke meje tečenja se doseže hiter prehod v plastično območje (npr. le z upoštevanjem gravitacije). Ob uporabi visokih dinamičnih obremenitev so strižne sile tako zanemarljive v primerjavi z vztrajnostnimi silami tekočine. Zrak je bil upoštevan le pri Eulerjevem in modelu po PLE.

Uporabljeni sta bili Mie-Gruneisenova enačba stanja (voda in zrak) in enačba stanja idealnega plina (le za zrak). Celoten model je bil izpostavljen nespremenljivem težnostnem pospešku (g = 9,81 m/s^2). V Lagrangevem in MHZD modelu je bil uporabljen avtomatski algoritem za določevanje stičnih sil, v Eulerjevem in modelu po PLE pa je bil stik med tekočino in strukturo definiran z uporabo posebnega algoritma ([6] in [10]).

3.2 Podatki računalniške simulacije

Izvedene so bile eksplicitne dinamične analize z uporabo štirih različnih modelov simuliranja tekočine: Lagrangev, Eulerjev, PLE in MHZD. Za izvedbo analiz je bil uporabljen program LS-DYNA Linux Version 970. Opazovani časovni interval je znašal 80 ms, časovni korak simulacije pa je bil določen glede na najnižjo resonančno frekvenco strukture in je znašal 0,01 ms.

plied method. The material model Null (Type 9) [6] was used for the water (ρ = 1000 kg/m^3 at 293 K) and the air (ρ = 1 kg/m^3 at 293 K) modelling. The fluid domain was described with a material model that neglects the deviatoric stresses. By defining a low yield stress, a rapid transition to plasticity can be achieved (e.g., by only considering the gravitation). Under high dynamic loading, the shear forces become negligible in comparison with the inertial forces of the fluid. The air was considered only in the Eulerian and ALE models.

The Mie-Gruneisen (water and air) and Ideal Gas (only for air) equations of states have been used. The model was also loaded with the constant gravitational acceleration (g = 9.81 m/s^2). In the Lagrangian and SPH model the automatic nodes to surface contact were used, and in the Eulerian and ALE models the contact between fluid and structure was defined with the keyword Constrained Lagrange in Solid ([6] and [10]).

3.2 Computational simulation data

Explicit dynamic analyses were carried out by using all four different fluid model approaches: Lagrangian, Eulerian, ALE and SPH. The models were solved with LS-DYNA Linux Version 970. The computational time frame was set to 80 ms and the time step of the simulation was defined according to the lowest resonant frequency of the structure and was equal to 0.01 ms.

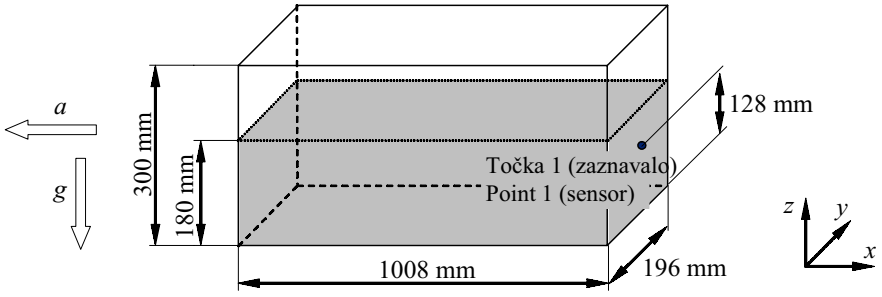

Sl. 8. *Izmere in začetne razmere analiziranega rezervoarja iz poliakrilnega stekla*
Fig. 8. *Dimensions and initial conditions of the analysed PMMA box*

3.3 Računalniški rezultati

Rezultati predvidene oblike proste površine za vse štiri simulacije so pri času $t = 38$ ms prikazane na sliki 9. Črtkana črta pomeni opazovano obliko proste površine v omenjenem trenutku pri preizkusu.

S slike 9 je razvidno, da sta Lagrangeva in MHZD formulacija na desni strani modela ustrezni le za približek gibanja tekočine, saj v resnici tekočina ne bi obdržala oblike posode, kar je razvidno iz simulacij na levi strani modela. Kljub temu pa se morajo omenjene omejitve vrednotiti glede na zahtevane računalniške rezultate. V primeru, kadar je iskan le udarec tekočine na steno rezervoarja, so deformacije in pomiki na nasprotni strani lahko zanemarljivi. Eulerjeva in PLE formulacija opišeta lego in obliko proste površine vode mnogo bolje, kar pa je odvisno od daljšega računskega časa (preglednica 2), kar ni vedno sprejemljivo. Potek gibanja tekočine v rezervoarju ponazarja slika 10. Pomembno je poudariti, da se z uporabo Lagrangevega modela pri zelo velikih deformacijah pojavijo zelo popačeni elementi in posledično velike numerične napake. Omenjeno ponovno potrjuje, da Lagrangeva zapis ni primeren za zelo velike deformacije.

Časovno spreminjanje tlaka vode v točki 1 je prikazano na sliki 11. Rezultati so bili določeni na dva različna načina. V Lagrangevem in MHZD modelu je bil tlak, ki se je pojavil v točki 1, merjen s stičnimi silami. Tlak pri Eulerjevem in PLE modelu pa je bil določen z merili poroznosti snovi in z določitvijo sile, ki je potrebna za vzpostavitev ravnotežja na vsakem opazovanem elementu na meji med tekočino in steno rezervoarja.

3.3 Computational results

The free-surface shape-prediction results of all four dynamic simulations at the time $t = 38$ ms are represented in Figure 9. The dotted line represents the free-surface shape observed in the experiment at the same time instance.

From Figure 9 it is obvious that the Lagrangian and SPH models are only good for approximations of the fluid motion at the right-hand side wall, since in reality the fluid would not retain the form of the container, which is the case observed in simulations at the left-hand side wall. However, this observation must be considered in view of the required computational results. In the case where only the impulse of the fluid towards the tank wall is needed, the deformations and deflections on the opposite side could be neglected. The Eulerian and ALE formulations perform much better when describing the position and the form of the water's free surface. However, this is only achieved by a dramatic increase of the calculation times, which is not always acceptable. Figure 10 represents the fluid motion in a reservoir during the calculation time. It is important to observe that using the Lagrangian formulation results in very distorted elements and, consequently, large computational errors. This again confirms the fact that the Lagrangian formulation is unsuitable for huge deformations.

The time variation of water pressure at point 1 is shown in Figure 11. The results have been determined by two different approaches. In the Lagrangian and SPH models the pressure at point 1 was measured with contact forces that appeared at the observed point. For the Eulerian and ALE model the pressure was determined by the leakage control, i.e., by determining the force that is needed to establish equilibrium in every observed element at the boundary between the fluid and the reservoir wall.

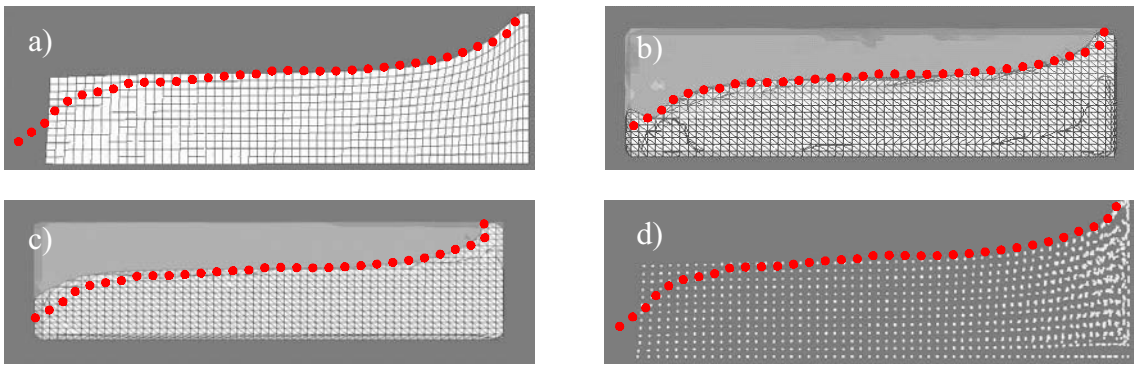

Sl. 9. *Oblika proste površine: a) Lagrangev model; b) Eulerjev model; c) PLE model; d) MHZD model*
Fig. 9. *Shape of the free surface: a) Lagrangian model; b) Eulerian model; c) ALE model; d) SPH model*

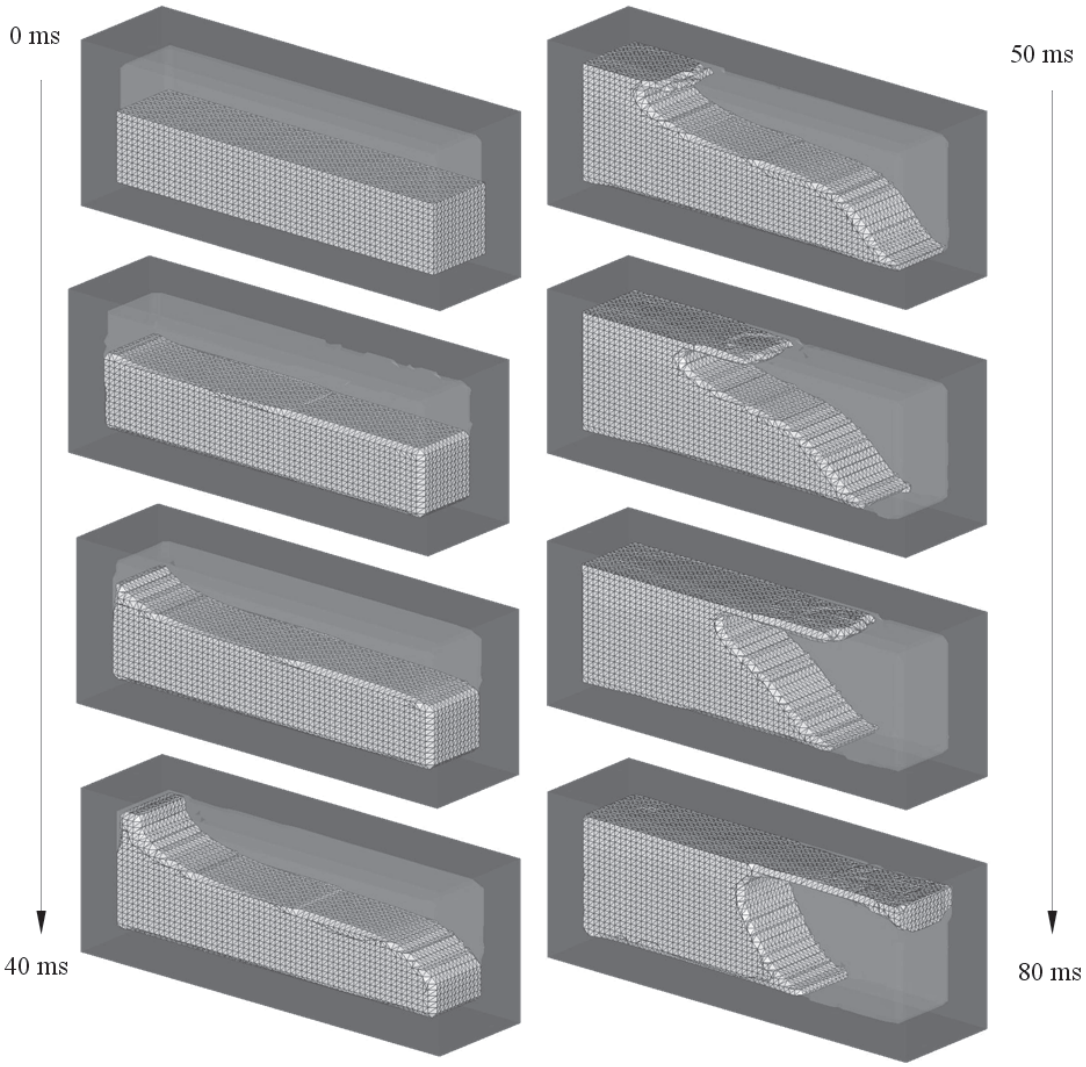

Sl. 10. *Gibanje tekočine, modelirane s PLE opisom*
Fig. 10. *Fluid motion modelled with ALE formulation*

Zelo dobro ujemanje z rezultati preizkusa je bilo doseženo z uporabo vseh štirih modelov. MHZD model zagotavlja zelo dobre rezultate, še posebej, če upoštevamo, da uporaba te metode omogoča zelo hitro in nezahtevno analizo (mreža sestoji le iz zglajenih delcev). Rezultati Lagrangevega modela so zelo dobri, kljub temu da se simulacija predčasno prekine zaradi velike popačenosti elementov. Razlog za nizek izmerjen tlak pri PLE modelu in Eulerjevem modelu se lahko pripiše vplivu zraka v rezervoarju, ki deluje kot dušilnik. Razlog za padec tlaka pri Eulerjevem zapisu pa je uporaba drugačnega modela zraka (drugačna enačba stanja), ki je potrebna za vzpostavitev stabilne analize.

Very good agreement with the experimental results was achieved by using all four formulations. The SPH formulation provided very good results, especially when taking into account that using this formulation results in a very quick and uncomplicated analysis (the mesh consists only of SPH particles). The results of the Lagrangian formulation are very good, although the simulation terminates because of the high element distortion. The reason for a lower pressure during the ALE and Eulerian models can be attributed to the air's influence inside the reservoir, where it acts like a damper. The drop in the pressure, observed for the Eulerian formulation, is also attributed to the need for a different air model (a different equation of state), which is necessary to ensure a stable analysis.

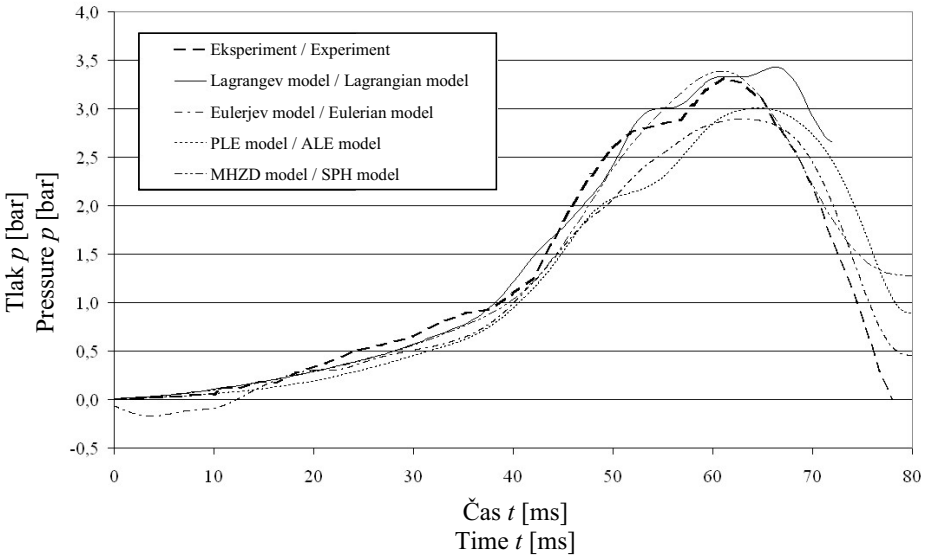

Sl. 11. *Primerjava časovne spremembe tlaka v točki 1*
Fig. 11. *Comparison of the pressure time-variation at point 1*

Velikost modelov in njihovi računski časi za posamezne analize so prikazani v preglednici 2, ki prikazuje zahtevane računske sposobnosti za rešitev izbranega problema z različnimi pristopi.

Deformacije samega rezervoarja so zaradi velike debeline njegovih sten zanemarljive. Za nazoren prikaz zmožnosti stika med tekočino in trdnino LS-DYNE je bila izvedena ponovna analiza z istim problemom, vendar je bila debelina sten rezervoarja zmanjšana na 10 odstotkov prvotne debeline, tj. 3 mm [6]. Deformacije sten rezervoarja, kot rezultat stika med tekočino in trdnino pri različnih časovnih korakih, so prikazane na sliki 12.

Iz opisanih simulacij je razvidno, da različni pristopi ponujajo alternativne možnosti za modeliranje toka tekočin in njihovega vpliva na strukturo. Prednost uporabe Lagrangevega in

The model size and the required CPU times for each analysis are listed in Table 2, to illustrate the required computational effort to solve the chosen problem with different approaches.

The deformation of the reservoir container is negligible, due to the thickness of the reservoir walls. To clearly illustrate the fluid-structure interaction capabilities of LS-DYNA, another analysis of the same problem was carried with reduced container reservoir walls to only 10% of the original thickness, i.e., 3 mm [6]. The resulting deformations of the container reservoir due to fluid-structure interaction at different time instances can be observed in Figure 12.

Following from the reported simulations it is obvious that these approaches offer an alternative means of fluid-flow modelling and its interaction with the structure. The advantage of using the SPH and

Preglednica 2. *Primerjava računskega časa*
Table 2. *CPU-time comparison*

Model	**Skupno število / Total number**		**Računski čas / CPU time**
	Vozlišča / Nodes	**Elementi / Elements**	min
Lagrangev / Lagrangian	2898	2420	16
Eulerjev / Eulerian	10162	8706	225
PLE / ALE	7462	6396	260
MHZD / SPH	2898	2896	13

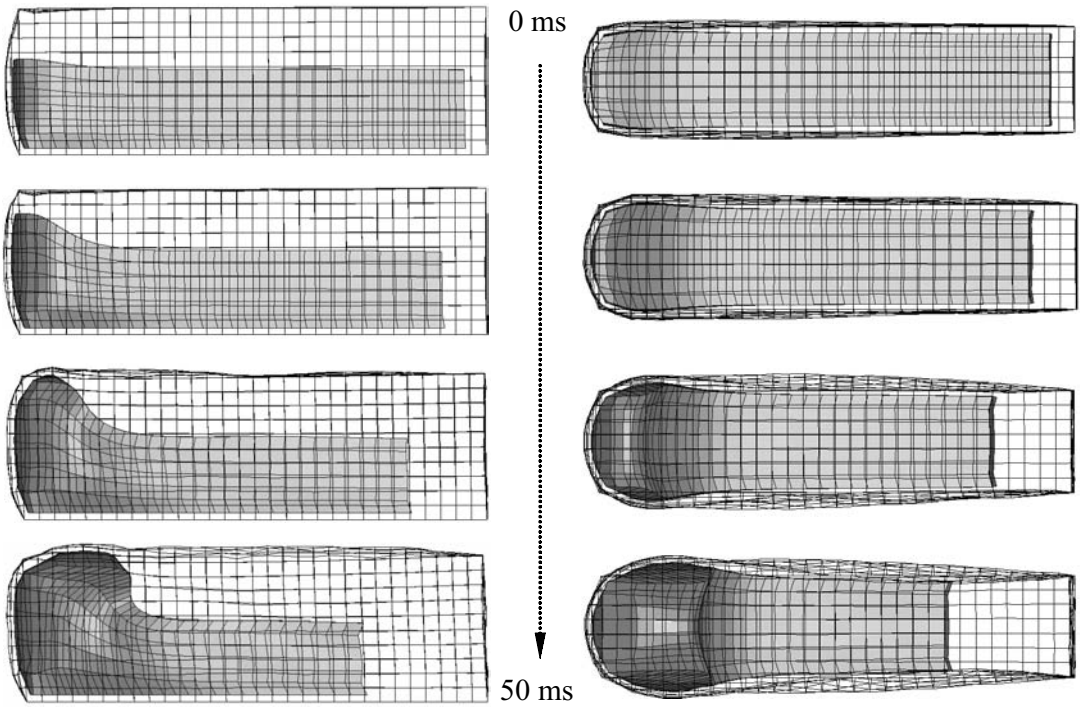

Sl. 12. *Medsebojni vpliv tekočine in trdnine*
Fig. 12. *Fluid-structure interaction*

MHZD modela je kratek čas za pripravo modela in sprejemljivi računski čas, medtem ko Eulerjev in PLE model opišeta gibanje tekočine natančneje. Kljub temu pa je bilo začetni udarec tekočine ob stene rezervoarja mogoče natančno simulirati z vsemi štirimi modeli tekočine, ki so vključeni v LS-DYNI.

4 SKLEP

V prispevku so predstavljeni štirje postopki modeliranja toka tekočine v LS-DYNI. Različne metode (Lagrangeova, Eulerjeva, PLE in MHZD) so bile uporabljene za analizo gibanja tekočine v deformabilnem rezervoarju, z namenom, da bi potrdili rezultate v primerjavi z znanimi preizkusnimi opazovanji. Računalniške simulacije so pokazale, da sta gibanje tekočine in medsebojni vpliv tekočine in trdnine natančno opisana z uporabo različnih izbirnih zapisov v LS-DYNI.

Predstavljeni modeli so osnova za komercialne računalniške modele, uporabljene za analizo zapletenejših problemov. Rezultati dejanskega rezervoarja za gorivo z zelo zahtevno geometrijsko obliko ob upoštevanju vpliva gibanja tekočine s PLE in MHZD formulacijami, so pokazali zelo dobro ujemanje s preizkusi [18].

Lagrangian models is a short pre-processing and a reasonable computational time, while the ALE and Eulerian models can describe the fluid motion more accurately. Nevertheless, the initial impact of the fluid on the reservoir wall could be simulated accurately with all four fluid models incorporated in LS-DYNA.

4 CONCLUSION

Four approaches to fluid-flow modelling in LS-DYNA have been presented in the paper. Different formulations (Lagrangian, Eulerian, ALE and SPH) were used to analyse the fluid motion in a deformable reservoir, with the purpose to validate the results in comparison with existing experimental observations. Computational simulations showed that the fluid motion and the fluid-structure interaction can be accurately described by applying different alternative formulations in the LS-DYNA.

The applied models provide a basis for economical computational models that can be used for analysing more complex problems. The results of the real fuel-tank with a very complex geometry, where the fluid motion's influence was considered with the ALE and SPH descriptions, showed a very good agreement with the experiments [18].

5 LITERATURA
5 REFERENCES

[1] Anghileri, M., Castelletti, L., Tirelli, M. (2003) Fluid-structure interaction of water filled tanks during the impact with the ground. *Int. Journal of Impact Engineering*.
[2] Belytschko, T., Liu, W.K., Moran B. (2000) Nonlinear finite elements for continua and structures, *John Wiley & Sons Ltd*, Chichester.
[3] Bois, P.D. (2003) Crashworthiness simulation using LS-DYNA. Stuttgart.
[4] Ferziger, J., Perić, M. (1997) Computational methods for fluid dynamics. *Springer Verlag*, Berlin.
[5] Gray, J.P., Monaghan J.J., Swift R.P. (2001) SPH elastic dynamics. Comput. Methods Appl. Mech. Engrg. 190, *Elsevier Science Ltd*.
[6] Hallquist, J.O. (1998) LS-DYNA Theoretical manual. Livermore.
[7] Idelsohn, S.R., Onate, E., Pin, F.D. (2003) A Lagrangian meshless finite element method applied to fluid-structure interaction problems. Computers and Structures 81, *Elsevier Science Ltd*.
[8] Lacome, L.L., Smoothed particle hydrodynamics. Part I, II.
[9] Liu, G.R., Liu, M.B. (2003) Smoothed particle hydrodynamics – a meshfree particle method. *World Scientific*, Singapore.
[10] Livermore Software Technology Corporation. (1998) LS-DYNA Theoretical manual. Livermore.
[11] Meywerk, M., Decker, F., Cordes, J. (1999) Fuel sloshing in crash simulation, *EuroPAM 99*.
[12] Müllerschön, H. (2004) Contact modeling in LS-DYNA. *DYNAmore*. Stuttgart.
[13] Olovsson, L. ALE and fluid-structure interaction capabilities in LS-DYNA. *LSTC*. Livermore.
[14] Olovsson, L., Soulli, M., Do, I. (2003) LS-DYNA – ALE capabilities, fluid-structure interaction modelling. *LSTC*. Livermore.
[15] Schwer, L.E. (2004) Preliminary assessment of non-Lagrangian methods for penetration simulation. *8th International LS-DYNA User Conference*.
[16] Souli, M. (2003) LS-DYNA advanced course in ALE and fluid/structure coupling. *LSTC*. Livermore.
[17] Škerget, L. (1994) Mehanika tekočin. *Tehniška fakulteta v Mariboru in Fakulteta za strojništvo v Ljubljani*.
[18] Vesenjak, M. (2004) Methoden um Fluid-Struktur Interaktion in LS-DYNA zu simulieren. *Daimler Chrysler*. Stuttgart.
[19] Vesenjak, M., Ren, Z., Hriberšek, M. (2004) Weakly coupled analysis of a blade in multiphase mixing vessel. *GAMM 2004*, Dresden.
[20] Zienkiewicz, O.C., Taylor, R.L. (2000) The finite element method. *McGraw-Hill Ltd.*, London.

Naslovi avtorjev: Matej Vesenjak
prof.dr. Zoran Ren
Univerza v Mariboru
Fakulteta za strojništvo
Smetanova 17
2000 Maribor
m.vesenjak@uni-mb.si
ren@uni-mb.si

dr. Heiner Müllerschön
DYNAmore GmbH
Industriestr. 2
70565 Stuttgart-Vaihingen, Nemčija
hm@dynamore.de

Stephan Matthaei
DaimlerChrysler AG, HPC B209
70322 Stuttgart, Nemčija
stephan.matthaei@daimlerchrysler.com

Authors' Addresses: Matej Vesenjak
Prof. Dr. Zoran Ren
University of Maribor
Faculty of Mechanical Eng.
Smetanova 17
2000 Maribor, Slovenia
m.vesenjak@uni-mb.si
ren@uni-mb.si

Dr. Heiner Müllerschön
DYNAmore GmbH
Industriestr. 2
70565 Stuttgart-Vaihingen, Germany
hm@dynamore.de

Stephan Matthaei
DaimlerChrysler AG, HPC B209
70322 Stuttgart, Germany
stephan.matthaei@daimlerchrysler.com

Prejeto: 6.10.2005
Received:
Sprejeto: 16.11.2005
Accepted:
Odprto za diskusijo: 1 leto
Open for discussion: 1 year

Strojniški vestnik - Journal of Mechanical Engineering 52(2006)2, 101-111
UDK - UDC 625.745.5:656.08
004.94:629.351:692.88
Izvirni znanstveni članek - Original scientific paper (1.01)

Simulacija naleta tovornega vozila ob cestno varnostno ograjo

Simulating the Impact of a Truck on a Road-Safety Barrier

Matej Borovinšek - Matej Vesenjak - Miran Ulbin - Zoran Ren
(Fakulteta za strojništvo, Maribor)

Cestno varnost lahko izboljšamo s postavitvijo cestnih varnostnih ograj, ki preprečujejo udeležencem cestnega prometa vstop v nevarna območja. Za dvig stopnje varnosti morajo biti cestne varnostne ograje oblikovane tako, da pri naletu vozila le-to preusmerijo nazaj na cestišče. Med preusmerjanjem vozila morajo s svojo deformacijo absorbirati čim večjo količino kinetične energije, da se zmanjšajo pojemki potnikov v vozilu. V prispevku je predstavljena računalniška simulacija naleta tovornega vozila ob cestno varnostno ograjo. Izvedene so bile parametrične računalniške analize za oceno primernosti različnih dodatnih elementov varnostne ograje. Za izvajanje eksplicitnih dinamičnih analiz je bil uporabljen program LS-DYNA. Računalniške simulacije dokazujejo, da je nosilnost analizirane ograje dovolj velika, da tovornjak zadrži in preusmeri nazaj na cestišče. Hkrati pa se pokaže tudi ustrezno visoka stopnja akumulacije kinetične energije vozila v obliki deformacije cestne varnostne ograje, kar zmanjša pojemke vozila in se kaže v povečani stopnji varnosti za potnike v vozilu.

(Ključne besede: varnost na cestah, ograje varnostne, analize trkov, simuliranje dinamično, LS-DYNA)

Road safety can be improved by applying appropriate road-safety barriers that prevent road-traffic participants from entering dangerous areas. In terms of preventing vehicles from veering off the road, a road-safety barrier should redirect the impacting vehicle back onto the road. In the process of doing so it should absorb as much of the vehicle's kinetic energy as possible through its deformation, so reducing the deceleration of the vehicle's occupants. This paper considers a computer simulation of a truck's impact on a steel road-safety barrier. Parametric computer simulations were used to evaluate the different additional safety elements of the road-safety barrier. The dynamic finite-element explicit code LS-DYNA was used for this purpose. The computer simulations prove that the analyzed road-safety barrier design is strong enough to retain and redirect the truck back onto the roadway. Appropriately, the high absorption of the impacting vehicle's kinetic energy through the safety-barrier deformation is observed at the same time, which indicates a reduction in a vehicle's deceleration, and with that, a higher safety level for the vehicle's occupants.

(Keywords: road safety, road safety barrier, impact simulations, dynamic simulations, LS-DYNA)

0 UVOD

Visoka stopnja varnosti je zelo pomembna v sodobnem cestnem prometu. Na eni strani avtomobilska industrija razvija nove pasivne in aktivne varnostne sisteme za povečanje varnosti potnikov v cestnem prometu, na drugi strani pa se varnost cest povečuje z uporabo učinkovitejših cestnih varnostnih elementov.

Zagotovitev dovolj visoke stopnje varnosti v cestnem prometu je primarnega pomena. Eden od

0 INTRODUCTION

A high level of safety is a very important aspect in modern road traffic. On the one hand, the car industry is developing new, passive and active vehicle-safety systems to increase the safety of road-vehicle occupants, and on the other hand, the roads are being made safer with the installation of more effective road-safety elements.

Ensuring appropriate safety levels in road traffic is of primary importance. One way to improve

načinov izboljšanja varnosti je postavitev varnostnih ograj. Namen cestnih varnostnih ograj je preprečiti zdrs vozila s ceste, torej preprečiti izlet vozila s cestišča ali prehod vozila na nasprotnosmerno vozišče. S tem se preprečijo oziroma popolnoma odpravijo možnosti poškodbe potnikov v vozilu ter oseb in objektov ob vozišču.

Novo postavljene cestne varnostne ograje v Sloveniji morajo izpolnjevati zahteve novega slovenskega pravilnika o postavitvi cestnih varnostnih ograj in standarda SIST EN 1317 [1]. Vsaka na novo postavljena ograja mora imeti uspešno opravljen preizkus naleta za stopnjo zadrževanja, za katero je namenjena. Zaradi visokih cen preizkušanj varnostnih ograj je smiselno njihovo konstrukcijo poprej preveriti z izvajanjem računalniških simulacij.

Tako so bile, z namenom, da bi izbrali najustreznejše konstrukcijske rešitve varnostne ograje, izvedene računalniške analize naleta tovornjaka ob ograjo. Za izvajanje teh simulacij je bil uporabljen programski paket LS-DYNA ([2] in [3]).

1 KONSTRUKCIJSKE ZAHTEVE ZA CESTNE VARNOSTNE OGRAJE

Cestne varnostne ograje morajo bili postavljene le na odsekih, kjer je možnost za hujše poškodbe pri naletu vozila manjša, kakor v primeru, če ograje ne bi bilo. Na javnih cestah v Sloveniji se lahko postavljajo le varnostne ograje, ki so atestirane po standardu SIST EN 1317.

Najpogosteje uporabljena vrsta cestnih varnostnih ograj v Sloveniji so jeklene varnostne ograje (sl. 1). Postavljene so predvsem na avtocestah, glavnih in regionalnih cestah. Na redkeje prevoznih cestah se uporabljajo le na nevarnih območjih, kjer je povečana verjetnost zdrsa vozila s cestišča.

Glavni konstrukcijski elementi enostranske jeklene varnostne ograje so (sl. 1):
- ščitnik – vzdolžni element ograje; s svojo deformacijo zmanjša moč udarca, hkrati pa mora biti dovolj tog, da se med trkom ne poruši;
- steber – nosilo distančnika in/ali ščitnika, ki zagotavlja lego ščitnika na določeni oddaljenosti in višini od vozišča oziroma nad njim;
- distančnik – zagotavlja določeno lego ščitnika glede na steber ograje;
- zaključni element – del varnostne ograje, ki je na njenem začetku oziroma koncu in je namenjen zmanjšanju posledic naleta vozila na ograjo.

road safety is to install road-safety barriers. The purpose of such systems is to restrain a vehicle from entering dangerous areas, i.e., to prevent it from veering off the road or on to the other side of the road. This effectively reduces or completely alleviates damage to vehicle occupants and other road-traffic participants and objects.

Newly installed road-restraint systems in Slovenia have to fulfill the new Slovenian regulation requirements for road-restraint systems and the SIST EN 1317 standard [1]. Every newly installed restraint system has to be certificated for the containment level it is designed for by a full-scale crash test. Since these tests are very expensive, it is advisable to preliminary check the adherence of safety-barrier design to the set regulations by means of a computer simulation.

This paper reports on a computer simulation of a truck impact into a road-safety barrier with the aim of determining the most effective safety-barrier design. The software system LS-DYNA ([2] and [3]) was used for this purpose.

1 DESIGN REQUIREMENTS FOR ROAD-SAFETY BARRIERS

Road-safety barriers only need to be installed on road sections where the possibility of severe injuries during vehicle impact is reduced by the installation of such barriers. Only certified road-safety barriers according to SIST EN 1317 may be installed on public roads in Slovenia.

The most frequently used type of road-safety barriers in Slovenia are steel road-safety barriers (Fig. 1). They are installed mainly on highways, main and regional roads. On roads with less traffic they are only used in dangerous areas with a high probability of the vehicle veering off the road.

The main design elements of a single-sided steel road-safety barrier are (Fig. 1):
- the guardrail – a longitudinally placed element, the deformation of which reduces the severity of an impact, but it should also be strong enough not to rupture during an impact;
- the post – carries the distance spacer and/or the guardrail and it ensures the guardrail position at a certain distance from and above the road;
- the distance spacer – ensures a certain position of the guardrail in relation to the post,
- the end element – a part of the safety barrier placed at its beginning and end, which reduces the consequences of a direct vehicle impact.

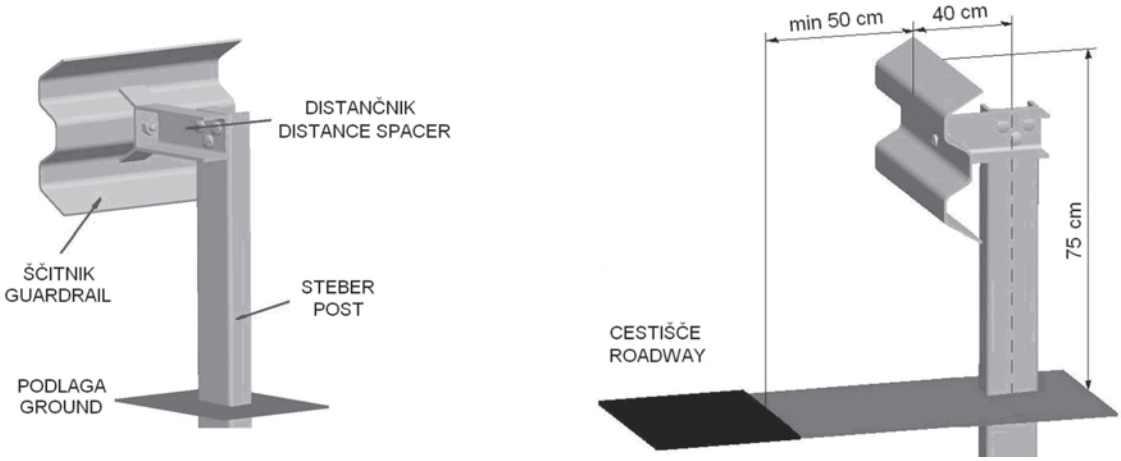

Sl. 1. *Konstrukcijski elementi in glavne mere jeklene cestne varnostne ograje*
Fig. 1. *Main elements and regulated dimensions of a steel road-safety barrier*

Pravila za postavitev cestnih varnostnih ograj v okviru tehnične specifikacije za javne ceste v Sloveniji še niso popolnoma določena, saj jih še zmeraj usklajujejo različne agencije [4].

2 ZAHTEVE STANDARDA SIST EN 1317

Glede na standard SIST EN 1317 ocenjujemo ustreznost varnostne ograje z ozirom na tri glavne kriterije [5]:

- raven zadrževanja vozila – pomeni raven zadrževanja za različne vrste vozil;
- moč udarca – se določa s tremi parametri: z merilom velikosti pospeškov (MVP - ASI), s pojemkom glave po udarcu (PGU - PHD) in s teoretično hitrostjo glave pri udarcu (THGU - THIV);
- deformacija ograje.

Najpomembnejši parameter ASI je brezrazsežna veličina, ki se uporablja kot splošno merilo za določanje posledic naleta vozila na potnike v vozilu. ASI je določen kot:

$$ASI = \max\left[ASI(t)\right] = \max\left[\sqrt{\left(\frac{\overline{a}_x}{\hat{a}_x}\right)^2 + \left(\frac{\overline{a}_y}{\hat{a}_y}\right)^2 + \left(\frac{\overline{a}_z}{\hat{a}_z}\right)^2}\right] \le 1,0\ (1,4) \qquad (1),$$

kjer $\overline{a}_x$, $\overline{a}_y$ in $\overline{a}_z$ pomenijo povprečne vrednosti pospeškov masnega središča vozila v njegovem lokalnem koordinatnem sistemu v tekočem časovnem koraku $\Delta t = 50$ ms (sl. 2). $\hat{a}_x$, $\hat{a}_y$ in $\hat{a}_z$ pomenijo mejne vrednosti pospeškov za posamezne koordinatne osi ter znašajo $\hat{a}_x = 12 \cdot g$, $\hat{a}_y = 9 \cdot g$ in $\hat{a}_z = 10 \cdot g$, kjer je $g = 9{,}81$ m/s^2.

Parameter moči udarca MVP mora biti merjen in izračunan samo za teste z vozili majhnih mas

The technical regulations for the installation of road-safety barriers on Slovenian public roads are not yet fully operational, as they are still in the process of final approval by various agencies [4].

2 SIST EN 1317 REQUIREMENTS

The suitability of a safety barrier is, according to the SIST EN 1317 standard, determined by three main criteria [5]:

- the containment level – represents the level of containment for different types of vehicles;
- the impact severity – defined by three parameters: the acceleration severity index (ASI), – the post-impact head deceleration (PHD) and the theoretical head-impact velocity (THIV),
- the deformation of the barrier.

The most important ASI parameter is a dimensionless variable, which is used as an overall measure of vehicle-impact consequences for the vehicle occupants. The ASI is determined as:

where $\overline{a}_x$, $\overline{a}_y$ and $\overline{a}_z$ represent the average values of the acceleration of the vehicle's center of gravity in a local coordinate system of the vehicle in a running-time interval of $\Delta t = 50$ ms (Fig. 2). $\hat{a}_x$, $\hat{a}_y$ and $\hat{a}_z$ stand for the acceptable acceleration limits for individual coordinate directions and are equal to $\hat{a}_x = 12 \cdot g$, $\hat{a}_y = 9 \cdot g$ and $\hat{a}_z = 10 \cdot g$, where $g = 9.81$ m/s^2.

The impact severity parameter ASI needs to be measured and determined only for tests with low

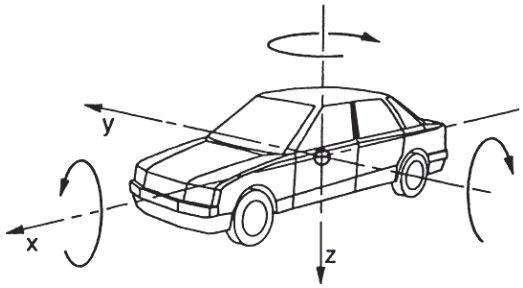

Sl. 2. *Lokalni koordinatni sistem vozila*
Fig. 2. *Local coordinate system of the vehicle*

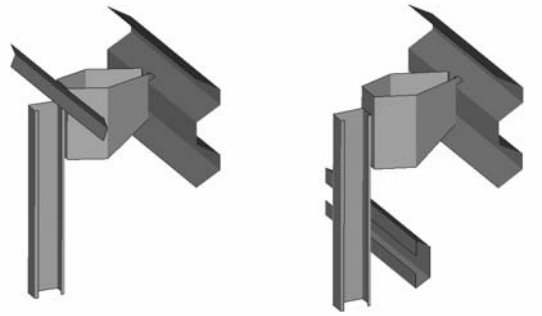

Sl. 3. *Konstrukcija ograje s pasnico (levo) in trapeznim vodilom (desno)*
Fig. 3. *Design of a barrier with tension belt (left) and wheel guidance (right)*

(osebna vozila), na katera med testom delujejo večji pojemki. Kljub temu je bil v tem prispevku parameter MVP uporabljen tudi za analizo razmer med naletom tovornjaka. Ta parameter pomeni dobro mero za normiran dejanski pospešek, saj se izračuna iz filtriranih koordinatnih pospeškov in je normiran z njihovimi mejnimi vrednostmi. Tako je bil tukaj uporabljen za prikaz vpliva različnih konstrukcijskih rešitev cestne varnostne ograje na skupno obnašanje vozila.

3 KONSTRUKCIJSKA IZVEDBA VARNOSTNE OGRAJE

S simulacijami je bilo preizkušenih več konstrukcijskih rešitev cestne varnostne ograje za raven zadrževanja H1. Po standardu SIST EN 1317 mora takšna ograja uspešno prestati nalet osebnega vozila (test TB11) in tovornjaka (test TB42). Osebno vozilo ima maso $m = 900$ kg, začetno hitrost $v = 100$ km/h in trči v cestno varnostno ograjo pod kotom $\alpha = 20°$ glede na postavitev ščitnika ograje. Tovornjak ima maso $m = 10.000$ kg in trči v varnostno ograjo z začetno hitrostjo $v = 70$ km/h pod vpadnim kotom $\alpha = 15°$. Test TB11 je namenjen določitvi parametrov moči udarca, medtem ko je test TB42 namenjen določitvi nosilnosti cestne varnostne ograje. Oba testa sta enako pomembna za končno odločitev o izbiri konstrukcijske rešitve cestne varnostne ograje.

Osnova za konstrukcijo nove cestne varnostne ograje je bila atestirana ograja za raven zadrževanja N2. Njeni glavni sestavni deli so v celoti izdelani iz konstrukcijskega jekla S 235. Ščitnik je narejen iz 3 mm debele pločevine in v dolžino meri 4.200 mm, kjer je 200 mm namenjenih spoju med sosednjimi ščitniki. Distančnik ima obliko šestkotnika [6], s tem ima največjo zmožnost absorpcije energije trka in predvidljivo deformacijo, narejen pa je iz 4 mm

weight vehicles (personal vehicles), which sustain significant deceleration during impact. However, in this paper the ASI parameter is also used to assess a truck's impact conditions. Since it is calculated from filtered coordinate acceleration data and normalized by their limiting values, it represents a good measure of the normalized effective acceleration. Thus, it was used here to illustrate the influence of different road-safety barrier designs on overall vehicle behavior.

3 ROAD-SAFETY BARRIER DESIGN

Simulations were used to test different designs of road-safety barrier for the containment level H1. According to the SIST EN 1317 standard such safety barrier has to successfully sustain the impact of a personal vehicle (TB11 test) and a truck (TB42 test). A personal vehicle has a mass of $m = 900$ kg, an initial velocity of $v = 100$ km/h and impacts the barrier at an angle of $\alpha = 20°$ with regard to the guardrail. The truck has a mass of $m = 10{,}000$ kg and impacts the barrier with an initial velocity of $v = 70$ km/h at an impact angle of $\alpha = 15°$. The TB11 test is used to determine the impact-severity parameters and the TB42 test is used to test the load-carrying capability of such a system. Both tests are equally important when making the final choice of road-safety barrier design.

The new H1 road-safety barrier was a design upgrade of an already-certified safety barrier for the containment level N2. The main components of this safety barrier are made of construction steel S 235. The guardrail is made from 3-mm-thick metal sheet and is 4,200 mm long, where the splice length is equal to 200 mm. The distance spacer is shaped in a hexagonal form [6] to provide the highest crash-energy absorption and controllable deformation and

pločevine. Steber je izdelan iz profila C izmer 100 × 55 × 4 mm, dolžine 1.900 mm. Ščitniki so medsebojno spojeni z vijačnimi zvezami z vijaki M16, v preostalih vijačnih zvezah pa so uporabljeni vijaki M10. Vsi uporabljeni vijaki so trdnostnega razreda 5.8.

Ta osnova cestne varnostne ograje je bila dodatno ojačana na dva različna načina. Enkrat z dodatno pasnico, ki je privijačena na hrbtni del distančnika, drugič pa s trapeznim vodilom, privijačenim neposredno na sprednji del stebra (sl. 3). Dodaten namen trapeznega vodila je preprečiti neposredni udarec kolesa vozila ob steber ograje ter tako zmanjšati pojemke v vozilu in zmanjšati moč udarca.

Pasnica in trapezno vodilo sta enake dolžine kakor ščitnik ograje in sta privijačena z vijaki M10. Debeline pločevin obeh ojačitev so bile predmet parametričnih numeričnih analiz. Debelina pločevine je obsegala vrednosti 3,0, 5,0 in 7,0 mm pri pasnici in 2,0, 2,5, 2,8 ter 3,0 mm pri trapeznem vodilu.

4 NUMERIČNE ANALIZE

4.1 Numerični model tovornega vozila

Za model tovornega vozila je bil uporabljen prosto dostopen model po MKE vozila Ford Single Unit Truck (poenostavljen) [7]. Dolžina tovornega vozila znaša 8,5 m, višina 3,3 m in širina 2,4 m (sl. 4.). Model po MKE sestavlja približno 22.200 linearnih končnih elementov z reducirano integracijsko shemo [8]. Od tega je okoli 1.000 prostorninskih, 500 linijskih elementov, ostalo pa predstavlja 20.700 lupinskih končnih elementov.

Model po MKE tovornega vozila je bil nekoliko spremenjen, da je ustrezal zahtevam standarda SIST EN 1317. Masa vozila je bila povečana iz 7.320 kg na

is made from 4-mm-thick sheet metal. The posts are C-shaped with dimensions of 100 × 55 × 4 mm and 1,900 mm long. The guardrails are joined together with M16 screws, while all other connections are made with M10 screws. All the screws are of strength class 5.8.

The basic design was additionally reinforced in two different ways. First, with a tension belt that is connected to the back of a distance spacer; and, second, with a wheel-guidance profile connected to the front of the post (Fig. 3). An additional purpose of the wheel guidance is to hinder the direct vehicle-wheel impact into the post, which results in smaller vehicle decelerations and lessens the severity of the impact.

The tension belt and the wheel guidance are of the same length as the guardrail and connected with M10 bolts. The sheet-metal thicknesses of both reinforcements were the subject of a parametrical analyses. Thicknesses of 3.0, 5.0, and 7.0 mm were used for the tension belt and 2.0, 2.5, 2.8, and 3.0 mm for the wheel-guidance profile.

4 COMPUTATIONAL SIMULATIONS

4.1 Computational model of a truck

A publicly accessible FEM model of a Ford Single-Unit Truck (Reduced Model) [7] was used as a basic truck model in the computational simulations. The truck is 8.5-m long, 3.3-m high and 2.4-m broad (Fig. 4). The FEM model is made of approximately 22,200 linear elements with a reduced integration scheme [8]. It consists of 1,000 solid elements, 500 beam elements and the rest is represented by 20,700 shell elements.

The FEM model of the truck was subjected to further changes to fulfill the SIST EN 1317 standard. The vehicle mass was raised from 7,320 kg to 10,000 kg by increasing the material density of all

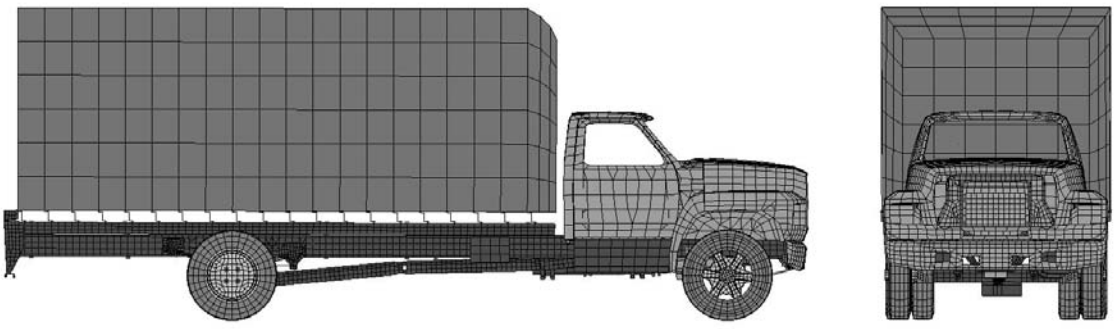

Sl. 4. *Model po MKE tovornega vozila Ford*
Fig. 4. *The FEM model of a Ford single-unit truck*

10.000 kg, tako da je bila povečana gostota vseh delov tovornjaka. V težišče tovornega vozila je bil dodan merilnik pospeškov kot tog lupinski končni element, ki omogoča zajem pomikov, hitrosti in pospeškov v lokalnem koordinatnem sistemu vozila.

4.2 Numerični model ograje

Podrobneje so bili modelirani ščitnik, steber in distančnik ograje, medtem ko so bile vijačne zveze modelirane poenostavljeno. Glede na rezultate prejšnjih simulacij in hitrost vozila je bila dolžina modelirane ograje omejena na 39 m, od tega 5 m ograje pred naletno točko tovornega vozila in 34 m za njo. Po celotni dolžini ograje je bilo razporejenih 19 stebrov in distančnikov na medsebojni razdalji 2 m.

Glavni sestavni deli cestne varnostne ograje so bili modelirani z lupinskimi elementi. Stebri in distančniki so bili modelirani z lupinskimi Belytschko-Tsayevimi končnimi elementi s tremi integracijskimi točkami po debelini, ščitniki, pasnice in trapezna vodila pa s polnimi integracijskimi lupinskimi elementi s petimi integracijskimi točkami po debelini, da je bil preprečen pojav nične deformacijske energije. Predpisana debelina končnih elementov je ustrezala konstrukcijski izvedbi posamezne ograje, kakor je navedeno v 3. poglavju. Vijačne zveze so bile modelirane z linijskimi Hughes-Liujevimi končnimi elementi. Celoten model ograje je tako sestavljen iz približno 100.000 elementov in 110.000 vozlišč.

Materialne lastnosti pločevin različnih debelin so bile določene s preizkusi. Glede na dobljene rezultate je bil izbran bilinearen izotropen elastoplastični model s kinematičnim utrjevanjem (preglednica 1). Porušitev materiala je bila predpisana z dejansko plastično deformacijo, ki je znašala 0,28.

Pri vijačnih zvezah z vijaki M10 je bil upoštevan trdnostni razred 5.8 z mejo plastičnosti 400 MPa in natezno trdnostjo 500 MPa, pri vijačnih zvezah z vijaki M16 pa so bile uporabljene vrednosti, navedene v preglednici 2. Te vrednosti so bile

the vehicle parts. A rigid shell element was added at the vehicle's center of gravity to act as an accelerometer and to record the displacements, velocities and accelerations in the local coordinate system of the truck.

4.2 Computational model of the safety barrier

The main safety barrier parts, the guardrail, the posts and the distance spacers were modeled in detail, while simplified modeling was used for the bolts. Based on previous simulations and the speed of the impacting vehicle the length of the modeled safety barrier was 39 m: 5 m before and 34 after the impact point. Along the whole length of the road-safety barrier 19 posts and distant spacers were placed 2-m apart.

Shell finite elements were used to model the main parts of the safety barrier. Posts and distance spacers were modeled with Belytschko–Tsay shell finite elements with three integration points through the shell thickness, while the guardrails, the tension belts and the wheel-guidance profiles were modeled using full-integration shell elements with five integration points through the thickness to prevent "hourglassing". The thicknesses of the shell elements were defined according to the construction plans of each design, as described in Section 3. The bolt connections were modeled with linear Hughes–Liu finite elements. The complete safety-barrier model consisted of approximately 100,000 finite elements and 110,000 nodes.

The material properties of the different sheet metal thicknesses were obtained experimentally. Experiment results were used to define an isotropic bilinear elastoplastic material model with kinematic hardening (Table 1). Material failure was prescribed according to the effective plastic deformation, which was set to 0.28.

A yield stress of 400 MPa and a limit stress of 500 MPa were prescribed for the M10 bolt connections of strength class 5.8, while the M16 bolt connections were modeled with the parameters presented in Table 2. The parameters were obtained from a correlation analysis

Preglednica 1. *Materialne lastnosti pločevin varnostne ograje*
Table 1. *Material properties of sheet-metal thicknesses*

d mm	E GPa	ν	σ_y MPa	E_t MPa	σ_u MPa
2,0 2,5 2,8 3,0	190	0,29	285	696	400
4,0 5,0 7,0	200	0,29	330	969	450

Preglednica 2. *Materialni podatki za vijačne zveze z vijaki M16*
Table 2. *Material properties for the M16 bolt connections*

E GPa	ν /	σ_y MPa	E_t MPa	ε_u %
190	0,29	240	0	170

dobljene s primerjavo med preizkusi in numeričnimi simulacijami vijačnih zvez z vijaki M16. Zaradi tega je dopustna dejanska plastična deformacija ε_u tako velika, saj zajema deformacijo celotne vijačne zveze in okoliškega materiala.

4.3 Začetni in robni pogoji

Robni in začetni pogoji za tovorno vozilo so predpisani s standardom SIST EN 1317. Vozilo pri testu TB42 je postavljeno pod kotom 15° glede na cestno varnostno ograjo s predpisano začetno hitrostjo, ki znaša 70 km/h.

Nadaljevanje ščitnika in ojačitev ograje je bila simulirana z vzmetnimi elementi (1 na sl. 5) ustrezne togosti in elastično linearno značilnico. Vpliv zemljine je bil simuliran z vzmetnimi elementi elasto-viskoplastičnih lastnosti spremenljivih po globini, ki je bila določena s predhodnimi parametričnimi simulacijami [9].

V modelu so bili predpisani štirje ločeni stiki: med posameznimi deli ograje, med posameznimi deli tovornega vozila, med desnim bokom tovornega vozila in ograjo ter med kolesi vozila in podlago. V prvih treh stikih je bila vrednost statičnega koeficienta trenja μ_s = 0,2, dinamičnega koeficienta trenja pa μ_d = 0,15. V zadnjem stiku pa je bila za oba koeficienta trenja uporabljena vrednost 0,3.

of the experimental measurements and the computational simulation of the M16 bolt connections. This explains the very high ultimate effective plastic deformation, ε_u, which actually accounts for the bolt and surrounding material deformation.

4.3 Initial and boundary conditions

The initial and boundary conditions for the vehicle are prescribed by the SIST EN 1317 standard. The impacting vehicle for the TB42 test is positioned at an angle of 15° to the safety barrier, and the initial velocity is equal to 70 km/h.

Continuation of the guardrail and the barrier reinforcement was modeled with spring elements (No. 1 in Fig. 5) with a linear elastic characteristic and an appropriate stiffness. The soil influence was simulated using spring elements with an elasto-viscoplastic characteristic varying with depth, which was obtained from previous parametric simulations [9].

Four different contact definitions were used in the model: between the safety-barrier parts, the contact between the vehicle parts, the contact between the impacting part of the vehicle and the barrier, and the contact between the wheels of the vehicle and the ground. The static and dynamic frictions in the first three contact definitions were set to μ_s = 0.2 and μ_d = 0.15, respectively. In the fourth contact definition, both friction coefficients were set to 0.3.

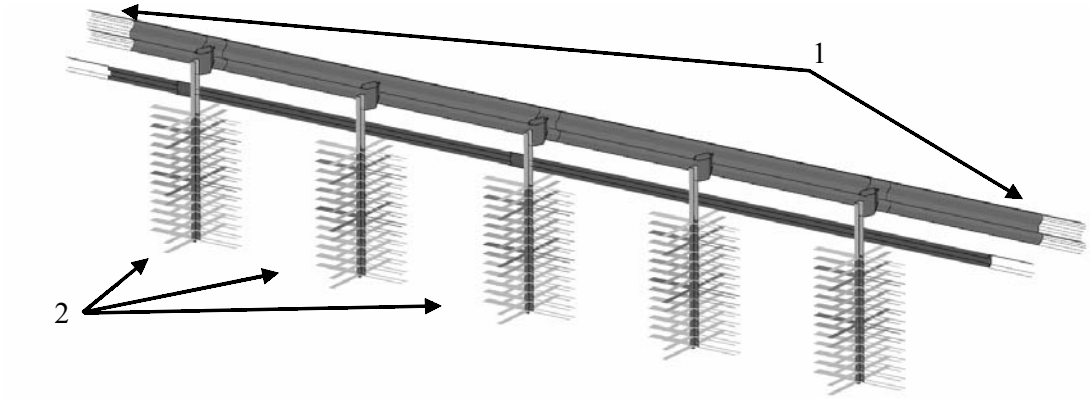

Sl. 5. *Robni pogoji za varnostno ograjo s stebri, zabitimi v zemljino*
Fig. 5. *Boundary conditions for a safety barrier with posts rammed into the soil*

4.4 Parametri računalniške simulacije

Analiza naleta vozila v cestno varnostno ograjo je bila simulirana s programskim paketom LS-Dyna Version MPP 970. Vse predstavljene analize so bile izvajane na sistemu z osmimi procesorji Intel Pentium IV 3,2GH s tehnologijo prepleta pod operacijskim sistemom Linux. Računalniške simulacije so bile izvedene v časovnem koraku $t = 1{,}6$ s, takoj po prvem stiku med vozilom in ograjo. Časovni korak analize je bil samodejno izračunan glede na najvišjo prvo resonančno frekvenco celotnega modela in je znašal 1,7 μs. Izvajanje ene same simulacije je na opisanem sistemu trajalo med 100 in 110 urami.

5 ANALIZA NUMERIČNIH REZULTATOV

Razlike med poteki trka parametričnih analiz različnih debelin pasnic in vodila so zanemarljive, zato je potek trka prikazan le za eno simulacijo (sl. 6). Rezultati vseh analiz kažejo, da vse konstrukcijske različice cestne varnostne ograje vozilo uspešno preusmerijo nazaj na vozišče. Največja deformacija varnostne ograje je dosežena v času $t = 0{,}8$ s. Vozilo se loči od ograje v času $t = 1{,}5$ s.

Pred izračunom časovnega poteka parametra MVP so bili vsi zbrani pospeški filtrirani z uporabo filtra CFC 180 (najmanjša frekvenca zbiranja podatkov znaša 1800 Hz) kakor zahteva standard SIST EN 1317.

4.4 Computational simulation properties

The computational simulation of a vehicle impact into a road-safety barrier was performed using the dynamic explicit software code LS-DYNA MPP Version 970. All the simulations were done on a PC cluster with eight Pentium-IV 3.2-GHz processors with hyper-threading technology and a Linux operating system. The simulations were done for the time interval of 1.6 s after the first contact between the vehicle and the barrier. The time-step increment was computed with regard to the highest first-resonant frequency of the model, and was equal to 1.7 μs. One simulation run on the reported configuration took from 100 to 110 hours.

5 ANALYSIS OF THE COMPUTATIONAL RESULTS

Due to the similarity of the vehicle behavior for different sheet-metal thicknesses of the tension belt and the wheel guidance only one vehicle-impact sequence is shown in Fig. 6. The results of all the simulations prove that all safety-barrier designs redirect the impacting vehicle back on to the road. The maximum system deformation is observed at time $t = 0.8$ s. The vehicle separates from the barrier at time $t = 1.5$ s.

Before calculating the ASI parameter all the measured vehicle-mass acceleration data was filtered using a CFC 180 filter (the minimum measurement frequency equals 1,800 Hz) according to SIST EN 1317.

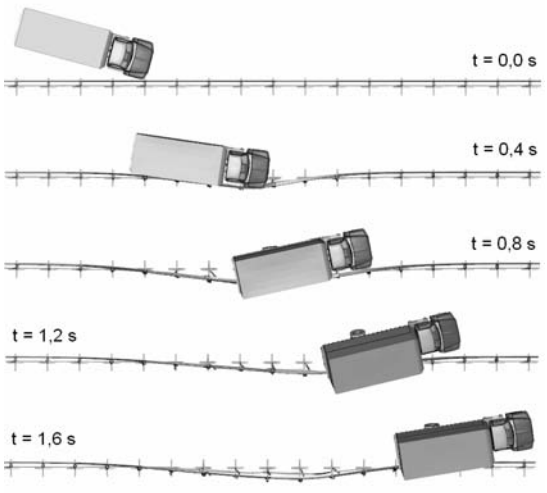

Sl. 6. *Potek naleta tovornega vozila ob cestno varnostno ograjo s pasnico*
Fig. 6. *The truck impact into a safety barrier reinforced with a tension belt*

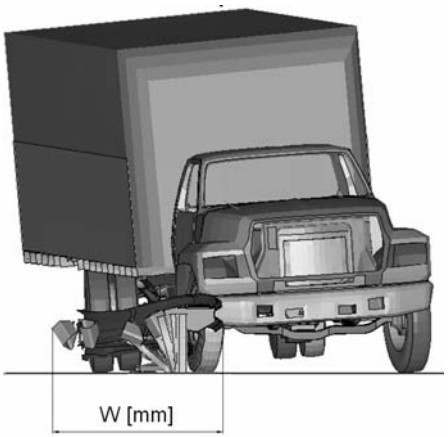

Sl. 7. *Delovna širina (W)*
Fig. 7. *Working width (W)*

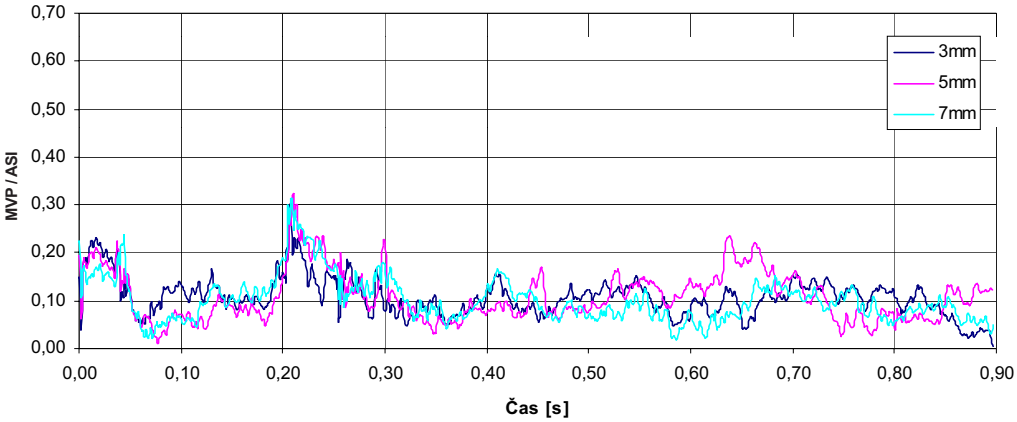

Sl. 8. *Potek parametra MVP pri ograji s pasnico*
Fig. 8. *ASI parameter for the barrier with the tension belt*

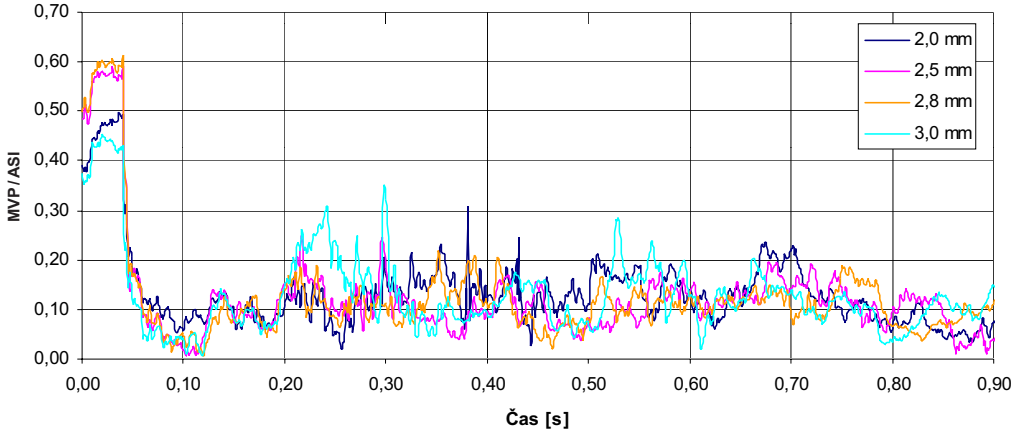

Sl. 9. *Potek parametra MVP pri ograji z vodilom*
Fig. 9. *ASI parameter for the barrier with the wheel guidance*

Potek parametra MVP v odvisnosti od časa pri analizah cestne varnostne ograje s pasnico je prikazan na sliki 8, pri ograji z vodilom pa na sliki 9. Največje dosežene vrednosti parametra MVP so podane v preglednici 3. Pri obeh časovnih potekih parametra MVP sta opazna dva izrazitejša vrha. Eden takoj v času $t = 0{,}0$ s, ko pride tovorno vozilo prvič v stik z ograjo in drugi v času $t = 0{,}2$ s, ko kolo vozila zadene steber varnostne ograje. Primerjava obeh slik pove, da so povprečne in največje vrednosti parametra MVP pri varnostni ograji s trapeznim vodilom večje. Razlog za večjo togost je večja dolžina razvitega profila pri trapeznem vodilu, ki znaša l = 285,0 mm in le 75,4 mm pri pasnici. Togost cestne varnostne ograje z vodilom je dodatno povečana še zaradi neposredne pritrditve trapeznega vodila na stebre, medtem ko je pasnica privijačena na distančnik.

Primerjava poteka parametra MVP med enakimi ojačitvami različnih debelin pokaže manjše

The time dependency of the ASI parameter for the road-safety design with a tension belt is given in Fig. 8, and for a wheel guidance in Fig. 9. The maximum values of the ASI are presented in Table 3. In both time dependencies of the AIS parameter two distinct peaks can be observed. One immediately after the time $t = 0.0$ s, when the vehicle impacts the barrier, and the second one at $t = 0.2$ s, when the wheel hits the barrier post. A comparison of both figures reveals that the average and maximum values of the ASI are higher for the barrier with the wheel guidance. The reason is in the greater length of the unfolded profile of the wheel guidance, which equals $l = 285.0$ mm, and only $l = 75.4$ mm for the tension belt. The stiffness is additionally increased due to the direct connection of the wheel guidance to the posts, while the tension belt is connected to the distance spacer.

The comparison of the ASI parameter for the same reinforcements of different thicknesses shows

razlike. Pri ograji s pasnico so največje dosežene vrednosti parametra MVP pri pločevinah različnih debelin enake, povprečne vrednosti pa pričakovano pokažejo manjše vrednosti pri tanjši pločevini. Pri ograji z vodilom je največja vrednost parametra MVP dosežena pri debelini pločevine d = 2,8 mm, kljub temu pa je pri tej debelini povprečna vrednost parametra MVP najmanjša. Večje povprečne vrednosti imata vodili debeline d = 2,0 mm in d = 3,0 mm, vendar imata manjšo največjo vrednost.

Razlike med vrednostmi delovnih širin (sl. 7) pri različnih debelinah pločevine cestne varnostne ograje ojačane s pasnico, so zanemarljive, medtem ko so razlike pri cestni varnostni ograji s trapeznim vodilom nekoliko večje. Pričakovali bi manjšo deformacijo ograje pri debelejši pločevini vodila, a izmerjeni rezultati kažejo drugače. Natančnejša analiza poteka trka pokaže, da je večji del te razlike posledica različne deformacije distančnikov in premikanja varnostne ograje med trkom. Primerjava vrednosti delovne širine med posameznima konstrukcijskima rešitvama pa pokaže manjše deformacije pri ograji z vodilom. To se sklada z ugotovitvijo o večji togosti te ograje.

6 SKLEP

Za oceno različnih konstrukcij varnostne ograje za raven zadrževanja H1 so bile izvedene računalniške simulacije naleta tovornega vozila v cestno varnostno ograjo na podlagi parametričnih nelinearnih dinamičnih analiz po metodi končnih elementov. Rezultati parametričnih analiz kažejo, da je z vidika moči udarca primernejša cestna varnostna ograja s pasnico. Ker vse konstrukcijske rešitve varnostne ograje s pasnico uspešno zadržijo vozilo na cestišču, je s cenovnega vidika najzanimivejša izbira najtanjše pasnice debeline 3,0 mm.

smaller differences. The maximum values of the ASI for the safety barrier with a tension belt are the same for all thicknesses, while the average values are lower for the thinner sheet metal, as expected. The highest value of ASI for the barrier with the wheel guidance is determined for the sheet-metal thickness d = 2.8 mm, while the average value of ASI is the lowest at the same time. Higher average values are recorded for metal thicknesses d = 2.0 mm and d = 3.0 mm, but with a lower maximum value.

The differences in working-width (Fig. 7) values for different sheet-metal thicknesses are negligible for the barriers reinforced with the tension belt, while they are more pronounced for the barriers reinforced with the wheel guidance. A lower working width is expected for the reinforcements with thicker sheet metal, but the results show otherwise. A more precise analysis of the impact shows that this effect can be attributed to the difference in the distance-spacer deformation and the barrier movement during impact. Comparisons of the working widths between both reinforcements show smaller deformations for the barrier reinforced with a wheel guidance. This is consistent with previous findings.

6 CONCLUSION

Computational simulations based on a parametric, nonlinear, dynamic finite-element analysis of a vehicle impact into a road-safety barrier were employed to evaluate different road-safety barrier designs for the containment level H1. The results of the parametric analyses showed that the barrier design reinforced with a tension belt is the appropriate choice when considering an impact severity. Because all the barrier designs with a tension belt successfully redirect the vehicle back onto the road the thinnest tension belt of thickness 3.0 mm is the best choice in terms of cost.

Preglednica 3. *Rezultati parametričnih simulacij cestnih varnostnih ograj*
Table 3. *Results of parametric simulations of road-safety barriers*

Ojačitev Reinforcement	d mm	maks MVP max ASI	Delovna širina Working width mm	Razred delovne širine Working width class
Pasnica Tension belt	3	17,5	1867	W6
	5	20,0	1820	W6
	7	19,3	1834	W6
Trapezno vodilo Wheel guidance	2,0	18,1	1519	W5
	2,5	18,3	1595	W5
	2,8	21,0	1682	W5
	3,0	13,9	1695	W5

Končna ocena o primernosti cestne varnostne ograje za raven zadrževanja H1, pa terja tudi upoštevanje delovne širine in preizkus cestne varnostne ograje z osebnim vozilom. Rezultati teh testov kažejo precej manjše vrednosti moči udarca pri varnostni ograji s trapeznim vodilom. Pri varnostni ograji s pasnico namreč pride do neposrednega udarca kolesa osebnega vozila v steber varnostne ograje, kar se kaže na večjih pojemkih, ki zaradi tega presežejo s standardom SIST EN 1317 predpisane mejne vrednosti. Tako lahko povzamemo, da je cestna varnostna ograja okrepljena s trapeznim vodilom najprimernejša konstrukcija varnostne ograje, ki izpolnjuje zahteve za raven zadrževanja H1.

Glede na rezultate simulacij je najprimernejša cestna varnostna ograja z vodilom iz pločevine debeline 2,0 mm, saj pomeni najboljšo poravnavo med povprečno in največjo vrednostjo parametra MVP ter ima hkrati tudi najmanjšo delovno širino.

For the final evaluation of the road-safety barrier's suitability for the containment level H1, the working width and the impact of a personal vehicle also had to be taken into account. The results of these computations show lower values of impact severity for the barrier with a wheel-guidance profile. In the case of the barrier with a tension belt the wheel of the personal car impacts directly into the post, and the higher accelerations that result in large impact-severity parameters exceed the limits defined in the SIST EN 1317 standard. It is, therefore, concluded that the safety-barrier design reinforced with the wheel-guidance profile is the most suitable choice to fulfill the H1 containment-level requirements.

According to the simulation results, the safety barrier with the 2.0-mm-thick wheel-guidance profile is the most appropriate design, since it offers the best compromise between average and maximum values of ASI and has the smallest working width.

7 LITERATURA
7 REFERENCES

[1] EN 1317-1 do 1317-5 Road restraint system (1998) *European Committee for Standardization*, Brussels.
[2] Livemore Software Technology Corporation (2003) LS-DYNA Keyword User's Manual. *Livemore*.
[3] Livemore Software Technology Corporation (1998) LS-DYNA Theoretical Manual. *Livemore*.
[4] Tehnična specifikacija za javne ceste TSC 02 (2003) Varnostne ograje, pogoji in načini postavitve. *Ministrstvo za promet, Urad za standardizacijo in meroslovje, Direkcija republike Slovenije za ceste*, oktober, 2003.
[5] Vesenjak, M., Ren Z. (2003) Dinamična analiza deformiranja cestne varnostne ograje pri naletu vozila. *IAT'03*, ZSIT Slovenije – SVM in FS Ljubljana – LAVEK, Ljubljana, pp. 349-357, 2003.
[6] Vesenjak, M., Ren Z. (2003) Dinamična simulacija deformiranja cestne varnostne ograje pri naletu vozila. *Kuhljevi dnevi '03*, Slovensko društvo za mehaniko, Ljubljana, pp. 207-216, 2003.
[7] Finite element model archive, FHWA/NHTSA National Crash Analysis Center, dostopno na WWW: http://www.ncac.gwu.edu/vml/models.html [3.10.2005].
[8] A finite element primer, 3rd Reprint (1992) *NAFEMS*, Glasgow.
[9] Sennah, K., Samaan, M., Elmarakbi, A. (2003) Impact performance of flexible guardrail systems using LS-DYNA, *4th European LS-DYNA Users Conference 2003*, DYNAmore GmbH, Ulm, pp. B-III-35-43.

Naslov avtorjev: Matej Borovinšek
Matej Vesenjak
dr. Miran Ulbin
prof.dr. Zoran Ren
Univerza v Mariboru
Fakulteta za strojništvo
Smetanova 17
2000 Maribor
ren@uni-mb.si
m.vesenjak@uni-mb.si
ulbin@uni-mb.si
matej.borovinsek@uni-mb.si

Authors' Address: Matej Borovinšek
Matej Vesenjak
Dr. Miran Ulbin
Prof.Dr. Zoran Ren
University of Maribor
Faculty of Mechanical Eng.
Smetanova 17
SI-2000 Maribor, Slovenia
ren@uni-mb.si
m.vesenjak@uni-mb.si
ulbin@uni-mb.si
matej.borovinsek@uni-mb.si

Prejeto: 5.10.2005
Received:

Sprejeto: 16.11.2005
Accepted:

Odprto za diskusijo: 1 leto
Open for discussion: 1 year

Strojniški vestnik - Journal of Mechanical Engineering 52(2006)2, 112-125
UDK - UDC 534.83:621.43.044
519.61/.64
Izvirni znanstveni članek - Original scientific paper (1.01)

Vibroakustično modeliranje alternatorja

Vibro-Acoustic Modelling of an Alternator

Martin Furlan[1] - Robert Rebec[1] - Andrej Černigoj[1] - Damjan Čelič[2] - Primož Čermelj[2] - Miha Boltežar[2]
([1]ISKRA Avtoelektrika, Šempeter pri Gorici; [2]Fakulteta za strojništvo, Ljubljana)

V prispevku so predstavljeni osnovni prijemi pri izdelavi sklopljenega modela alternatorja za ovrednotenje vibroakustičnega odziva kot posledice različnih vzbujanj alternatorja; vibracij motorja z notranjim zgorevanjem, neuravnoteženosti rotorja ter magnetnih sil. Prikazani sta izdelava in preverjanje strukturnih trirazsežnih (3D) modelov metode končnih elementov (MKE) za osnovne sestavne dele; posamezne povezane sklope in za alternator kot celoto. Preverjanje strukturnih modelov je izvedeno z eksperimentalno modalno analizo (EMA), ki je obenem namenjena za ovrednotenje dušenja ter posodobitev strukturnega modela alternatorja. Natančneje je opisan poseben primer izračuna vibroakustičnega odziva kot posledice vzbujanja magnetnih sil. Pri tem je bil za ovrednotenje magnetnih sil izdelan trirazsežni model MKE za magnetno polje, tako da je omogočal harmonsko analizo magnetnih sil in njihov neposreden prenos v strukturni model MKE alternatorja. Na podlagi poznanega vzbujanja alternatorja, tj. magnetnih sil v določenih obratovalnih razmerah, je bil ovrednoten in analiziran strukturni in akustični odziv alternatorja.

(Ključne besede: alternatorji, vibracije, metode končnih elementov, metode robnih elementov, analize modalne)

In this paper we present the basic approaches to building a sequentially coupled model of an alternator to evaluate the vibro-acoustic response resulting from different excitations, such as engine vibration, rotor unbalance and magnetic forces. Special emphasis is given to the set-up and verification of the three-dimensional (3D) structural finite-element (FE) model for the whole alternator and for the alternator components. The verification of the structural model was carried out using experimental modal analysis (EMA), which was also applied for the estimation of the modal damping and for the structural FE model updating. Special emphasis is given to the evaluation of magnetic noise, generated due to the magnetic force excitation in the alternator. To estimate the magnetic forces and their harmonic components a 3D magnetic FE model of the alternator was prepared. Finally, the exciting magnetic forces, calculated for the specific operation conditions of the alternator, were transferred into a structural FE model, where the structural and acoustic responses were calculated and analysed.

(Keywords: alternators, vibrations, finite element methods, boundary element methods, modal analysis)

0 UVOD

Osnovni cilj izdelave sklopljenega numeričnega modela alternatorja za ovrednotenje vibroakustičnega odziva sta optimizacija in razvoj novih konstrukcij alternatorjev z notranjim ventilatorjem, ki naj po tehničnih značilnostih dosegajo ali celo presegajo primerljive konkurenčne izdelke. Slednje pomeni, da pri alternatorju dosežemo zadovoljiv odvod toplote oz. povečamo izkoristek pri majhni stopnji

0 INTRODUCTION

The optimisation of an alternator with an internal ventilator was the major driving force for setting up a coupled numerical model of the alternator intended to evaluate its vibro-acoustic response. Additionally, this model will be used in the development process of new designs of alternators, helping to improve their technical characteristics and make them comparable or even better than their competitors. In the case of the alternator,

aerodinamičnega hrupa ventilatorja ter pri tem ne ogrozimo dobe trajanja alternatorja ali povečamo njegovega vibracijskega in akustičnega odziva. Enako pomembna je optimizacija konstrukcije alternatorja z vidika magnetike, ki prav tako omogoča izboljšanje izkoristka ter zmanjšanje magnetnega hrupa alternatorja, povzročenega z magnetnimi silami, ki vzbujajo strukturo alternatorja.

Pri doseganju omenjenega cilja se srečujemo z izključujočimi se zahtevami in omejitvami, ki iskanje optimalne rešitve zelo otežujejo. Pri iskanju takih rešitev so v veliko pomoč računalniška tehnologija in numerične metode. Predvsem razmah računalniške tehnologije v zadnjem času je omogočil, da se zahtevni večdisciplinarni problemi, npr. nastajanje hrupa, v doglednem času rešijo z numeričnimi simulacijami. Bistvena prednost, ki jo omogočajo numerične simulacije, je možnost uporabe optimizacije, kar zmanjša število prototipov in posledično količino eksperimentalnega dela. Skupno se to kaže v krajšem razvojnem času in večji kakovosti izdelka.

1 SKLOPLJENI VIBROAKUSTIČNI MODEL ALTERNATORJA

V splošnem vibroakustični model alternatorja združuje tri fizikalne probleme, tj. magnetni, strukturni in akustični problem, in njim pripadajoče modele, ki jih lahko predstavimo kot celovit – zaporedno

improvements could be achieved with better heat transfer, which corresponds to higher efficiency, where the aerodynamic noise of the ventilators needs to be kept under control. Besides this, the alternator's durability should not be threatened by either an increase in the alternator's vibration and/or acoustic response. Optimising the design of the alternator from the thermal and structural dynamic points of view is not enough.

When achieving the above-mentioned goal one can meet many limitations and contradictory demands that make the search for the optimum design of the alternator very difficult. At this point numerical simulations can be applied as a very effective tool to help the engineer. The recent development of computer technology and numerical methods have also made it possible to simulate very demanding multidisciplinary problems such as the generation of the magnetic noise in a reasonable time. The major advantage of the computer technology and numerical methods is the possibility to make the optimisation and the evaluation in a virtual environment. This significantly decreases the number of prototypes and the quantity of the experimental work and finally shortens the development time and increases the quality of the product.

1 A COUPLED VIBRO-ACOUSTIC MODEL OF THE ALTERNATOR

In general, the vibro-acoustic model of the alternator unites three physical problems, i.e., the magnetic, the structural dynamic and the acoustic. With regard to the physical nature of the alternator,

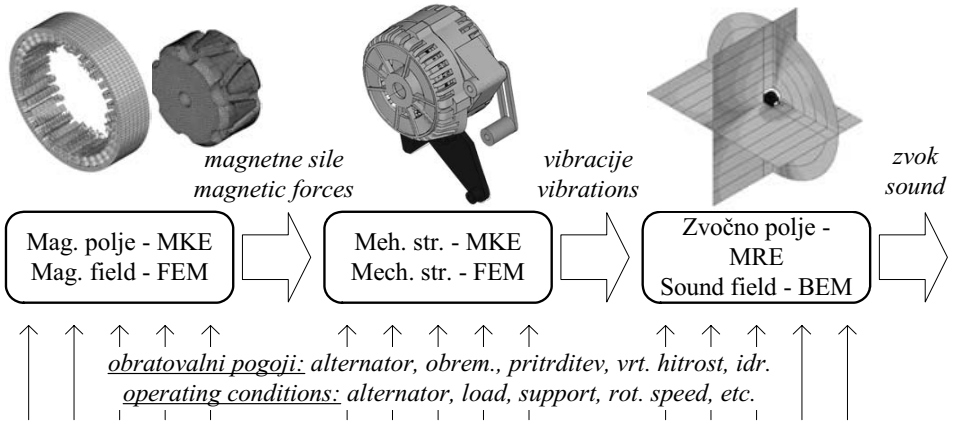

Sl. 1. *Zaporedno povezani magnetni, strukturni in akustični problem alternatorja*
Fig. 1. *The sequentially coupled magnetic, structural dynamic and acoustic problem of the alternator*

Sl. 2. *Obravnavani alternator*
Fig. 2. *The investigated alternator*

sklopljeni problem. Značilnost takega problema je, da ga lahko obravnavamo v treh ločenih zaporednih korakih (sl. 1).

Da bi potrdili verodostojnost tako postavljenega modela, je potrebno preverjanje na dejanskih modelih. Zaradi omenjenega smo se pri gradnji sklopljenega modela alternatorja odločili, da ga izvedemo za že obstoječi alternator (sl. 2).

Z uporabo MKE za magnetno polje izračunamo velikosti in porazdelitev magnetnih sil, ki delujejo na zunanje površine rotorja in statorja alternatorja. Ker vrtenje rotorja vpliva na spreminjanje gostote magnetnega pretoka v zračni reži alternatorja, ima to za posledico periodičen značaj magnetnih sil.

Da bi tako zahteven model magnetnega polja lahko rešili, smo predpostavili, da je porazdelitev magnetnih sil neodvisna od same obremenitve alternatorja. To pomeni, da v magnetni model nismo vnesli statorskih tokov, ampak le nespremenljiv rotorski tok, ki pomeni magnetno vzbujanje alternatorja. Porazdelitev magnetnih sil smo izračunali z magnetostatičnim modelom za različne medsebojne lege rotorja in statorja. Tako dobimo potek spreminjanja magnetnih sil pri vrtenju rotorja alternatorja, na katerem izvedemo harmonsko razdružitev.

Rezultate spremenljivih magnetnih sil pri vrtenju rotorja, izračunanih z MKE za magnetno polje, smo uporabili kot vzbujevalne sile v strukturnem modelu po MKE. Temeljna naloga pri določitvi strukturnega odziva sta bili gradnja in ovrednotenje strukturnega modela po MKE. Strukturni model po MKE smo preverili z eksperimentalno modalno analizo (EMA), ki smo jo izvedli za različne sklope in

each problem can be treated independently, and then they can all be linked into one sequentially coupled problem, Figure 1.

To validate the presented model of the alternator it is necessary to verify it with real cases. For this reason we decided to set-up the vibro-acoustic model for the existing alternator, Figure 2.

The magnetic forces and their distribution, acting on the exterior surfaces of the rotor and stators, are calculated using the finite-element method (FEM) for the magnetic field. In this case it is assumed that a consequence of the stationary rotation of the rotor is a periodic varying of the magnetic forces caused by changes of the magnetic flux densities in the air gap of the alternator.

To simplify the solution of the magnetic problem of the alternator it was necessary to make a few assumptions. The major one relates to the stator excitation. Here we assumed that the distribution of the magnetic forces is load independent. By assuming this, we avoid having to take into account the stator currents, so the rotor current was considered as the only magnetic excitation in the magnetic model. The distribution of the magnetic forces was calculated using a magneto-static model for different rotor positions which describes the changing of the magnetic forces during the rotation and finally allows a calculation of their harmonic components.

The results of the changing magnetic forces during the rotor rotation, calculated using FEM for the magnetic field, are used as the excitation forces in the structural FEM model. The basic job in the process of the evaluation of the structural dynamic response is to build and to verify the structural FEM model. The verification of the structural FEM model was done using experimental modal analysis (EMA)

podsklope alternatorja ter za alternator v celoti. Ovrednotenje strukturnega odziva modela po MKE alternatorja na vzbujanje z magnetnimi silami smo obravnavali kot problem harmonskega vzbujanja, pri čemer je vzbujanje podano s harmonskimi komponentami magnetnih sil.

Zadnji korak v postopku vibroakustičnega modeliranja alternatorja obravnava zvočno polje kot posledico strukturnega odziva. Zvočno polje, ki je rešitev Helmholtzove valovne enačbe, smo obravnavali z metodo robnih elementov (MRE). Glede na numerično zahtevnost omenjenega problema [1] smo numerične simulacije izvedli le za omejeno število diskretnih vrednosti valovnih števil oz. frekvenc. Pri tem smo se omejili na frekvence z največjim prispevkom k magnetnemu hrupu oz. na frekvence prvih nekaj harmonskih komponent, ki nastanejo zaradi harmonske razdružitve magnetnih sil.

2 MAGNETNE SILE V ALTERNATORJU

Ovrednotenje magnetnih sil v alternatorju smo izvedli z uporabo MKE. Zaradi oblike rotorja oz. rotorskih krempljastih polov smo morali ovrednotenje sil izvesti na trirazsežnem modelu, saj je omenjeno geometrijsko lastnost neposredno nemogoče opisati z dvorazsežnim modelom. Glede na simetrično obliko rotorja, ki ima 6 polovih parov, smo zgradili model, ki obsega le eno šestino celotnega alternatorja (sl. 3).

on every single part of the alternator and its substructures as well as on the whole structure of the alternator. The evaluation of the structural response of the alternator FEM model, as a consequence of the magnetic force excitation, is considered as a harmonic problem.

The last step in the process of the vibro-acoustic modelling of the alternator deals with the sound field as a result of the structural response, i.e., vibrations on the alternator structure. The sound field, governing by the Helmholtz wave equation, is evaluated by the boundary-element method (BEM). Due to the numerical extensivenesses of the mentioned problem [1], we limited the simulations of the sound field to only a few wave numbers or discrete frequencies. Only the frequencies with a significant contribution to the magnetic noise or a few first harmonics of the magnetic forces are taken into account for the sound-field calculation.

2 MAGNETIC FORCES IN THE ALTERNATOR

The evaluation of the magnetic forces was carried out using the FEM. Because of the claw pole shape of the rotor it was necessary to build up a three-dimensional (3D) FEM model for the magnetic field. For that reason a two-dimensional FEM model cannot be used. As a result of the cyclic symmetry of the rotor with six pole pairs, only one sixth of the complete alternator was modelled, Figure 3.

Taking into account the cyclic symmetry of

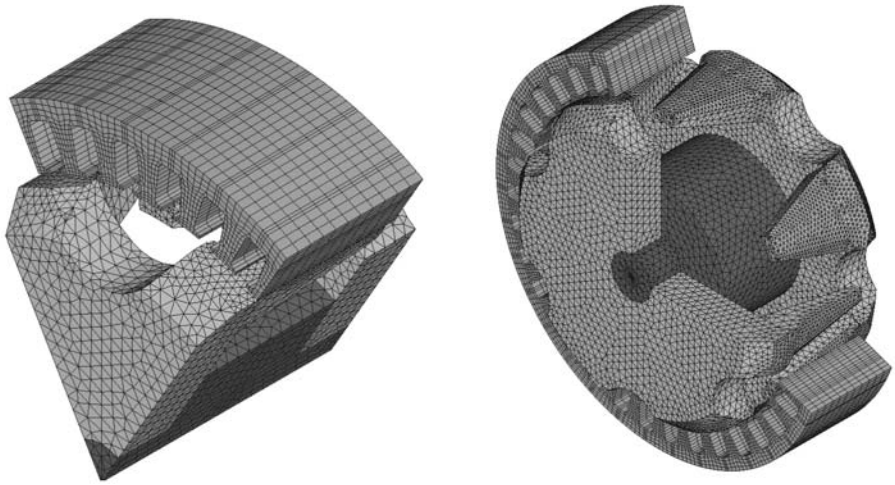

Sl. 3. *Pogled v trirazsežni model po MKE alternatorja za magnetno polje (levo) in celoten alternator (desno)*
Fig. 3. *The 3D FEM magnetic model of the alternator (left) and the complete alternator (right)*

Zaradi simetrije alternatorja smo vrtenje izvedli za 60° v enakomerno razporejenih korakih. Pri izbiri velikosti koraka smo se odločili na podlagi potrebe po razločevanju harmonskih komponent, ki nastanejo pri razvoju magnetnih sil v Fourierjevo vrsto. Glede na predhodne izkušnje in poznavanje karakterja magnetnega hrupa ([1], [5] in [6]), pri katerem se vpliv višjih harmonskih komponent zmanjšuje in njihove frekvence segajo v frekvenčna področja, ki so glede vibroakustičnega odziva manj zanimiva, smo za ovrednotenje izbrali le prvih 12 harmonskih komponent. Iz omenjenega izhaja, da je treba izpeljati izračun magnetnih sil za vsaj 24 korakov, da izpolnimo Nyquistov pogoj. V našem primeru so bili izračuni sil izvedeni za vrtenje v 60 korakih po 1°. To omogoča, da ovrednotimo tudi višje harmonske komponente, kar pripomore k natančnejšemu ovrednotenju magnetnih sil. Slika 4 prikazuje harmonsko analizo za magnetne sile, ki delujejo v vozliščih vzdolž sredine statorskega zoba.

Poleg vpliva vrtenja na magnetne sile je bilo treba ovrednotiti tudi vpliv razmer pri obratovanju. Zaradi zahtevnosti smo se na tem mestu omejili na obratovanje neobremenjenega alternatorja, ko ni statorskega vzbujanja. Glede na naravo delovanja obravnavanega alternatorja smo razmere obratovanja opredelili s tokom v rotorskem navitju. Tako smo ovrednotenje magnetnih sil pri vrtenju rotorja izvedli za različne rotorske tokove. Pri izbiri velikosti tokov smo izhajali iz poznavanja obratovalnih razmer alternatorja in upoštevali dejstvo, da se v običajnih razmerah vrednosti tokov gibljejo med 2A in 4,2A.

the rotor, the magnetic forces calculation was performed in evenly distributed steps in a rotation over 60 degrees. The step size was chosen on the basis of distinguishing the harmonic components that arise from the discrete Fourier transform. Based on previous practice and expertise in the modelling of electric machine noise ([1], [5] and [6]), where the influence of higher harmonics decrease and their frequencies range out of vibro-acoustic interest, for the evaluation of magnetic forces only the first 12 harmonics were chosen. From those facts it follows that at least 24 steps must be executed to fulfil the Nyquist criterion. In our case the magnetic forces calculations during the rotation was performed in steps of 1 degree. This enables us to evaluate the higher harmonics that contribute to a precise presentation of the magnetic forces. Figure 4 shows the harmonic decomposition of the magnetic forces acting on nodes along the centre of the stator tooth.

Besides the influence of rotation on the magnetic forces, the evaluation of the operating conditions of the alternator is also important. For the sake of simplicity we have studied only the unloaded alternator so there is no magnetic excitation on the stator side. Regarding the physical nature of the alternator, the operating conditions were defined with current in the rotor winding. Finally, the magnetic forces calculation was performed for different rotor currents. Knowing that under normal operating conditions the rotor current is generally between 2A and 4.2A, the appropriate rotor current was determined.

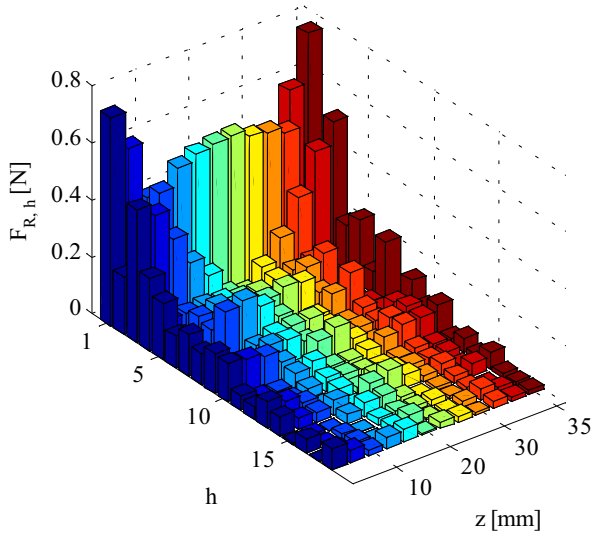

Sl. 4. *Harmonske komponente magnetnih sil vzdolž statorskega zoba*
Fig. 4. *Harmonic components of the magnetic forces along the centre of stator tooth*

Prenos magnetnih sil iz modela po MKE za magnetiko v strukturni model po MKE je lahko zelo zahteven predvsem zaradi različnih postopkov reševanja magnetnega problema na eni in strukturnega problema na drugi strani. Različne zahteve po diskretizaciji pri obravnavi magnetike na eni strani in mehanske strukture na drugi strani onemogočajo uporabo enotne diskretizacije trirazsežnega modela po MKE za reševanje sklopljenega magnetomehanskega problema. Gostota mreže trirazsežnega modela po MKE, ki jo zahteva obravnava problema magnetike, je namreč preveliko breme pri reševanju strukturnega problema. Nasprotno lahko rečemo, da je diskretizacija strukturnega modela neprimerna ali celo neuporabna za reševanje magnetike.

Glede na značaj magnetnih sil, predvsem v smislu krajevne in časovne porazdelitve na površini statorja in krempljastih polov rotorja, je njihov učinek nemogoče v celoti nadomestiti z rezultirajočimi silami in momenti ([1], [5] in [6]). Slednje smo predpostavili le za učinek magnetnih sil, ki delujejo na krempljaste pole rotorja in so znotraj zelo toge strukture krempljastih polov zaradi simetrije vedno v ravnotežju. Nasprotno je za resničen prenos magnetnih sil, ki vzbujajo "elastičen" stator, potrebno ohraniti njihov krajevni značaj. Časovni značaj magnetnih sil pa je opredeljen s harmonskimi komponentami.

3 STRUKTURNI ODZIV ALTERNATORJA

V drugi fazi vibroakustičnega modeliranja alternatorja je treba določiti strukturni odziv kot posledico vzbujanja alternatorja, tj. vibracij motorja z notranjim zgorevanjem, neuravnoteženosti rotorja ali magnetnih sil. Predstavljena je gradnja strukturnega modela po MKE, čemur je namenjen največji poudarek. Opisano je preverjanje modela ter končno ovrednotenje strukturnega odziva, pri čemer smo se omejili le na odziv kot posledico vzbujanja magnetnih sil. Z najmanjšimi dopolnitvami strukturnega modela je mogoče priti tudi do odziva kot posledice vibracij motorja z notranjim zgorevanjem ali neuravnoteženosti rotorja.

Pri ovrednotenju strukturnega odziva se omejimo na ustaljeno delovanje alternatorja. Magnetne sile, ki v takem načinu obratovanja vzbujajo strukturo alternatorja, imajo periodičen značaj. Ob predpostavki, da je mehanska struktura linearen sistem z majhnim dušenjem, lahko obravnavani problem prevedemo na problem

The transfer of magnetic forces from the magnetic FEM model to the structural FEM model can be very difficult to carry out because of there being one way to solve the magnetic model and another way to solve the structural model. A dissimilar requirement for the mesh density of the magnetic and structural problems is the reason why the same mesh cannot be used for the 3D FEM coupled magneto-structural problem. The mesh density required in the 3D FEM magnetic problem is too dense for solving 3D FEM structural problem. Put another way, the mesh density of the 3D FEM structural problem is too coarse to be used in the 3D FEM magnetic problem.

Observing the character of the magnetic forces in terms of time and space distribution over the surface of the stator and the rotor claw pole it is impossible to entirely substitute their effect with the resulting magnetic forces and moments ([1], [5] and [6]). The latter is assumed for the affect of the magnetic forces acting on the rotor claw poles, which are a very rigid structure, and because of their symmetry the magnetic forces are always in counterbalance. In contrast to the credible transfer of magnetic forces, which excite the "elastic" stator, the preservation of their space distribution is required. Meanwhile, their time distribution is characterized with harmonic components.

3 STRUCTURAL RESPONSE OF THE ALTERNATOR

In the second phase of the vibro-acoustic modelling of the alternator it is necessary to determine its structural response as a consequence of the excitation of the alternator, i.e., vibrations due to the operation of an internal combustion engine, rotor unbalance or magnetic forces. Great stress is laid on building a structural FEM model, which is introduced here. The model checking and the final verification of the structural response are described with the assumption that only the response as a consequence of the magnetic forces excitation was taken into account. With a minimum of modal updating it would also be possible to describe the response due to vibrations of an internal combustion engine and rotor unbalance.

The steady state operation of the alternator was assumed during the verification of the structural response. The magnetic forces, which excite the structure, are in this case periodic. Taking into consideration the mechanical structure as a low-damped linear system, our problem can be

vsiljenega nihanja za celoten spekter harmonskih komponent magnetnih vzbujevalnih sil. Nazadnje iz znanega odziva posameznih harmonskih komponent obnovimo celotni strukturni odziv.

V našem primeru smo za ovrednotenje strukturnega odziva na izbranem alternatorju uporabili MKE. Prvotno je bilo treba strukturni model po MKE zgraditi ter preveriti njegovo skladnost na dejanski izvedbi. Gradnje strukturnega modela smo se lotili korakoma. Strukturo alternatorja smo obravnavali po delih, ki smo jih na koncu združili v celoto. Za vsak posamezni del alternatorja smo izdelali model po MKE in ga tudi preverili. Sklepno dejanje pri gradnji strukturnega modela po MKE je bilo povezovanje posameznih delov v celoto. Za potrebe ovrednotenja smo izvedli različne meritve strukturnega odziva, tako posameznih delov kakor celotnega alternatorja, pri čemer smo uporabili eksperimentalno modalno analizo (EMA). To je poleg ovrednotenja strukturnega modela po MKE omogočilo tudi ovrednotenje dušenja za posamezne sklope alternatorja.

3.1 Gradnja strukturnega modela alternatorja

Glede na zapletenost strukture obravnavanega alternatorja smo strukturni model po MKE gradili postopoma. Pri tem smo izhajali iz razdelitve obravnavanega alternatorja, ki se ponuja sama po sebi. Celotno strukturo smo razdelili v štiri sklope: *prednji ležajni pokrov (PLP)*, *zadnji ležajni pokrov (ZLP)*, *stator* in *rotor* (sl. 5). Ker je že vsak sklop sam po sebi dovolj zahteven, je bilo treba tudi pri gradnji strukturnega modela po MKE posamezni sklop graditi v več korakih, kolikor je pač konstrukcija to dopuščala. Tako smo pri gradnji strukturnega modela MKE za posamezen sklop izhajali iz osnovnih podsestavov, ki jih lahko z MKE preprosto modeliramo in v nadaljevanju s preizkusi preverimo. Postopoma smo model sklopa dopolnjevali in ga sproti večkrat preverili. Lahko rečemo, da smo pri gradnji strukturnega modela in njegovih sklopov sledili tehnološkemu postopku izdelave alternatorja. Tak postopek je zahteval veliko število prototipov in preizkusnega dela.

Sklepno dejanje v izgradnji strukturnega modela po MKE obravnavanega alternatorja je povezava predhodno izdelanih sklopov v celoto. Zato da bi lahko čimbolj prepričljivo izvedli mehanske povezave v strukturnem modelu po MKE, moramo spoje dobro poznati. Glede na naravo spojev oz. mehanskih povezav, ki se pojavljajo med PLP, ZLP, statorjem in rotorjem, smo delali s tremi različnimi

transformed into a forced vibration problem for the whole spectrum of excitation, magnetic-force harmonics. Finally, from the known response of the particular harmonic components, the entire structural response can be reconstructed.

For the verification of the structural response of the selected alternator, a FEM was used. The structural FEM model had to be built and verified on a real structure first. The modelling of the whole structure was done using a step-by-step procedure. Each part of the alternator was taken apart, modelled by means of the FEM and verified. Combining those FEM sub-models together was the most difficult step in the structural FEM building up. From the necessity of the verification, various measurements of the structural response, not only on subsystems but also on assemblies, were carried out using experimental modal analysis (EMA). This was necessary for the verification of the structural FEM model, as well as for the verification of the damping on different assemblies of the alternator.

3.1 Structural model of the alternator

With regard to the complexity of the alternator's structure the structural FEM model was built up gradually. In this case we used alternator subpart definitions as they are defined in production, so the structure was divided into four basic subparts: the drive-end bracket (DEB), the rear-end bracket (REB), the stator and the rotor (Figure 5). Due to the great complexity of the subpart FEM models, some of them had to be built gradually, as the design so allowed. In this way we proceeded from the construction of very basic element FEM models, the characteristics of which were then experimentally verified. The main FEM model was progressively built and experimentally verified at every coupling step. We can say that we followed the technological production process during the building up of the FEM model of the alternator. This kind of process required many different prototypes and types of experimental work.

The final action in the structural FEM model construction of the investigated alternator is the coupling of the previously made subassemblies into an integrity. To design the structural FEM model connections as realistically as possible, we should know them very well. Regarding the nature of the connection that occurs between the DEB, the REB, the stator and the rotor, we applied three different

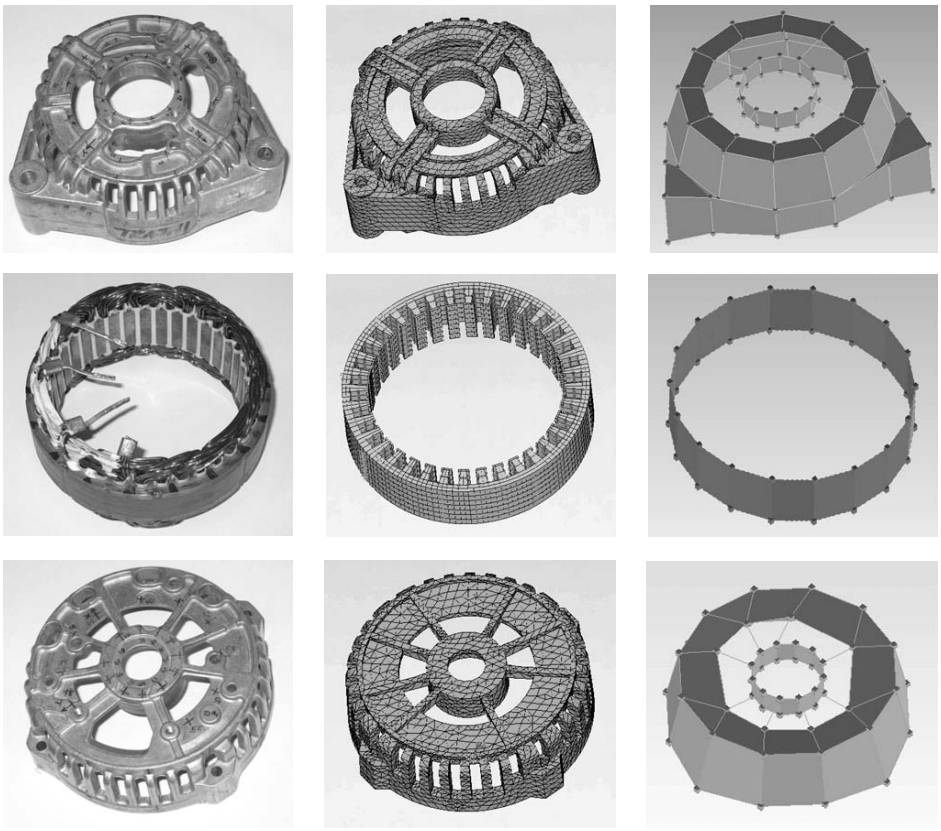

Sl. 5. *Sklopi alternatorja: PLP (zgornja vrsta), stator (srednja vrsta) in ZLP (spodnja vrsta) ter njim pripadajoča dejanska struktura (stolpec levo), strukturni model po MKE (stolpec sredina) in model EMA (stolpec desno)*

Fig. 5. *Alternator subparts; drive-end bracket (upper row), stator (middle row) and rear-end bracket (lower row); and belonging real structure (left column), structural FEM model (middle column) and EMA model (right column)*

mehanskimi povezavami. Najprej smo opredelili povezavo, ki jo predstavljata ležaja in se pojavlja v stiku med rotorjem in PLP ter ZLP. V našem primeru smo togosti ležajev izračunali ([1] in [2]) ter njune lastnosti uporabili v strukturnem modelu po MKE. Drugo obliko mehanske povezave, ki povezuje PLP, ZLP in stator, ter daje alternatorju značaj celote, predstavljajo štiri vijačne zveze. Glede na to, da obravnavani spoj združuje okrov in prednji pokrov s silo in obliko, smo ga v strukturnem modelu po MKE izvedli z združitvijo vseh prostostnih stopenj v vozliščih, ki se pojavljajo na mestu vijačne zveze. Tretja oblika mehanske povezave je stik, ki nastaja pri naleganju med statorjem in PLP ter ZLP. Ker smo se odločili, da mehansko strukturo opišemo z linearnim modelom, stika nismo mogli modelirati v pravem pomenu. Zato da smo ohranili linearnost strukturnega modela po MKE, smo ga modelirali tako, da smo spojili pomike na stičnih površinah.

mechanical connections. First of all we defined the connection between the rotor and both end brackets – the DEB and the REB. In our case we calculated the stiffness matrix of the bearings ([1] and [2]) and used them in the structural FEM model. The next type of coupling was used to connect the alternator as an integrity and represents four screws between the DEB and the REB. Taking into account that the mentioned connections couple subparts with shape and force, we modelled them by coupling all the degrees of freedom (DOFs) of the nodes situated in the proximity of the screw joint. A third different kind of connections was used to model the contact conditions between the stator and the DEB or REB. As we have decided to describe the mechanical structure with a linear model, we did not have the option to model the contact conditions as they should be. To ensure the structural FEM model's linearity, we used just connections that couple the nodal DOFs on the contact surfaces.

Ovrednotenje strukturnega modela po MKE smo izvajali na podlagi primerjave modalnih parametrov (lastnih frekvenc in vektorjev). Kot dodatna kriterija smo uporabili kriterij modalnega zaupanja (KMZ - MAC) ter vidno primerjavo modalnih oblik, ki nam jo omogoča EMA. Nenazadnje tudi masa strukturnega modela po MKE govori o resničnosti, zato smo jo vseskozi primerjali z maso dejanske strukture. Če so izpolnjeni vsi navedeni kriteriji, imamo zagotovilo, da model dobro opisuje masne in togostne lastnosti dejanske strukture. Vprašanje dušenja smo rešili tako, da smo v modelu po MKE uporabili nespremenljivi razmernik strukturnega dušenja en odstotek. Ker vemo, da ima gostota diskretizacije strukturnega modela po MKE vpliv na natančnost izračuna, smo njen vpliv omejili takole. Vsaka podvojitev števila elementov v modelu, bodisi celotnega alternatorja, sklopa ali podsestava, vodi do razlik v izračunanih vrednostih lastnih frekvenc v območju do 4 kHz, ki pa so manjše od enega odstotka. V nadaljevanju je kot primer prikazano ovrednotenje strukturnega modela po MKE za PLP (pregl. 1 in sl. 6) ter za celotni strukturni model alternatorja (pregl. 2 in sl. 7).

The validation of the structural FEM model was done by comparing the modal parameters to real subparts (natural frequencies and mode shapes). As additional criteria, we used the modal assurance criterion (MAC) and a visual comparison of the modal shapes, which was done by using means of the EMA. As a frequently used comparison criterion during model validation, we must also mention the mass of the structural FEM model. If we fulfil all the mentioned criteria we can be sure that our model properly describes the mass and stiffness properties of the real structure. The issue of damping the structural FEM model was solved by using a 1% constant-damping ratio. As we know, the FEM model mesh density has an influence on the accuracy of the calculation. It turns out that every doubling of the elements, irrespective of whether this is performed on just one subpart or on the whole alternator, leads to differences between the natural frequencies and the measured ones. This discrepancy is less than 1% in the range 0–4 kHz. The structural FEM model of the DEB (Figure 6, Table 1) and the whole alternator (Figure 7, Table 2) are shown as examples.

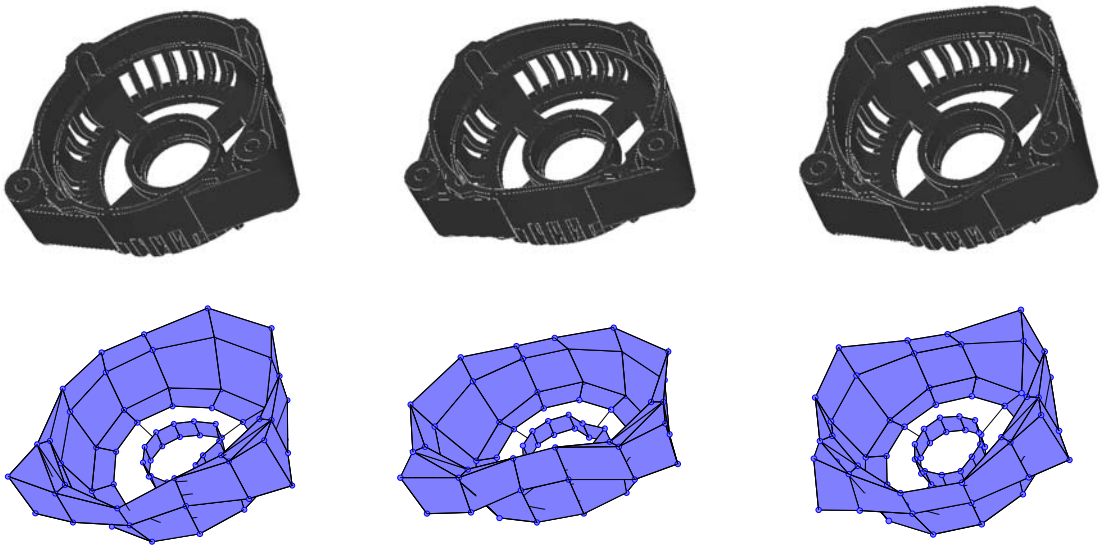

Sl. 6. *Primerjava lastnih oblik PLP, strukturni model po MKE (zgoraj), model EMA (spodaj); prva (na levi), druga (na sredini) in tretja (na desni)*

Fig. 6. *Comparison of the DEB mode shapes, the structural FEM model (above), the EMA model (below); first mode shape (left), second (middle), third (right)*

Preglednica 1. *Izračunane in izmerjene lastne frekvence za PLP*
Table 1. *Calculated and measured natural frequencies of DBE*

MKE		EMA			Δ_f
n	*f* [Hz]	*n*	*f* [Hz]	δ [%]	[%]
1	913	1	969	0,06	-5,8
2	1367	2	1457	0,04	-6,2
3	2547	3	2742	0,37	-7,1
4	2760	4	3062	0,17	-9,9
5	3107	5	3348	0,06	-7,2
6	3252	6	3693	0,07	-11,9
7	4062	7	3922	0,10	3,6

m_{MKE} [kg]	m_{EMA} [kg]	Δ_m [%]
0,829	0,844	-1,8

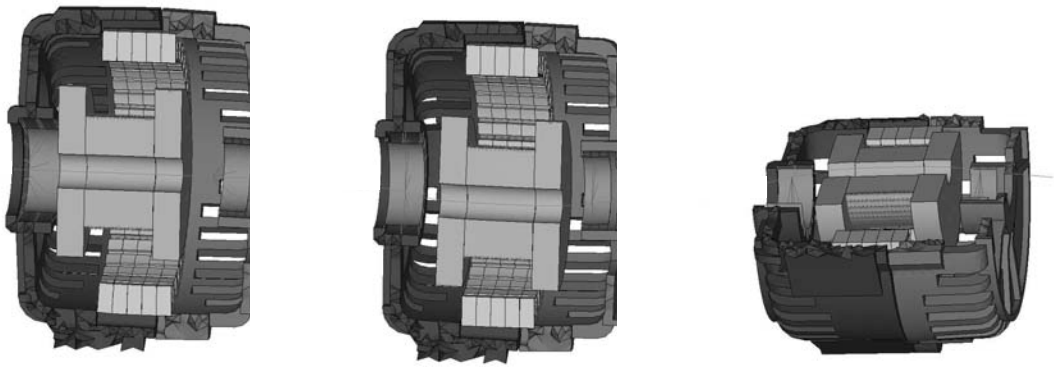

Sl. 7. *Oblike strukturnega modela po MKE alternatorja; prva (levo), druga (sredina) in tretja (desno)*
Fig. 7. *Alternator structural FEM model mode shapes; first mode shape (left), second (middle), third (right)*

Preglednica 2. *Izračunane in izmerjene lastne frekvence za alternator kot celoto*
Table 2. *Calculated and measured natural frequencies of the alternator*

MKE		EMA			Δ_f
n	*f* [Hz]	*n*	*f* [Hz]	δ [%]	[%]
1	412	1	587	2,02	-29,8
2	889	2	908	0,44	-2,1
3	900	3	951	0,69	-5,4
4	1726	4	1272	1,29	35,7

3.2 Prenos magnetnih sil v strukturni model ter odziv

V nadaljevanju je opisano ovrednotenje strukturnega odziva alternatorja na podlagi predhodno zgrajenega strukturnega modela po MKE, pri čemer je alternator vpet na motor z notranjim zgorevanjem. Pri določitvi narave vzbujevalnih sil smo izhajali iz rezultatov, dobljenih pri ovrednotenju magnetnih sil z MKE. Zato da bi lahko izvedli

3.2 Transfer of magnetic forces to a structural model and to the response

Work proceeds with the evaluation of the structural response of the alternator based on the previously built structural FEM model, while the alternator is mounted on the internal combustion engine. The nature of the excitation forces was determined from the results of the magnetic forces verification using the FEM. In order to compare measured and calculated data, the

primerjavo med meritvami in izračunom, je bilo treba določiti jakost magnetnih sil in njihovo osnovno frekvenco vzbujanja. Pri tem smo se oprli na izmerjene vrednosti toka, ki so določale moč magnetnih sil, ter na izmerjene vrednosti vrtilnih frekvenc, ki so določale osnovne frekvence vzbujanja.

Ker je odziv strukture alternatorja močno odvisen od frekvence vzbujanja in zaradi tega od vrtilne frekvence alternatorja, smo osnovno frekvenco vzbujanja za harmonske komponente magnetnih sil vzeli iz meritev vrtilne frekvence. Le-ta se giblje med 3000 min^{-1} in 7500 min^{-1}. Tako je frekvenca osnovne harmonske komponente magnetnih sil (šest polovih parov na rotorju) v različnih razmerah obratovanja nahaja v območju od 300 Hz do 750 Hz.

Ker med posameznimi harmonskimi komponentami enakega reda, vendar za različne smeri rezultirajočih magnetnih sil, obstajajo fazni odmiki, je bilo pri prenosu magnetnih sil na strukturni model treba upoštevati tudi to. Fazno usklajenost smo ohranili tako, da smo harmonske komponente magnetnih sil v strukturni model po MKE vnesli v kompleksni obliki. Slika 8, na levi, prikazuje strukturni model po MKE statorja alternatorja s prirejenimi trenutnimi vrednostmi magnetnih sil, medtem ko slika 8, na desni, prikazuje strukturni odziv kot posledico obratovanja neobremenjenega alternatorja zaradi delovanja pete harmonske komponente magnetnih sil, katere frekvenca pri vrtilni frekvenci 3000 min^{-1} ustreza 1500 Hz.

intensity and the fundamental excitation frequency of the magnetic forces must be determined. This was done using the measured values of current, which determine the intensity of the magnetic forces, and the measured values of the rotational velocity, which determine the fundamental excitation frequencies.

The structural response of the alternator is strongly dependent on the excitation frequency and, consequently, on the rotational velocity of the alternator. For this reason, the fundamental excitation frequency for the harmonic components of the magnetic forces was adopted from the measurement of the rotational velocity. The latter varies from 3000 min^{-1} to 7500 min^{-1}. So, the frequency of the fundamental harmonic component of magnetic forces (six pole pairs on the rotor), on various working conditions, occurs in the range between 300 Hz and 750 Hz.

Between some particular harmonic components of the same order, but for different directions of the resulting magnetic forces, a phase shift occurs. During the transfer of magnetic forces to structural model this also had to be considered. The harmonic components of the magnetic forces were entered into the structural FEM model in a complex form, and a phase adjustment was preserved. Figure 8, on the left, shows the structural FEM model of the stator (of the alternator) with arranged instantaneous values of the magnetic forces, while Figure 8, on the right, depicts the structural response as a consequence of the operation of the unloaded alternator due to the effect of the 5^{th} harmonic component of the magnetic forces. The frequency of the 5^{th} harmonic component at rotational velocity of 3000 min^{-1} corresponds to 1500 Hz.

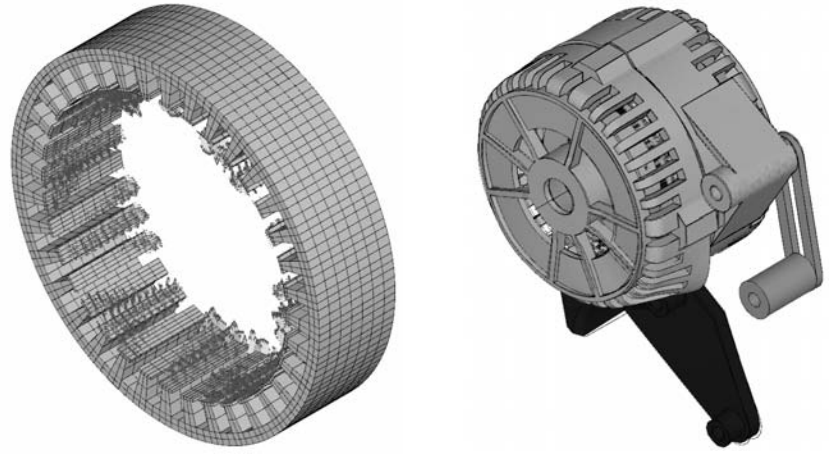

Sl. 8. *Magnetne sile na statorju (na levi) ter strukturni odziv modela po MKE alternatorja kot posledice 5-te harmonske komponente magnetnih sil (na desni)*

Fig. 8. *Magnetic forces on the stator (left) and structural response of the FEM model of the alternator as a consequence of the 5 th harmonic component of the magnetic forces (right)*

4 AKUSTIČNI ODZIV ALTERNATORJA

Zadnja faza vibroakustičnega modeliranja alternatorja je bila določitev zvočnega polja v njegovi okolici na podlagi predhodnega poznavanja strukturnega odziva modela MKE alternatorja. Pri numeričnem ovrednotenju, pri katerem z metodo robnih elementov (MRE) na podlagi znanega strukturnega odziva, izračunamo zvočno polje.

Pri ovrednotenju zvočnega polja smo se držali enakih omejitev, kakor smo jih navedli pri ovrednotenju strukturnega odziva. Bistvena je zahteva po ustaljenem obratovanju alternatorja. Strukturni odziv oz. vibracije, ki se pri takem obratovanju pojavijo na zunanjih površinah alternatorja, povzročajo zvočno valovanje ali ti. magnetni hrup. Ob predpostavki, da mehansko strukturo alternatorja in pojav zvočnega polja v njegovi okolici opišemo z linearnim modelom, lahko reševanje obravnavanega sklopljenega problema prevedemo na problem vsiljenega nihanja oz. na reševanje za posamezne harmonske komponente. Tako vsaka obratovalna oblika oz. strukturni odziv posamezne harmonske komponente povzroča pripadajočo harmonsko komponento zvočnega polja. Poznavanje zvočnega polja za vse harmonske komponente v končni fazi omogoča rekonstrukcijo celotnega zvočnega polja kot posledico strukturnega odziva alternatorja zaradi vzbujanja z magnetnimi silami.

Pri gradnji akustičnega modela MRE smo izhajali iz strukturnega modela po MKE. Celotno zunanjo površino alternatorja, ki jo v strukturnem modelu po MKE sestavljata mreži PLP in ZLP, smo prekrili z redkejšo mrežo trikotnih robnih elementov. Pri tem je mreža robnih elementov zgrajena tako, da si robni elementi delijo vozlišča strukturnega modela po MKE, kar omogoča preprost prenos robnih pogojev iz strukturnega modela po MKE na akustični model MRE. V našem primeru akustičnega modela MRE je največja dolžina robnega elementa manjša od 9 mm, kar zagotavlja dovolj natančno reševanje v frekvenčnem območju do 6,4 kHz. Za opis akustičnega medija smo vzeli lastnosti zraka v normalnih okoliščinah. Z namenom, da bi se seznanili z zvočnim poljem v okolici alternatorja, smo zvočno polje okolice ovrednotili le za nekaj izbranih primerov obratovanja. Slika 9 prikazuje zvočno polje v okolici alternatorja pete harmonske komponente magnetnega hrupa neobremenjenega alternatorja pri obratovanju s 3000 min^{-1}.

4 ACOUSTIC RESPONSE OF THE ALTERNATOR

In the final step of the vibro-acoustic modelling of the alternator, a sound field in its surroundings was determined. This was obtained from the known structural response of the alternator FEM model. The numerical verification of the sound field is basically just an upgrade in the solving of the structural problem, where, on the basis of known structural response and by means of the boundary-element method (BEM), the sound field is calculated.

During the verification of the sound field the same restriction as at the verification of the structural response was used. The demand to have a stationary operation of the alternator is essential. The structural response during such an operation on the external surfaces of the alternator causes a sound radiation or the so-called magnetic noise. Suppose that the mechanical structure of the alternator and the phenomenon of the sound field in its surrounding can be described using a linear model, the solving of the discussed combined problem can then be transformed to a forced vibration problem or to solve a particular harmonic component. Thus, each operational shape, or the structural response at a particular harmonic component, contributes a belonging component to the sound field. Knowing the sound field for each harmonic component makes it possible to reconstruct the entire sound field as a consequence of the structural response of the alternator due to the magnetic force excitations.

The basis for the acoustic BEM model was the structural FEM model. The entire external surface of the alternator, which had been formed in the structural FEM model from the DEB and REB meshes, was covered with a less dense mesh consisting of triangular boundary elements. The mesh of the boundary elements was formed in such a way that its nodes coincided with the nodes of the structural FEM model. This enables an easy transfer of the boundary conditions from the structural FEM model to the acoustic BEM model. In our case of an acoustic BEM model, the maximum length of the boundary element was smaller than 9 mm, so an accurate solving in the region of 6.4 kHz was ensured. For the description of the acoustic medium, the air properties under regular conditions were adopted. In order to get to know the sound field in the surroundings of the alternator, the sound field was evaluated for just a few selected cases of the operation. Figure 9 shows the sound field in the surroundings of the unloaded alternator at 3000 min^{-1} as a consequence of the 5^{th} harmonic component of the magnetic noise.

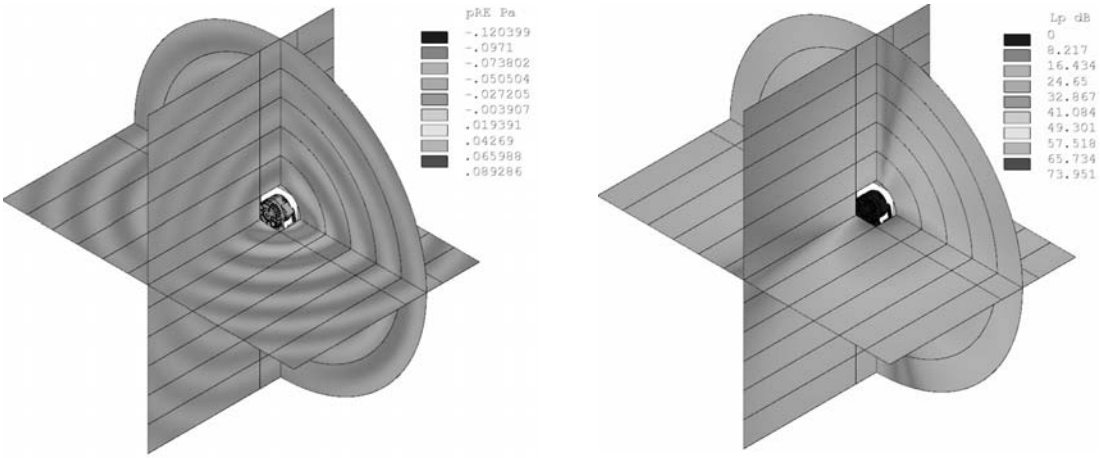

Sl. 9. *Zvočno polje v okolici alternatorja kot posledica 5-te harmonske komponente magnetnih sil; trenutna vrednost zvočnega tlaka (na levi) in raven zvočnega tlaka (na desni)*

Fig. 9. *The sound field in the surroundings of the alternator as a consequence of the 5th harmonic component of the magnetic forces; the instantaneous value of sound pressure (left) and the level of sound pressure (right)*

5 SKLEP

Prispevek predstavlja postopek izdelave in deloma tudi ovrednotenja sklopljenega vibroakustičnega modela alternatorja, ki združuje tri fizikalne probleme, tj. magnetni, strukturno-dinamični ter akustični problem. Predhodno je ovrednoten vibroakustični odziv alternatorja kot posledica vzbujanja z magnetnimi silami. S tem je postavljen postopek, ki omogoča preprosto in hitro posodabljanje parametrov modela ter razpoznavanje in raziskavo vpliva ključnih parametrov konstrukcije alternatorja na njegove tehnične značilnosti. Glede na dejstvo, da je izdelava vibroakustičnega modela v začetni fazi, je treba izvesti dodatno preverjanje in posodobitve modela predvsem v smislu izboljšanja modela mehanske strukture alternatorja.

5 CONCLUSION

This paper presents the process of building, and partly also of verifying, a coupled vibro-acoustic model of an alternator that unites three physical problems, i.e., the magnetic, the structural dynamic and the acoustic. The vibro-acoustic response as a result of the magnetic excitation is evaluated and it shows a preliminary study of the magnetic noise of the alternator. This means that we have successfully established the process where it is easily possible to change almost any parameters of the model and update the response results. In addition, this makes it possible to identify and to analyse the important design parameters of the alternator and find their influence on the technical characteristic of the alternator. Due to the fact that the vibro-acoustic model of the alternator is in its early stages, it needs additional verification and updating, especially the structural FEM model.

6 LITERATURA
6 REFERENCES

[1] Furlan M. (2003) Karakterizacija magnetnega hrupa enosmernega elektromotorja: doktorsko delo, *Univerza v Ljubljani, Fakulteta za strojništvo*, Ljubljana.

[2] Rebec R. (2004) Karakterizacija vibracij alternatorja AAN: Diplomska naloga univerzitetnega študija, *Univerza v Ljubljani, Fakulteta za strojništvo*, Ljubljana.

[3] Furlan M., Černigoj A. in Boltežar M. (2003) A coupled electromagnetic-mechanical-acoustic model of a DC electric motor, *Compel*, 2003, letn. 22, št. 4, str. 1155-1165.

[4] Boltežar M., Čelič D., Jakšić N., Keber M. in Čermelj P. (2004) Analiza in modeliranje alternatorja AAN: poročilo, *Univerza v Ljubljani, Fakulteta za strojništvo*, Ljubljana.

[5] Ramesohl I., Bauer T. in Henneberger G. (1998) Calculation procedure of the sound field caused by magnetic excitations of the claw-pole alternator, *International seminar on vibations and acoustic noise of electric machinery*, Bethune.
[6] Ramesohl I., Henneberger G., Kueppers S. in Hadrys W. (1996) Three dimensional calculation of magnetic forces and displacements of a claw-pole generator, *IEEE Transactions on Magnetic*s, 32(3):1685–1688, 1996.

Naslova avtorjev: dr. Martin Furlan
Robert Rebec
Andrej Černigoj
ISKRA Avtoelektrika d.d.
Polje 15
5290 Šempeter pri Gorici
martin.furlan@iskra-ae.com
robert.rebec@iskra-ae.com
andrej.cernigoj@iskra-ae.com

Damjan Čelič
dr. Primož Čermelj
prof.dr. Miha Boltežar
Univerza v Ljubljani
Fakulteta za strojništvo
Aškerčeva 6
1000 Ljubljana
damjan.celic@fs.uni-lj.si
primoz.cermelj@fs.uni-lj.si
miha.boltezar@fs.uni-lj.si

Authors' Addressses: Dr. Martin Furlan
Robert Rebec
Andrej Černigoj
ISKRA Avtoelektrika d.d.
Polje 15
SI-5290 Šempeter pri Gorici, Slovenia
martin.furlan@iskra-ae.com
robert.rebec@iskra-ae.com
andrej.cernigoj@iskra-ae.com

Damjan Čelič
Dr. Primož Čermelj
Prof.Dr. Miha Boltežar
University of Ljubljana
Faculty of Mechanical Engineering
Aškerčeva 6
SI-1000 Ljubljana, Slovenia
damjan.celic@fs.uni-lj.si
primoz.cermelj@fs.uni-lj.si
miha.boltezar@fs.uni-lj.si

Prejeto: 9.10.2005
Received:
Sprejeto: 16.11.2005
Accepted:
Odprto za diskusijo: 1 leto
Open for discussion: 1 year

Strojniški vestnik - Journal of Mechanical Engineering 52(2006)2, 126-137
UDK - UDC 531.36/.38:621.313.13
Izvirni znanstveni članek - Original scientific paper (1.01)

Modeliranje in analiza dinamike ščetke elektromotorja

Modeling and analyzing the dynamics of an electric-motor brush

Janko Slavič[1] - Miha Nastran[2] - Miha Boltežar[1]
([1]Fakulteta za strojništvo, Ljubljana; [2]Domel, Železniki)

V prispevku je na kratko predstavljen Pfeiffer-Glockerjev postopek modeliranja dinamike togih teles z enostranskimi stiki. Mogoča stična stanja: lepenje, drsenje, trk s trenjem, sprostitev stika se preoblikujejo na linearni komplementarni problem, ki omogoča reševanje več sočasnih stičnih stanj. Predstavljeno teoretično ozadje je prilagojeno za telesa nepravilnih oblik. Uporaba predstavljenih zamisli je prikazana na dinamičnem modelu ščetke elektromotorja. Dinamični model je definiran z več ko 40 parametri, podrobni popis geometrijske oblike pa vključuje tudi površinsko hrapavost. V numeričnem preizkusu prispevek prikaže, kako obraba in togost ščetke vplivata na njeno stabilnost.

(Ključne besede: dinamika teles, telesa toga, simuliranje numerično, modeli dinamični)

This paper briefly presents the Pfeiffer-Glocker formulation for the multibody dynamics of rigid bodies with unilateral contacts. The multiple, concurrent contact situations of stick-slip, detachment and impact with friction are solved as a linear complementarity problem. The theory is extended toward the discretely defined bodies of complex body shapes with nonlinearities. As shown in the numerical example of the electric-motor-brush dynamics the presented extensions can be used to simulate the influence of a detailed geometry, including surface roughness. The influences of brush-wear and brush-stiffness on the dynamic stability are presented from more than 40 parameters that define the brush system.

(Keywords: multibody dynamics, rigid bodies, numerical simulations, dynamic stability)

0 UVOD

Dinamika sistema togih teles v zadnjem času pridobiva pozornost, saj se uporablja tako pri krmiljenju robotov, podajnih mehanizmov, kakor tudi pri izdelavi navideznih prototipov in pri simuliranju navidezne resničnosti [1]. V nasprotju s postopki simuliranja sistemov z dvostranskimi stiki (npr.: vrtljive zveze, vodila itn.), ki so že dobro uveljavljeni, so se načini vključevanja enostranskih stikov (npr.: trk, trk dveh teles) razvili do primerne matematično-fizikalne doslednosti šele v zadnjem desetletju.

V tem prispevku se bomo osredotočili na enostranske stike, zapisane v obliki linearnega komplementarnega problema (LKP - LCP), tak zapis je prvi uporabil Lötstedt [2]. Med pomembnejše raziskovalce tega področja sodijo še Murty [3], Baraff [4], Panagiotopoulos [5], Moreau [6], Pfeiffer in Glocker ([7] in [8]) itn.

Podrobneje si bomo ogledali enega od bolj obetavnih postopkov popisa dinamike togih teles z

0 INTRODUCTION

The mathematical formulation of multibody dynamics with unilateral contacts has received much interest in recent decades. This is particularly so for various control systems, such as the control of robots and industrial feeding mechanisms. Furthermore, it is included into research on virtual prototyping and virtual reality [1]. Despite the fact that bilateral contacts (e.g., rotating joints, linear joints) have been theoretically covered for several decades, the general formulation of unilateral contacts (e.g., impact with the friction of two bodies) was developed to the necessary mathematical and physical consistency only in the past decade.

This paper focuses on the research of unilateral contacts written as a Linear Complementarity Problem (LCP), which was initiated by Lötstedt [2]. Some of the more important researchers in this field are Murty [3], Baraff [4],

enostranskimi stiki: to je Pfeiffer-Glockerjev postopek [7]. Njuno delo pomeni matematično pravilen in fizikalno dosleden način reševanja dinamike togih teles z več sočasnimi stičnimi stanji. Pfeiffer in Glocker stični problem (lepenje, drsenje, sprostitev stika in trk s trenjem) preoblikujeta na pregleden in zgoščen zapis v obliki linearnega komplementarnega problema. Raziskovalca sta v svojih raziskavah uvedla novo razstavitev trenja, ki v primeru odvisnih koordinat nima težav s singularnostjo in vodi v rešitev tudi v primeru predoločenih sistemov; kot prva sta trk s trenjem predstavila v obliki linearnega komplementarnega problema.

Namen prispevka je prilagoditev Pfeiffer-Glockerjevega postopka za diskretno definirana telesa. V ta namen je v drugem poglavju na kratko predstavljen njun postopek simuliranja dinamike togih teles, ki temelji na komplementarnosti stičnih stanj. Uporaba v drugem poglavju predstavljenih zamisli za reševanje diskretno definiranih teles je nato prikazana v tretjem poglavju na dinamičnem modelu ščetke elektromotorja z 11 prostostnimi stopnjami; kot primer analize je predstavljen vpliv nekaterih parametrov modela na stabilnost delovanja ščetke. Zadnje sledi poglavje s sklepi.

1 DINAMIKA SISTEMA TOGIH TELES KOT LINEARNI KOMPLEMENTARNI PROBLEM

Zaradi celovitosti si bomo v tem poglavju na kratko pogledali bistvene zamisli Pfeiffer-Glockerjevega postopka reševanja sistemov togih teles z enostranskimi stiki ([7] do [9]).

Gibalne enačbe sistema togih teles s f prostostnimi stopnjami (vključujoč dvostranske stike) so:

$$\boldsymbol{M}(\boldsymbol{q},t)\ddot{\boldsymbol{q}} - \boldsymbol{h}(\boldsymbol{q},\dot{\boldsymbol{q}},t) = 0 \quad \in R^f \tag{1},$$

kjer so $\boldsymbol{M}$ masna matrika, $\boldsymbol{q}$ vektor posplošenih (generaliziranih) koordinat in $\boldsymbol{h}$ vektor posplošenih aktivnih sil. Če imamo v nekem trenutku množico stičnih točk $i \in I_N$, potem se (1) spremeni:

$$\boldsymbol{M}\,\ddot{\boldsymbol{q}} - \boldsymbol{h} = \sum_{i \in I_N} \boldsymbol{Q}_i^C \quad \in R^f \tag{2},$$

kjer je $\boldsymbol{Q}_i^C$ posplošena nekonservativna sila (kot posledica stične sile v stiku i). Načeloma je treba posplošene koordinate prilagajati trenutnim prostostim, ki pa so odvisne od rešitve stičnega problema. Za primer navedimo, da bi za rešitev sistema z n_N stičnimi točkami morali

Panagiotopoulos [5], Moreau [6], and Pfeiffer and Glocker ([7] and [8]).

One of the more promising and complete theories for including unilateral contacts was presented by Pfeiffer and Glocker [7]; their theory presents a sound and physically consistent basis for including concurrent multiple contact situations. They were also the first to present concurrent impacts with friction as a LCP. Furthermore, their decomposition of stick-slip and the detachment problem avoids the singularity of overdefined dynamical systems.

This paper is organized as follows: the second section presents the Pfeiffer-Glocker formulation for simulating unilateral contact problems in general. In addition, some modifications for discretely defined bodies are given. The ideas are presented in a numerical example of electric-motor-brush dynamics with 11 degrees of freedom, given in the third section. As an example of an analysis the stability of electric-motor-brush dynamics is studied. The last section gives conclusions.

1 MULTIBODY DYNAMICS AS A LINEAR COMPLEMENTARITY PROBLEM

For the sake of completeness this section gives a brief review of the mathematical modeling of multibody dynamics with unilateral contacts as presented by Glocker and Pfeiffer ([7] to [9]).

The equations of motion for a multibody system with f degrees of freedom (including only bilateral contacts) can be written as:

where $\boldsymbol{M}$ is the mass matrix, $\boldsymbol{q}$ is the vector of generalized coordinates and $\boldsymbol{h}$ is the vector of generalized active forces. If there is a set of $i \in I_N$ contact forces (as a result of unilateral contacts) then the equations of motion will be:

where $\boldsymbol{Q}_i^C$ are the generalized, non-conservative active forces. Note that the contact forces change the number of degrees of freedom. In general it is not known which degrees of freedom disappear; this problem is usually solved by looking at all the possible solutions and finding the one that is physically consistent. If there are n_N

najti fizikalno komplementarno rešitev med 3^{n_N} mogočimi rešitvami [7][1]. Tako iskanje ustrezne rešitve postane hitro praktično nemogoče izvedljivo. Zraven tega pa je z vidika numeričnega reševanja zelo neprimerno neprestano prilagajanje števila posplošenih koordinat.

Kakor bomo videli pozneje, se tem težavam z uporabo LKP elegantno izognemo, saj bo število posplošenih koordinat vedno enako številu prostosti sistema brez enostranskih stikov (2).

Poglejmo si najprej povezavo relativnih stičnih sil s posplošenimi stičnimi silami. Z uporabo Jacobijeve matrike lahko normalno stično silo $\boldsymbol{F}_{A,N}$ v točki C_A na telo A (sl. 1) zapišemo kot posplošeno silo:

possible contact points with a stick-slip transition or detachment, then there are 3^{n_N} possible solutions [7][1]. It is clear that the search for a physically consistent combination is time consuming. Furthermore, for numerical simulations it is not appropriate to change the minimum number of coordinates during each time-step.

As we see later, the linear complementarity problem (LCP) method solves this problem in an elegant way, and the number of generalized coordinates is constant at all times. The number of generalized coordinates is always equal to the number of degrees of freedom of the system without unilateral contacts (2).

The real contact forces are linked with the generalized contact forces via the Jacobian matrix. In Figure 1 two bodies are shown, the centers of gravity being denoted by A and B. The normal contact force $\boldsymbol{F}_{A,N}$ at point C_A on the body A as a generalized contact force is:

$$\boldsymbol{Q}^c_{A,N} = \left(\frac{\partial\, {}_I r_{C_A}}{\partial \boldsymbol{q}} \right)^T \boldsymbol{F}_{A,N} = J^T_{C_A} \cdot {}_I\, \boldsymbol{n}_A \cdot \lambda_N \tag{3}$$

in če dodamo še silo na telo B:

and when including the normal force at point B:

$$\boldsymbol{Q}^c_N = \left(J^T_{C_A}\ {}_I \boldsymbol{n}_A + J^T_{C_B}\ {}_I \boldsymbol{n}_B \right) \lambda_N = \boldsymbol{w}_N\, \lambda_N \tag{4}$$

$\boldsymbol{w}_N$ vsebuje kinematične lastnosti stika C, λ_N je stična amplituda sile in I označuje inercialen koordinatni sistem.

Zgornja izpeljava velja za zvezno definirana telesa v splošnem. Kako določimo Jacobijevo matriko stične točke, če ima telo definirano obliko glede na svoje težišče pa sta izpeljala Slavič in Boltežar ([10] in [11]).

Analogno normalni smeri nadaljujemo s tangentno stično silo (indeks T) in izraz (2) preoblikujemo v:

$\boldsymbol{w}_N$ includes the kinematical properties of the contact, λ_N is the amplitude of the force and I denotes the inertial frame.

To adopt the formulation for bodies with discretely defined shapes the Jacobian matrix of the contact point can be further simplified, as shown by Slavič and Boltežar ([10] and [11]).

By using a similar notation for the tangential force (index T), Equation (2) is rewritten as:

$$\boldsymbol{M}\,\ddot{\boldsymbol{q}} - \boldsymbol{h} - \sum_{i \in I_N} \left(\boldsymbol{w}_N\, \lambda_N + \boldsymbol{w}_T\, \lambda_T \right)_i = 0 \quad \in \mathbb{R}^f \tag{5}.$$

Z uporabo matričnega zapisa:

Or by using matrix notation:

$$\boldsymbol{W}_N = \{\boldsymbol{w}_{N_i}\}, \qquad \boldsymbol{W}_T = \{\boldsymbol{w}_{T_i}\}, \qquad i \in I_N \tag{6}$$

gibalne enačbe preoblikujemo v:

the equations of motion are:

$$\boldsymbol{M}\,\ddot{\boldsymbol{q}} - \boldsymbol{h} - \left(\boldsymbol{W}_N \quad \boldsymbol{W}_T \right) \begin{pmatrix} \lambda_N \\ \lambda_T \end{pmatrix} = 0 \quad \in \mathbb{R}^f \tag{7}.$$

Stična stanja rešimo v dveh korakih: najprej na ravni impulzov rešimo nezvezni problem trka s trenjem, nato pa na ravni sil še lepenje, drsenje ali sprostitev stika. Če ni trčnih stanj, prvi korak odpade.

The contact situations are solved in two steps: in the first, the non-smooth impact with friction is solved; in the second, the stick-slip or detachment situation is solved. While the impact is solved in the impulse-domain, the stick-slip or detachment is solved in the force-domain.

[1]Trčna stanja so v podanem primeru izključena; vsaka stična točka je lahko v eni od naslednjih faz: lepenje, drsenje in sprostitev stika.

[1]In this example the impact situations are excluded. Each of the contacts can be in one of the states: sticking, slipping or detachment of the contact.

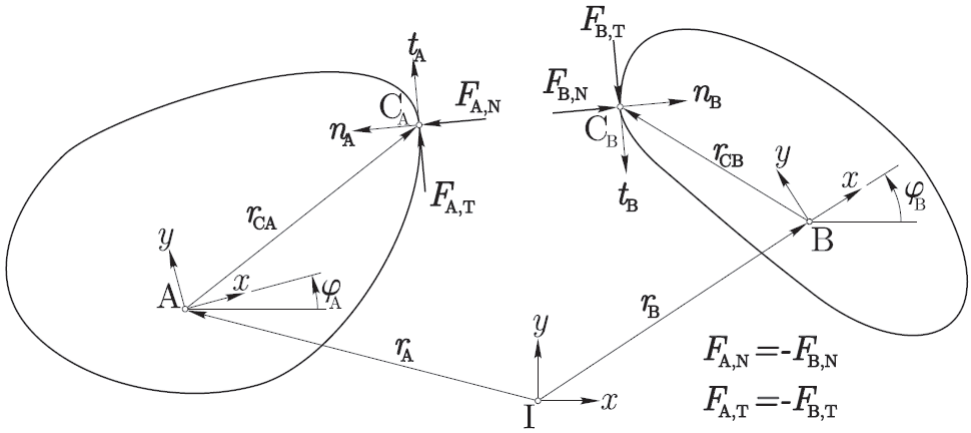

Sl. 1. *Stične sile*
Fig. 1. *Contact forces*

Preden v nadaljevanju podrobneje spoznamo oba koraka, si poglejmo množice stičnih točk:

All the possible contact points I_G are organized in four sets during each time-step:

$$\begin{aligned} I_G &= \{1,2,..,n_G\} \\ I_S &= \{i \in I_G ; g_N = 0\} \quad n_S \text{ elementov/elements} \\ I_N &= \{i \in I_S ; \dot{g}_N = 0\} \quad n_N \text{ elementov/elements} \\ I_H &= \{i \in I_N ; \dot{g}_T = 0\} \quad n_H \text{ elementov/elements} \end{aligned} \tag{8}$$

Množica l_S vključuje v nekem koraku aktivne stike, l_N samo tiste z nično normalno relativno hitrostjo in l_H možne lepene stike. Stične množice se lahko v vsakem časovnem koraku spremenijo.

The set l_S contains all the closed contacts, the set l_N contains only the contacts with vanishing relative normal velocities (stick-slip or detachment), and the set l_H contains the possibly sticking contacts. The number of elements in the sets can change during each time-step.

1.1 Lepenje, drsenje ali sprostitev stika

Lepenje, drsenje (in prehod med njima) in sprostitev stika rešujemo na množici stičnih točk. Gibalne enačbe (7) in relativni stični pospeški $\ddot{g}$ so ([7], [8] in [12]):

1.1 Stick-slip transition or detachment

First, the stick-slip transition or detachment problem is solved on an impact-free set l_N. The equations of motion (7) and the relative contact accelerations $\ddot{g}$ are ([7], [8] and [12]):

$$\boldsymbol{M}\ddot{\boldsymbol{q}} - \boldsymbol{h} - \begin{pmatrix} \boldsymbol{W}_N + \boldsymbol{W}_G \bar{\bar{\mu}}_G & \boldsymbol{W}_H \end{pmatrix} \begin{pmatrix} \lambda_N \\ \lambda_H \end{pmatrix} = 0 \qquad \in \mathbb{R}^f \tag{9}$$

$$\begin{pmatrix} \ddot{g}_N \\ \ddot{g}_H \end{pmatrix} = \begin{pmatrix} \boldsymbol{W}_N^T \\ \boldsymbol{W}_H^T \end{pmatrix} \ddot{\boldsymbol{q}} + \begin{pmatrix} \bar{w}_N \\ \bar{w}_H \end{pmatrix} \qquad \in \mathbb{R}^{n_N + n_H} \tag{10}.$$

Indeks N označuje normalno smer in H tangentno smer možnih lepenih stikov iz množice l_H. Indeks G označuje drseče stike (tangentna sila je znana iz Coulombovega zakona) iz množice $l_N \setminus l_H$. $\bar{\bar{\mu}}_G$ je diagonalna matrika koeficientov trenja.

Za vsak aktiven stik $i \in I_N$ velja, da je relativna normalna razdalja $g_{N_i} = 0$ in podobno za relativno stično hitrost $\dot{g}_{N_i} = 0$. Zaradi nepredirljivosti teles velja $g_{N_i} \geq 0$; sledi, da lahko za vsak stik v normalni smeri zapišemo komplementarni pogoj:

The index N denotes the normal direction, and the index H denotes the tangential direction of the possibly sticking set l_H. The new index G denotes the sliding contacts (the tangential force is known) of the set $l_N \setminus l_H$ and the $\bar{\bar{\mu}}_G$ diagonal matrix of the friction coefficients.

Each closed contact $i \in I_N$ is characterized by a vanishing contact distance $g_{N_i} = 0$ and a normal relative velocity $\dot{g}_{N_i} = 0$. Because of the impetrability of the bodies $g_{N_i} \geq 0$, a complementary solution for each contact in the normal direction can be found:

$$\ddot{g}_{N_i} = 0 \wedge \lambda_{N_i} \geq 0 \qquad \text{stik se ohranja/contact is maintained} \tag{11}$$

$$\ddot{g}_{N_i} > 0 \wedge \lambda_{N_i} = 0 \qquad \text{sprostitev stika/detachment of contact} \tag{12}$$

in tudi $i \in I_N$:

and also $i \in I_N$:

$$\ddot{g}_{N_i} \lambda_{N_i} = 0 \tag{13}.$$

Taka komplementarnost je prikazana na sliki 2. Nekaj podobnega lahko ugotovimo za vsak stik v tangentni smeri (sl. 3a), vendar moramo še prej Coulombov zakon razdeliti na dve veji: ena za pozitivno in ena za negativno smer. Taka razdelitev in komplementarni prikaz stičnega zakona v tangentni smeri je prikazana na sliki 3b. Da bi se izognili težavam s singularnostjo, smo dejansko uporabili bolj zapleteno razdelitev stika v tangentni smeri, ki je tukaj zaradi pomanjkanja prostora ne bomo obravnavali [7].

Z zamudno matematično izpeljavo komplementarni problem za vse stične točke v normalni in tangentni smeri hkrati zapišemo v obliki [7]:

Such a complementarity is sometimes also referred to as the corner law [9], and is shown in Figure 2. In the following we will also try to represent the idea of the corner law in the tangential direction. Figure 3a presents the Coulomb friction law. Figure 3b shows the friction law decomposed into two branches: one for positive sliding and one for negative sliding. To avoid singularity problems, the actually used decomposition is more complicated and is covered in [7].

By extensive mathematical manipulation [7] the normal and tangential directions are written together in the form:

$$\boldsymbol{y} = A\,\boldsymbol{x} + b \tag{14}$$

$$\boldsymbol{y} \geq 0, \qquad \boldsymbol{x} \geq 0, \qquad \boldsymbol{y}^T\,\boldsymbol{x} = 0 \tag{15},$$

kjer (14) in (15) pomenita linearni komplementarni problem (LKP) razsežnosti n_N+4n_H in se kot neznanki pojavljata vektorja $\{\boldsymbol{y}, \boldsymbol{x}\} \in \mathbb{R}^{n_N+4n_H}$. V komplementranih pogojih (15) je treba zapis $\boldsymbol{y}^T\boldsymbol{x} = 0$ razumeti na ravni posameznih elementov: $y_i x_i = 0$ za vse *i*. Vektor $\boldsymbol{y}$ med drugim vsebuje neznane stične pospeške $\ddot{g}$ in vektor $\boldsymbol{x}$

Equations (14) and (15) represent an LCP where the vectors $\{\boldsymbol{y}, \boldsymbol{x}\} \in \mathbb{R}^{n_N+4n_H}$ are not known, but they comply with the complementary conditions (15), where $\boldsymbol{y}^T\boldsymbol{x} = 0$ should be understood on the element basis: $y_i x_i = 0$ for all *i*. Vector $\boldsymbol{y}$ includes the unknown contact accelerations $\ddot{g}$, and the vector $\boldsymbol{x}$ includes

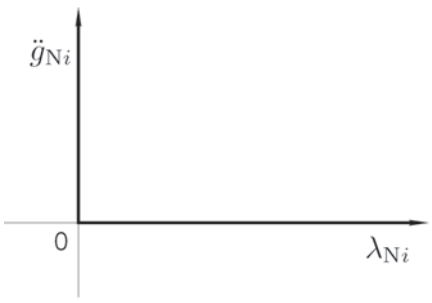

Sl. 2. *Dopolnilnost v normalni smer*i
Fig. 2. *Complementarity in the normal direction*

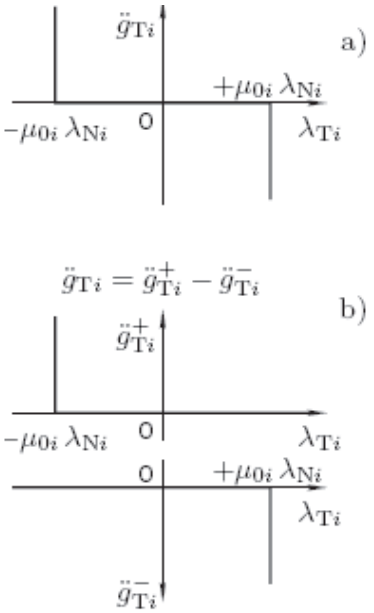

Sl. 3. *Dopolnilnost v tangentni smeri*
Fig. 3. *Complementarity in the tangential direction*

neznane stične sile λ. Matriki $\boldsymbol{A}$ in $\boldsymbol{b}$ sta znani in določeni z masno matriko, vektorjem aktivnih sil, koeficienti trenja in kinematiko stičnih točk/obliko teles.

1.2 Trk s trenjem

V trku sodelujejo stiki iz množice l_S in ga rešujemo na ravni impulzov, zato moramo gibalno enačbo (7) najprej integrirati [7], nato pa impulz v fazi kompresije s Poissonovim zakonom povežemo z impulzom v fazi ekspanzije. Pri tem uporabimo naslednje poenostavitve: čas trka je zanemarljivo majhen, lega teles in vse neimpulzne sile se ne spremenijo, ne spremeni se tudi število stičnih točk.

Podobno kakor smo pri lepenju, drsenju in sprostitvi stika zapisali komplementarne pogoje, tako lahko tudi za fazo kompresije in ekspanzije zapišemo komplementrane pogoje. Pri čemer pa se pri trku v komplementarnem paru namesto sil in pospeškov pojavljajo hitrosti in impulzi. Faza se konča, ko so relativne stične hitrosti v normalni smeri enake nič; takrat se začne faza ekspanzije [7]. Podrobneje tukaj ne bomo šli v zapis LKP. Je pa treba izpostaviti, da moramo pri več sočasnih trkih paziti na pogoj nepredirljivosti. V fazi ekspanzije lahko namreč lokalna ekspanzija v neki točki povzroči prediranje v neki drugi točki; to preprečimo tako, da v komplementarnem pogoju omogočimo večji impulz ekpanzije, kakor ga dovoljuje Poissonov zakon, vendar je v tem primeru relativna stična hitrost ob koncu ekspanzije enaka nič. Glocker [8] je pokazal, da je zakon trka v takem primeru celotno raztresen.

Omeniti velja, da je Pfeiffer-Glockerjeva formulacija ena redkih, ki omogoča simuliranje tudi popolnega povračljivega trka v tangentni smeri[2].

2 NUMERIČNI PREIZKUS

V nadaljevanju si bomo ogledali uporabo predstavljenih postopkov na primeru dinamike ščetke elektromotorja (sl. 4). Dinamični sistem sestavljajo štiri telesa: kolektor, ščetka, vodilo in vzmet.

2.1 Definiranje dinamičnega sistema

Kolektor je definiran s polmerom, ekscentričnostjo, številom lamel, površinsko hrapavostjo Rz (sl. 4, detajl B) in širino reže.

[2]Popolno povračljivost v tangentni smeri ima npr. zelo elastična žoga; medtem, ko je npr. trk pingpong žoge v tangentni smeri nepovračljiv.

the unknown contact forces λ. $\boldsymbol{A}$ and $\boldsymbol{b}$ are the known matrix and vector defined by the mass matrix, the friction coefficients and the contact shapes.

1.2 Impact with friction

While the stick-slip or detachment transition is solved in the force-acceleration domain, the impact is solved in the impulse-velocity domain. Some common assumptions for rigid-body impacts are made: the duration of the impact is infinitely short, the wave effects are not taken into account, during the impact all the positions and orientations, and all the non-impulsive forces and torques, remain constant.

As it is possible to write the stick-slip and detachment problem in the form of an LCP, it is also possible to do it for the compression and expansion phase; the only difference is that the solution is found in the impulse-velocity domain, and that the decomposition of the contact law is more complicated. One of the additional complications is posed by the multiple concurrent contacts that have mutual influences; the physically consistent formulation needs to guarantee non-penetration at such contact situations. As shown by Glocker [8], the Pfeiffer-Glocker formulation can deal with multiple contacts in a physically consistent way, and it maintains the globally dissipative criteria. After the compression phase ends when the relative contact velocities at contacts diminish, the expansion phase continues. The amount of impulse transferred from the compression to the expansion phase is defined by the friction and Poisson laws.

More details on impacts with friction are given in [7]; the same publication gives more details on how to include the reversibility in the tangential direction[2].

2 NUMERICAL EXPERIMENT

This section presents an 11-degrees-of-freedom model of electric-motor-brush dynamics, Figure 4. The dynamical system consists of four bodies: commutator, brush, and spring holder.

2.1 Characterization of the dynamical system

The commutator is defined by the radius, the eccentricity, the number of commutator bars, the surface roughness, Rz, and the slot-width between the bars, Fig. 4B.

[2]As an example of reversibility in the tangential direction the super-elastic ball is usually given. On the other, hand a ping-pong ball impulse in the tangential direction is completely irreversible.

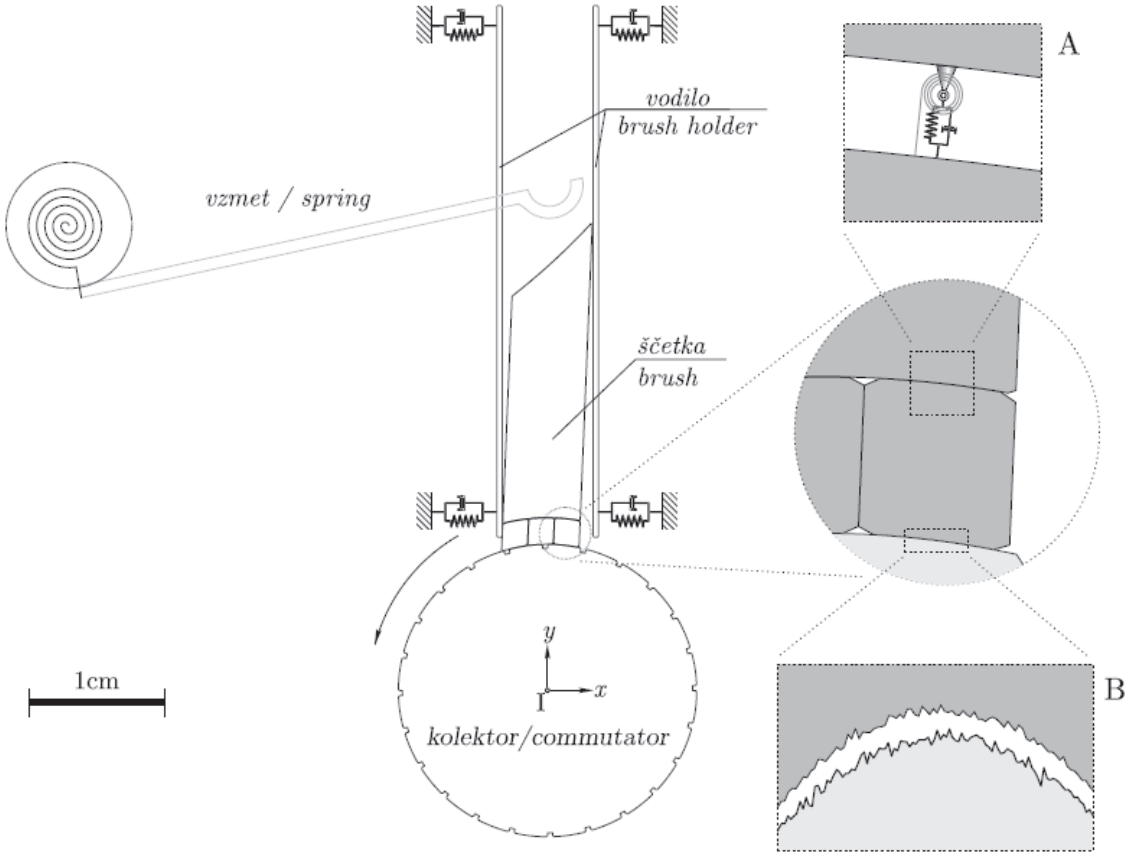

Sl. 4. *Shematičen prikaz dinamičnega modela ščetke z 11 prostostnimi stopnjami*
Fig. 4. *Scheme of the model with 11 degrees of freedom*

Ščetka elektromotorja je definirana s širino, dolžino, ukrivljenostjo in hrapavostjo stične površine s kolektorjem, nagibom stične površine z vzmetjo in togostjo. Da se doseže lokalna deformabilnost ščetke v stiku s kolektorjem, je le-ta modelirana kot sistem štirih togih teles. Toga telesa, ki sestavljajo ščetko, so med seboj povezana z vibroizolacijo (sl. 4, detajl A), katere parametri so pridobljeni s preizkusom. Ščetka ima kot sistem togih teles 9 prostostnih stopenj.

Vodilo ščetke je definirano z dolžino, zračnostjo glede na ščetko, zračnostjo glede na kolektor, togostjo vpetja in lego težišča glede na inercialni koordinatni sistem $_{r}xy$ (sl. 4). Vodilo ima eno prostostno stopnjo: vrtenje okoli težišča.

Vzmet je definirana z dolžino, polmerom vrtenja, togostjo, prednapetjem vzmeti in lego glede na inercialni koordinatni sistem $_{r}xy$. Vzmet ima eno prostostno stopnjo.

Potem ko so posamezna telesa definirana, je treba določiti gibalne enačbe sistema brez enostranskih stikov in jih zapisati v matrično

The electric-motor brush is defined by the width, the length, the radius of curvature of the contact surface with commutator, the roughness of the contact surface with the commutator, the slope of the contact surface with the spring and with the brush stiffness. To achieve local deformability the brush is modeled as a system of four rigid bodies (9 degrees of freedom) that are connected with viscoelastic elements, Fig. 4A. The parameters of the viscoelastic elements were obtained experimentally.

The holder of the brush is defined by the length, the clearance between the holder and the brush, the clearance between the holder and the commutator, the stiffness of the attachment to the surroundings and the position of the center of gravity, see Figure 4. The holder has 1 degree of freedom.

The spring is defined with the length, the radius of rotation, the stiffness, the pre-stress rate and the position. The spring has one degree of freedom.

The 11 equations of motion for the given system need to be written in the matrix form (1). The equations of motion for a contact-free case can be

obliko (1). Celoten sistem ima 11 prostostnih stopenj in je definiran z 11 gibalnimi enačbami. Izpeljava gibalnih enačb z uporabo Lagrangevih enačb II. vrste je razmeroma preprosto, vendar zamudno opravilo in ga bomo tukaj zaradi obsežnosti izpustili. Popis sistema nadaljujemo s stičnimi parametri med telesi: ščetka – kolektor, ščetka – vodilo, ščetka – vzmet. Stični parametri so: koeficient trenja μ, koeficient trka v normalni ε_n in tangentni smeri ε_t ter koeficient povračljivosti trka v tangentni smeri ν [7].

Ščetka kot bistveni stični element je narejena iz grafit-epoksidnega materiala. Ker je kristalna rešetka grafit-epoksidnega materiala šesterokotna, so materialne lastnosti anizotropne (tako električne kot mehanske); poleg tega se materialne lastnosti zelo spreminjajo: predvsem s temperaturo in gostoto toka skozi ščetko. Pri vzpostavitvi dinamičnega modela je tako zelo pomembno preizkusno pridobivanje ustreznih materialnih podatkov:

- elastični in dušilni parametri v odvisnosti od temperature in gostote toka,
- trčni parametri v odvisnosti od temperature, gostote toka, hitrosti trka in izmere trčnih teles (dolžine ščetke),
- koeficienta trenja v odvisnosti od temperature, gostote toka in relativne hitrosti drsenja.

Vsaka od zgoraj naštetih nalog je sama zase zahtevna naloga, vendar se je kot najbolj zahtevna izkazala meritev koeficienta trenja v odvisnosti od temperature in gostote toka, ki smo jo predstavili v ločeni objavi [13].

Ker je oblika togih teles definirana z robom iz diskretnih točk, lahko kinematične podatke trka (4) določimo neposredno iz oblike [11].

2.2 Vpliv spreminjanja parametrov sistema na obratovalne razmere ščetke

V prejšnjem poglavju so našteti bistveni parametri, ki definirajo obravnavani dinamični sistem ščetke. Zaradi velikega števila parametrov bo tukaj kot primer prikazan vpliv samo nekaterih parametrov.

2.2.1 Vpliv dolžine ščetke na njeno stabilnost

Na sliki 5 je prikazan fazni diagram nove ščetke; opazimo, da je kotna hitrost omejena s ±30 rad/s in da je ščetka praktično vedno znotraj nagiba $-7\cdot10^{-3}$ rad do $-2\cdot10^{-3}$ rad. Kadar se ščetka obrabi, kakor je prikazano na sliki 6, pa postane ščetka

obtained relatively easily with the help of Lagrange equations, but because this is a lengthy task it will be omitted here. For a complete definition of the system the contact parameters between the brush-commutator, the brush-holder and the brush-spring need to be set. The contact parameters are as follows: the coefficient of friction μ, and the coefficient of restitution in the normal and tangential directions, ε_n and ε_t , respectively. If necessary, the coefficient of reversibility in the tangential direction ν needs to be set [7].

The most important body in the system is the brush, which consists of graphite/epoxy material whose characteristics are highly sensitive to temperature. In addition, because the crystal lattice is hexagonal the mechanical and electrical properties are highly anisotropic. Because of the anisotropy and the temperature sensitivity the experimental work was focused on determining:

- the stiffness and damping properties as a function of temperature and current density,
- the impact properties as a function of temperature, current density, impact velocity and the dimensions of the impacting bodies (length of brush),
- the coefficient of friction as a function of temperature, current density and sliding velocity.

The quality of the simulation results critically depends on the quality of the experimental work; how we measured the coefficient of friction for various temperatures and current densities we present in a separate paper [13].

The kinematical properties (4) of the contact points are determined automatically from the discretely defined bodies [11].

2.2 Influence of the parameter variation on the working conditions of the brush

The dynamical system is defined by more than 40 parameters. As an example of influence-analysis, the influence of selected parameters on the working conditions will be given.

2.2.1 Influence of brush-length on the dynamic stability

A phase plot of a new brush is shown in Figure 5: the angular velocity is in the range ±30 rad/s, while the angle is in the range from $-7\cdot10^{-3}$ rad to $-2\cdot10^{-3}$ rad. When the brush is at the end of its lifetime it becomes considerably less stable, see Figure 6.

bistveno bolj nemirna: kotna hitrost sega tudi izven področja ±100 rad/s in tudi nagib ščetke je v bistveno širšem področju kakor pri novi ščetki. Obrabljena ščetka je torej bistveno bolj nemirna, kar seveda vpliva na kakovost električnega stika in s tem tudi na obrabo, dobo in zanesljivost delovanja elektromotorja.

Na sliki 7 je prikazana povprečna absolutna kotna hitrost ščetke za več ko 1400 različnih numeričnih simulacij. Simulirani sistemi se razlikujejo v naboru 11 različnih parametrov, kakor so: hrapavost kolektorja, ekscentričnost kolektorja, nagib ščetke glede na os vrtenja, togost ščetke, zračnost med ščetko in vodilom, togost napenjalne vzmeti itn.

Ker je izraba ščetke neizogibna, je dolžina ščetke težko vir izboljšav, ki pa jih lahko dosežemo s spreminjanjem vrste drugih parametrov. Izbira

The angular velocity can also be above ±100 rad/s and also a broader range of angles of the brush is observed. The stability of the brush considerably influences the quality of the electrical contact and consequently the lifetime and the reliability of the electric motor.

From more then 1400 simulation results obtained from systems with different parameter values we can see that the brush-length has a major influence on the stability, see Figure 7. Altogether, 11 parameters were varied: commutator roughness, commutator eccentricity, relative position of the brush, brush stiffness, clearance between the brush and the holder, stiffness of the spring, etc.

Because of the wear the change of the brush-length cannot be omitted, and therefore we are seeking another property to increase the stability. One of the obvious options is the change of the brush-material, i.e.,

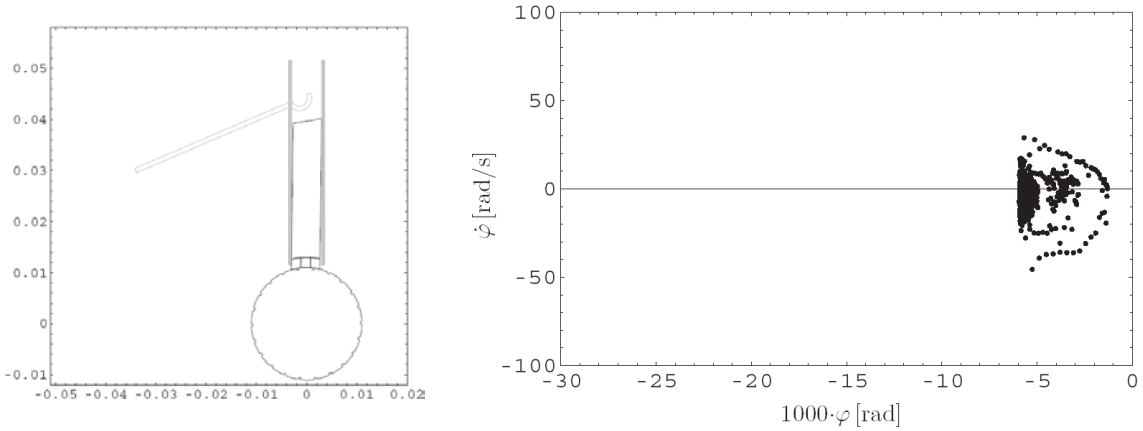

Sl. 5. *Fazni diagram za φ pri novi ščetki*
Fig. 5. *Phase diagram for φ for a new brush*

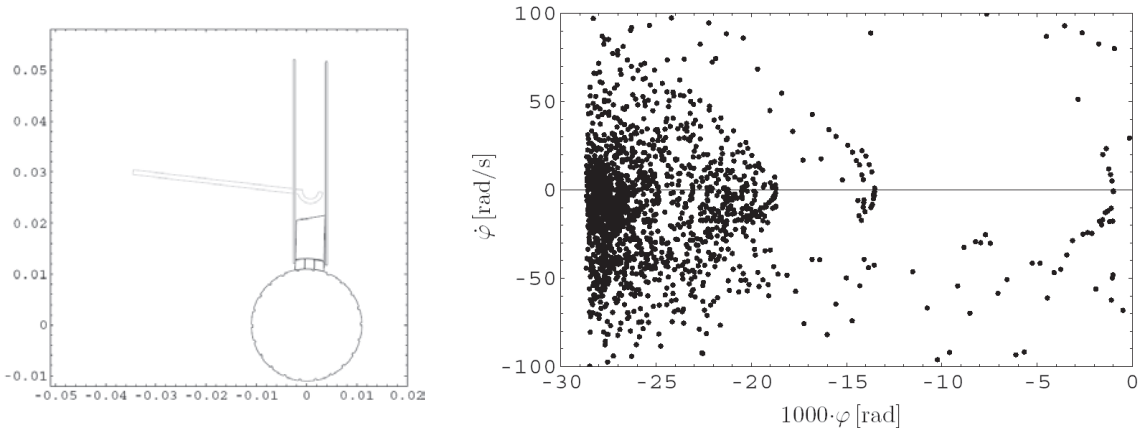

Sl. 6. *Fazni diagram za φ pri obrabljeni ščetki*
Fig. 6. Phase diagram for φ for a used brush at end of its lifetime

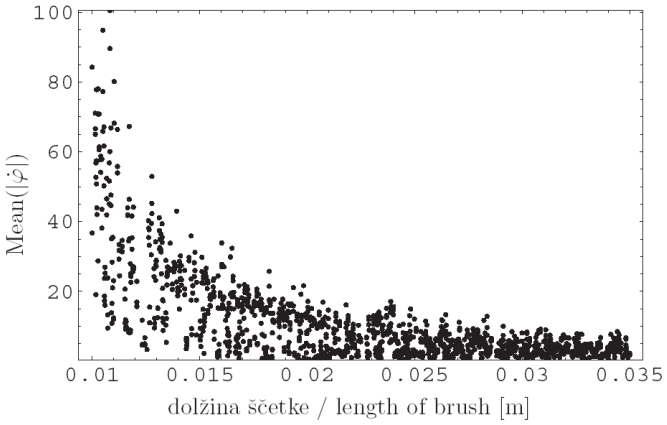

Sl. 7. *Povprečna absolutna kotna hitrost ščetke v odvisnosti od njene obrabe*
Fig. 7. *Average absolute angular velocity as a function of the length of the brush*

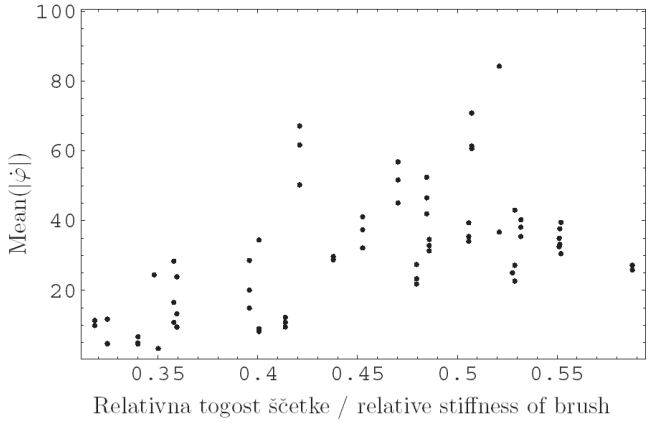

Sl. 8. *Povprečna absolutna kotna hitrost ščetke v odvisnosti od relativne togosti ščetke (69 različnih numeričnih simulacij)*
Fig. 8. *Average absolute angular velocity as a function of relative brush stiffness (69 different simulations)*

drugačnega materiala je ena od možnosti in na sliki 8 je prikazan vpliv relativne togosti na povprečno absolutno kotno hitrost ščetke; prikazanih je 69 rezultatov ščetke dolžine od 10 mm do 15 mm. Očitno je, da bolj elastična ščetka prispeva k stabilnosti lete.

3 SKLEPI

V prvem delu prispevka predstavljeni postopki so predvsem namenjeni simuliranju analitično zapisanih problemov in jasno izraženih stičnih stanj; za take primere lahko kinematične lastnosti stičnih točk določimo analitično in vnaprej. V primeru geometrijsko zahtevnejših teles in v primeru dinamičnih sistemov z geometrijskimi nelinearnostmi pa se izkaže, da je določevanje kinematičnih lastnosti kontaktnih točk vnaprej praktično nemogoče. V

the stiffness and damping parameters of the brush. The influence analysis of the brush-stiffness on the brush stability at the end of its lifetime shows an increased stability of softer materials, see Figure 8. The Figure shows the results of 69 different simulations with a brush length ranging from 10 to 15 mm

3 CONCLUSIONS

The second section of the paper introduces the concepts needed to simulate the dynamics of analytically defined systems with clear contact situations. However, in geometrically more complicated and nonlinear cases the contact properties of the contact situations cannot be defined *a priori* and the extension of the concepts toward discretely defined bodies is necessary. The

tem prispevku uporabljen diskreten postopek definiranja geometrijske oblike teles pa to omejitev odpravlja, saj se kinematične lastnosti stičnih točk glede na geometrijsko obliko teles določajo sproti (v vsakem časovnem koraku).

Predstavljeni postopki omogočajo numerično simulacijo sistema togih teles z zelo zahetvno geometrijsko obliko, katera, kakor je nakazano v numeričnem preizkusu, vključuje tudi hrapavost.

V numeričnem preizkusu predstavljen dinamični model ščetke elektromotorja ima 11 prostostnih stopenj in ga definira več kot 40 različnih parametrov. Na primeru vpliva obrabe/dolžine ščetke in togosti ščetke je prikazano, kako lahko z numeričnim preizkusom iščemo nove zamisli za izdelavo prototipnih izvedb in dejanskih preizkusnih potrditev. Pri ujemanju rezultatov numeričnega in dejanskega preizkusa pa je vsaj toliko kot uporaba fizikalno dosledne teorije pomembna tudi uporaba kakovostnih preizkusnih podatkov, ki se v preizkusnih načelih ujemajo z uporabljenimi teoretičnimi postopki. Velik pomen predstavljenega dela je zato bil tudi na preizkusnih meritvah.

discretely defined bodies are therefore used to define the contact parameters during each time-step.

As shown in the numerical example, the extensions for discretely defined bodies can therefore be used to simulate the dynamics of complex body shapes, including such local details as a geometrically exact simulation of the roughness.

The numerical experiment of the electric-motor-brush presents a rigid body model with 11 degrees of freedom defined by more than 40 parameters. The study of how brush-wear and brush-roughness influence the stability of the electric brush shows how new ideas for improvements can be found. However, the ideas have to be tested on prototypes. We believe that the quality of the simulations critically depends on the quality of the theoretical background and—at least as important—on the quality of the experimental work.

4 LITERATURA
4 REFERENCES

[1] P. Song (2002) Modeling, analysis and simulation of multibody systems with contact and friction. PhD thesis, *University of Pennsylvania*.

[2] P. Lötstedt (1981) Coulomb friction in two-dimensional rigid body systems. *Z. Angewandte Math. Mech.*, 61:605–615.

[3] K.G. Murty (1988) Linear complementarity, Linear and nonlinear programming. *Heldermann Verlag*, Berlin.

[4] D. Baraff (1992) Dynamic simulations of non-penetrating rigid bodies. PhD thesis, *Cornell University*, NY.

[5] P.D. Panagiotopoulos (1993) Hemivariational inequalities: applications in mechanics and engineering. *Springer Verlag*, Berlin, Heidelberg.

[6] J.J. Moreau (1976) Sur les mesures différentialles de fonctions vectorielles et certains problèmes d'évolution. *Comptes Rendus Acad. Sci. Paris*, 282:837–840, Sér. A.

[7] F. Pfeiffer and C. Glocker (1996) Multibody dynamics with unilateral contacts. *John Wiley & Sons, Inc*, New York.

[8] C. Glocker (1995) Dynamik von Starrkörpesystemen mit Reibung und Stößen. PhD Thesis, *Technische Universität München*.

[9] F. Pfeiffer (2003) The idea of complementarity in multibody dynamics. *Archive of Applied Mechanics*, 72:807–816.

[10] J. Slavič and M. Boltežar (2004) Dinamika diskretno definiranega sistema togih teles z enostranskimi kontakti = Multibody dynamics of discrete bodies with unilateral contacts. In J. Korelc and D. Zupan, editors, *Kuhljevi dnevi 2004*, Otočec, 30. september - 1. oktober 2004, pages 285–292. Slovensko društvo za mehaniko.

[11] J. Slavič and M. Boltežar (2005) Nonlinearity and non-smoothness in multi body dynamics: application to woodpecker toy. *Journal of Mechanical Engineering Science*, 2005. In press.

[12] R.I. Leine, C. Glocker, and D.H. Van Campen (2003) Nonlinear dynamics and modelling of some wooden toys with impact and friction. *Nonlinear Dynamics*, 9:25–78.

[13] J. Slavič and M. Boltežar (2005) Measuring the dynamic forces to identify the friction of a graphite-copper contact for variable temperature and current. *Wear*, 2005. In press.

Strojniški vestnik - Journal of Mechanical Engineering 52(2006)2, 126-137

Naslova avtorjev: dr. Janko Slavič
prof.dr. Miha Boltežar
Univerza v Ljubljani
Fakulteta za strojništvo
Aškerčeva 6
1000 Ljubljana
janko.slavic@fs.uni-lj.si
miha.boltezar@fs.uni-lj.si

dr. Miha Nastran
Domel d.d.
Otoki 21
4228 Železniki
miha.nastran@domel.si

Authors' Addressses: Dr. Janko Slavič
Prof.Dr. Miha Boltežar
University of Ljubljana
Faculty of Mechanical Engineering
Aškerčeva 6
SI-1000 Ljubljana, Slovenia
janko.slavic@fs.uni-lj.si
miha.boltezar@fs.uni-lj.si

Dr. Miha Nastran
Domel d.d.
Otoki 21
SI-4228 Železniki, Slovenia
miha.nastran@domel.si

Prejeto: 3.10.2005
Received:
Sprejeto: 16.11.2005
Accepted:
Odprto za diskusijo: 1 leto
Open for discussion: 1 year

Osebne vesti - Personal Events

Doktorat, magisterija in diplome - Doctor's, Master's and Diploma Degrees

DOKTORAT

Na Fakulteti za strojništvo Univerze v Ljubljani je z uspehom zagovarjal svojo doktorsko disertacijo:

dne *30. januarja 2006*: **mag. Simon Krašna**, z naslovom: "Modeliranje mehanike človeškega telesa za analizo dinamike in poškodb potnikov pri trkih vozil".

S tem je navedeni kandidat dosegel akademsko stopnjo doktorja znanosti.

MAGISTERIJA

Na Fakulteti za strojništvo Univerze v Mariboru so z uspehom zagovarjali svoja magistrska dela:

dne 5. januarja 2006: **Janez Makovšek**, z naslovom: "Nadzor čistilnega procesa v tlačnih posodah procesne tehnike s pomočjo analize vibracij";

dne 6. januarja 2006: **Alenka Pšeničnik**, z naslovom: "Sistemska ureditev pretoka materialov in informacij v proizvodnji valjev".

S tem sta navedena kandidata dosegla akademsko stopnjo magistra znanosti.

DIPLOMIRALI SO

Na Fakulteti za strojništvo Univerze v Ljubljani je pridobil naziv univerzitetni diplomirani inženir strojništva:

dne *25. januarja 2006*: David VIŽINTIN.

*

Na Fakulteti za strojništvo Univerze v Ljubljani so pridobili naziv diplomirani inženir strojništva:

dne *13. januarja 2006*: Boris GUZELJ, Primož KOKALJ, Gorazd LAPANJA, Boštjan ŠKRLJ;

dne *27. januarja 2006*: Gregor CVETKOVIČ, Janez FIREDER, Boštjan IRŠIČ, Andrej JESENOVEC.

Na Fakulteti za strojništvo Univerze v Mariboru sta pridobila naziv diplomirani inženir strojništva:

dne 26. januarja 2006: Borut MEKE, Robert POLOVIČ.

Strojniški vestnik - Journal of Mechanical Engineering 52(2006)2, 139-140
Navodila avtorjem - Instructions for Authors

Navodila avtorjem - Instructions for Authors

Članki morajo vsebovati:
- naslov, povzetek, besedilo članka in podnaslove slik v slovenskem in angleškem jeziku,
- dvojezične preglednice in slike (diagrami, risbe ali fotografije),
- seznam literature in
- podatke o avtorjih.

Strojniški vestnik izhaja od leta 1992 v dveh jezikih, tj. v slovenščini in angleščini, zato je obvezen prevod v angleščino. Obe besedili morata biti strokovno in jezikovno med seboj usklajeni. Članki naj bodo kratki in naj obsegajo približno 8 strani. Izjemoma so strokovni članki, na željo avtorja, lahko tudi samo v slovenščini, vsebovati pa morajo angleški povzetek.

Za članke iz tujine (v primeru, da so vsi avtorji tujci) morajo prevod v slovenščino priskrbeti avtorji. Prevajanje lahko proti plačilu organizira uredništvo. Če je članek ocenjen kot znanstveni, je lahko objavljen tudi samo v angleščini s slovenskim povzetkom, ki ga pripravi uredništvo.

VSEBINA ČLANKA

Članek naj bo napisan v naslednji obliki:
- Naslov, ki primerno opisuje vsebino članka.
- Povzetek, ki naj bo skrajšana oblika članka in naj ne presega 250 besed. Povzetek mora vsebovati osnove, jedro in cilje raziskave, uporabljeno metodologijo dela,povzetek rezulatov in osnovne sklepe.
- Uvod, v katerem naj bo pregled novejšega stanja in zadostne informacije za razumevanje ter pregled rezultatov dela, predstavljenih v članku.
- Teorija.
- Eksperimentalni del, ki naj vsebuje podatke o postavitvi preskusa in metode, uporabljene pri pridobitvi rezultatov.
- Rezultati, ki naj bodo jasno prikazani, po potrebi v obliki slik in preglednic.
- Razprava, v kateri naj bodo prikazane povezave in posplošitve, uporabljene za pridobitev rezultatov. Prikazana naj bo tudi pomembnost rezultatov in primerjava s poprej objavljenimi deli. (Zaradi narave posameznih raziskav so lahko rezultati in razprava, za jasnost in preprostejše bralčevo razumevanje, združeni v eno poglavje.)
- Sklepi, v katerih naj bo prikazan en ali več sklepov, ki izhajajo iz rezultatov in razprave.
- Literatura, ki mora biti v besedilu oštevilčena zaporedno in označena z oglatimi oklepaji [1] ter na koncu članka zbrana v seznamu literature. Vse opombe naj bodo označene z uporabo dvignjene številke[1].

OBLIKA ČLANKA

Besedilo članka naj bo pripravljeno v urejevalnilku Microsoft Word. Članek nam dostavite v elektronski obliki.

Ne uporabljajte urejevalnika LaTeX, saj program, s katerim pripravljamo Strojniški vestnik, ne uporablja njegovega formata.

Enačbe naj bodo v besedilu postavljene v ločene vrstice in na desnem robu označene s tekočo številko v okroglih oklepajih

Papers submitted for publication should comprise:
- Title, Abstract, Main Body of Text and Figure Captions in Slovene and English,
- Bilingual Tables and Figures (graphs, drawings or photographs),
- List of references and
- Information about the authors.

Since 1992, the Journal of Mechanical Engineering has been published bilingually, in Slovenian and English. The two texts must be compatible both in terms of technical content and language. Papers should be as short as possible and should on average comprise 8 pages. In exceptional cases, at the request of the authors, speciality papers may be written only in Slovene, but must include an English abstract.

For papers from abroad (in case that none of authors is Slovene) authors should provide Slovenian translation. Translation could be organised by editorial, but the authors have to pay for it. If the paper is reviewed as scientific, it can be published only in English language with Slovenian abstract, that is prepared by the editorial board.

THE FORMAT OF THE PAPER

The paper should be written in the following format:
- A Title, which adequately describes the content of the paper.
- An Abstract, which should be viewed as a mini version of the paper and should not exceed 250 words. The Abstract should state the principal objectives and the scope of the investigation, the methodology employed, summarize the results and state the principal conclusions.
- An Introduction, which should provide a review of recent literature and sufficient background information to allow the results of the paper to be understood and evaluated.
- A Theory
- An Experimental section, which should provide details of the experimental set-up and the methods used for obtaining the results.
- A Results section, which should clearly and concisely present the data using figures and tables where appropriate.
- A Discussion section, which should describe the relationships and generalisations shown by the results and discuss the significance of the results making comparisons with previously published work. (Because of the nature of some studies it may be appropriate to combine the Results and Discussion sections into a single section to improve the clarity and make it easier for the reader.)
- Conclusions, which should present one or more conclusions that have been drawn from the results and subsequent discussion.
- References, which must be numbered consecutively in the text using square brackets [1] and collected together in a reference list at the end of the paper. Any footnotes should be indicated by the use of a superscript[1].

THE LAYOUT OF THE TEXT

Texts should be written in Microsoft Word format. Paper must be submitted in electronic version.

Do not use a LaTeX text editor, since this is not compatible with the publishing procedure of the Journal of Mechanical Engineering.

Equations should be on a separate line in the main body of the text and marked on the right-hand side of the page with numbers in round brackets.

Enote in okrajšave

V besedilu, preglednicah in slikah uporabljajte le standardne označbe in okrajšave SI. Simbole fizikalnih veličin v besedilu pišite poševno (kurzivno), (npr. *v, T, n* itn.). Simbole enot, ki sestojijo iz črk, pa pokončno (npr. ms^{-1}, K, min, mm itn.).

Vse okrajšave naj bodo, ko se prvič pojavijo, napisane v celoti v **slovenskem jeziku**, npr. časovno spremenljiva geometrija (ČSG).

Slike

Slike morajo biti zaporedno oštevilčene in označene, v besedilu in podnaslovu, kot sl. 1, sl. 2 itn. Posnete naj bodo v ločljivosti, primerni za tisk, v kateremkoli od razširjenih formatov, npr. BMP, JPG, GIF. Diagrami in risbe morajo biti pripravljeni v vektorskem formatu.

Pri označevanju osi v diagramih, kadar je le mogoče, uporabite označbe veličin (npr. *t, v, m* itn.), da ni potrebno dvojezično označevanje. V diagramih z več krivuljami, mora biti vsaka krivulja označena. Pomen oznake mora biti pojasnjen v podnapisu slike.

Vse označbe na slikah morajo biti dvojezične.

Preglednice

Preglednice morajo biti zaporedno oštevilčene in označene, v besedilu in podnaslovu, kot preglednica 1, preglednica 2 itn. V preglednicah ne uporabljajte izpisanih imen veličin, ampak samo ustrezne simbole, da se izognemo dvojezični podvojitvi imen. K fizikalnim veličinam, npr. *t* (pisano poševno), pripišite enote (pisano pokončno) v novo vrsto brez oklepajev.

Vsi podnaslovi preglednic morajo biti dvojezični.

Seznam literature

Vsa literatura mora biti navedena v seznamu na koncu članka v prikazani obliki po vrsti za revije, zbornike in knjige:

[1] A. Wagner, I. Bajsić, M. Fajdiga (2004) Measurement of the surface-temperature field in a fog lamp using resistance-based temperature detectors, *Stroj. vestn.* 2(2004), pp. 72-79.
[2] Vesenjak, M., Ren Z. (2003) Dinamična simulacija deformiranja cestne varnostne ograje pri naletu vozila. *Kuhljevi dnevi '03*, Zreče, 25.-26. september 2003.
[3] Muhs, D. et al. (2003) Roloff/Matek Maschinenelemente – Tabellen, 16. Auflage. *Vieweg Verlag*, Wiesbaden.

Podatki o avtorjih

Članku priložite tudi podatke o avtorjih: imena, nazive, popolne poštne naslove in naslove elektronske pošte.

SPREJEM ČLANKOV IN AVTORSKE PRAVICE

Uredništvo Strojniškega vestnika si pridržuje pravico do odločanja o sprejemu članka za objavo, strokovno oceno recenzentov in morebitnem predlogu za krajšanje ali izpopolnitev ter terminološke in jezikovne korekture.

Avtor mora predložiti pisno izjavo, da je besedilo njegovo izvirno delo in ni bilo v dani obliki še nikjer objavljeno. Z objavo preidejo avtorske pravice na Strojniški vestnik. Pri morebitnih kasnejših objavah mora biti SV naveden kot vir.

Units and abbreviations

Only standard SI symbols and abbreviations should be used in the text, tables and figures. Symbols for physical quantities in the text should be written in italics (e.g. *v, T, n,* etc.). Symbols for units that consist of letters should be in plain text (e.g. ms^{-1}, K, min, mm, etc.).

All abbreviations should be spelt out in full on first appearance, e.g., variable time geometry (VTG).

Figures

Figures must be cited in consecutive numerical order in the text and referred to in both the text and the caption as Fig. 1, Fig. 2, etc. Pictures may be saved in resolution good enough for printing in any common format, e.g. BMP, GIF, JPG. However, graphs and line drawings sholud be prepared as vector images.

When labelling axes, physical quantities, e.g. *t, v, m,* etc. should be used whenever possible to minimise the need to label the axes in two languages. Multi-curve graphs should have individual curves marked with a symbol, the meaning of the symbol should be explained in the figure caption.

All figure captions must be bilingual.

Tables

Tables must be cited in consecutive numerical order in the text and referred to in both the text and the caption as Table 1, Table 2, etc. The use of names for quantities in tables should be avoided if possible: corresponding symbols are preferred to minimise the need to use both Slovenian and English names. In addition to the physical quantity, e.g. *t* (in italics), units (normal text), should be added in new line without brackets.

All table captions must be bilingual.

The list of references

References should be collected at the end of the paper in the following styles for journals, proceedings and books, respectively:

[1] A. Wagner, I. Bajsić, M. Fajdiga (2004) Measurement of the surface-temperature field in a fog lamp using resistance-based temperature detectors, *Stroj. vestn.* 2(2004), pp. 72-79.
[2] Vesenjak, M., Ren Z. (2003) Dinamična simulacija deformiranja cestne varnostne ograje pri naletu vozila. *Kuhljevi dnevi '03*, Zreče, 25.-26. september 2003.
[3] Muhs, D. et al. (2003) Roloff/Matek Maschinenelemente – Tabellen, 16. Auflage. *Vieweg Verlag*, Wiesbaden.

Author information

The information about the authors should be enclosed with the paper: names, complete postal and e-mail addresses.

ACCEPTANCE OF PAPERS AND COPYRIGHT

The Editorial Committee of the Journal of Mechanical Engineering reserves the right to decide whether a paper is acceptable for publication, obtain professional reviews for submitted papers, and if necessary, require changes to the content, length or language.

Authors must also enclose a written statement that the paper is original unpublished work, and not under consideration for publication elsewhere. On publication, copyright for the paper shall pass to the Journal of Mechanical Engineering. The JME must be stated as a source in all later publications.